AD-A245 906

# TATION PAGE

Form Approved
OMB No. 0704-0188



| 1. AGENCY USE ONLY (Leave blank) | 2. REPORT DATE | 3. REPORT TYPE AND DATES COVERED |
|---|---|---|
| | April, 1991 | Final 7/1/87 - 6/30/90 |

**4. TITLE AND SUBTITLE**
Theoretical Studies of the Electronic Structure of Metal/Semiconductor/Hydrogen Systems

**5. FUNDING NUMBERS**
AFOSR-87-0302

**6. AUTHOR(S)**
Prof. Walter C. Ermler

DTIC
ELECTE
FEB 10 1992
S D
D

**7. PERFORMING ORGANIZATION NAME(S) AND ADDRESS(ES)**
Stevens Institute of Technology
Hoboken, NJ 07030

**8. PERFORMING ORGANIZATION REPORT NUMBER**
5-27061

**9. SPONSORING/MONITORING AGENCY NAME(S) AND ADDRESS(ES)**
Air Force Office of Scientific Research
Bolling Air Force Base, DC 20332-6448

**10. SPONSORING/MONITORING AGENCY REPORT NUMBER**
AFOSR-TR 91 0502

NP

**11. SUPPLEMENTARY NOTES**

**12a. DISTRIBUTION/AVAILABILITY STATEMENT**
Approved for public release;
distribution unlimited.

**12b. DISTRIBUTION CODE**
92-03242

**13. ABSTRACT** (Maximum 200 words)

Cesium, hydrogen and oxygen adsorption on beryllium clusters are studied using restricted Hartree-Fock (RHF) calculations and ab initio relativistic effective core potentials. The clusters are taken as cylindrical plugs from Be wafers. Cs-, H- and O-to-substrate internuclear distances are optimized. For each system numerous low-lying electronic states are investigated and Mulliken electron populations analyzed. RHF calculations show that $Be_{19}$, with three layers of atoms, is too small to adequately model the Be surface, while $Be_{33}$, a five-layered system, and $Be_{45}$, a seven-layered system, are more accurate representations of the bulk metal. The emitted electron is clearly seen as vacating a molecular orbital which is localized in the surface layer of the cluster, thereby giving further credence to the model. RHF calculations are completed for PbI and BiI semiconductor clusters. Blue shifts in optical spectra and geometry changes are shown to be due to quantum size effects. Scanning tunneling microscopy is used to investigate the nature of colloidal particles in the 15 nm diameter size range. Images show a near monodispersion of small Au clusters. A model of the STM tip as a polyatomic crystalline surface is shown to correctly explain observations of anomalous long range order.

| 14. SUBJECT TERMS | 15. NUMBER OF PAGES |
|---|---|
| | 119 |
| | 16. PRICE CODE |

| 17. SECURITY CLASSIFICATION OF REPORT | 18. SECURITY CLASSIFICATION OF THIS PAGE | 19. SECURITY CLASSIFICATION OF ABSTRACT | 20. LIMITATION OF ABSTRACT |
|---|---|---|---|
| Unclassified | Unclassified | Unclassified | Unclassified |

92 2 04 060

AD-A245906

POOR
ORIGINAL
DOC.

# DISCLAIMER NOTICE

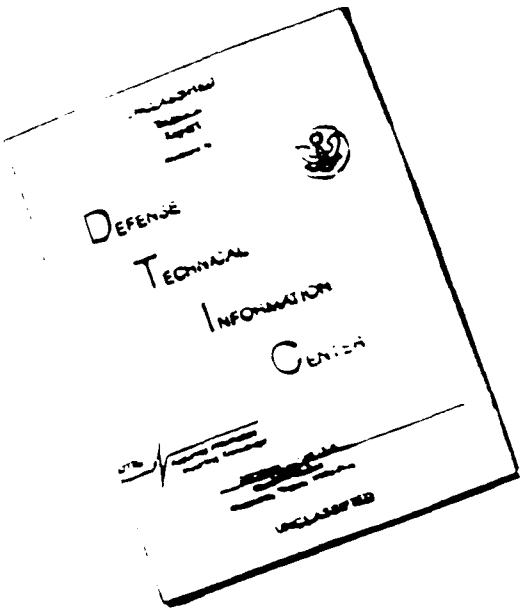


THIS DOCUMENT IS BEST QUALITY AVAILABLE. THE COPY FURNISHED TO DTIC CONTAINED A SIGNIFICANT NUMBER OF PAGES WHICH DO NOT REPRODUCE LEGIBLY.

## Table of Contents

Grant AFOSR-86NP309

# Theoretical Studies of the Electronic Structure of Metal/Semiconductor/Hydrogen Systems

Walter C. Ermler, Professor of Chemistry and Physics
Department of Chemistry and Chemical Engineering
Stevens Institute of Technology
Hoboken, New Jersey 07030
(201) 420-5520

## Final Report

One area of concentration during the first year of the grant involved a series of ab initio self-consistent field (SCF) calculations on clusters of beryllium atoms together with associated cesium and hydrogen atoms. They were completed by Maria M. Marino, the doctoral student whose stipend and tuition were covered under the conditions of this grant. An analysis of both the experimental and theoretical aspects of exposing Be metal surfaces to Cs and H was begun.

SCF calculations were carried out on clusters of 19, 33 and 45 Be atoms. The clusters were defined as cylindrical plugs from a thin wafer of Be metal; an arrangement that is consistent with experimental measurements taken by Tompa and Seidl. Adatoms were made to approach the clusters along the three-fold symmetry axis from above and below the cylinder faces. This is also consistent with the experimental procedure of exposing a foil of Be to Cs and H. The internuclear distances between the Be atoms were held fixed at values corresponding to the hcp metal lattice constants.

The calculations were carried out to examine the nature of the effects of cesium and of hydrogen adsorption on the work function of Be metal. While it is well known that cesium adsorption appreciably lowers the work function of many metals, details of the mechanism by which it occurs is still not well understood. In the case of hydrogen, the interaction with a metal such as Be provides a good, simple model for the process in which we are most interested, that of negative hydrogen production from surfaces. Theoretical studies of the

adsorption process can provide detailed information about the interaction that is not obtainable from experiment. For example, results related to charge distributions and orbital structure at the interface are calculated.

A good model of the interaction between adsorbate and substrate requires the use of clusters large enough to adequately describe the metal surface, while remaining small enough for the application of accurate theoretical methods. In the study recently completed we used relatively small clusters and made use of relativistic pseudopotentials and the high ($D_{3h}$) symmetry of the systems to render the calculations tractable. The calculations were carried out on a Cray X-MP supercomputer at the NSF's Pittsburgh Supercomputing Center and at the Ohio Supercomputer Center. Closed- and open-shell SCF calculations were completed for each cluster system for a range of low-lying electronic states and positive ion states.

Activities during the second year of the grant proceeded essentially along the directions described in the original proposal. A series of ab initio self-consistent field (SCF) calculations on clusters of beryllium atoms together with associated cesium, hydrogen, and oxygen atoms was completed. An analysis of both the experimental and theoretical aspects of exposing Be metal surfaces to Cs and H was published in Surface Science. Prof. Milos Seidl of the Stevens Physics Department and his graduate student Gary Tompa were co-authors of the article. In addition, studies detailing the results of SCF calculations on the simultaneous cesiation and hydrogenation, as well as the simultaneous cesiation and oxygenation, of the $Be_{45}$ surface were initiated.

The SCF calculations were carried out on clusters of 19, 33 and 45 Be atoms. The clusters were defined as cylindrical plugs from a thin wafer of Be metal; an arrangement that is consistent with experimental measurements taken by Prof. Seidl's research group. Adatoms were made to approach the clusters along the three-fold symmetry axis from above and below the cylinder faces. This is also consistent with the experimental procedure of exposing a foil of Be to Cs, H and O. The internuclear distances between the Be atoms were held fixed at values corresponding to the hcp metal lattice constants.

The calculations were carried out to examine the nature of the effects of cesium, hydrogen and oxygen adsorption on the work function of Be metal. While it is well known that cesium adsorption appreciably lowers the work function of

many metals, details of the mechanism by which it occurs is still not well understood. In the case of hydrogen, the interaction with a metal such as Be provides a good, simple model for the process in which we are most interested, that of negative hydrogen production from surfaces. Theoretical studies of the adsorption process can provide detailed information about the interaction that is not obtainable from experiment. For example, results [illegible] to charge distributions and orbital structure at the interface are [illegible].

The adsorption energies of Cs on $Be_{33}$ and on $Be_{45}$ were calculated as 21.8 and 15.1 kcal/mol·atom, respectively, whereas the adsorption of H on $Be_{33}$ and on $Be_{45}$ was not predicted to occur at all. Optimum Cs-to-Be-surface and H-to-Be-surface distances were 3.70 and 0.86 Å, with the latter value corresponding to a local energy minimum. The decreases in the ionization potentials of $Be_{33}Cs_2$ relative to $Be_{33}$ and of $Be_{45}Cs_2$ relative to $Be_{45}$ were 1.5 and 0.54 eV, respectively. This compares favorably with the experimental bulk work function lowering of 2.3 eV. Theoretically, H is predicted to adsorb on $Be_{19}$ but not on $Be_{33}$ nor on $Be_{45}$, consistent with the fact that there is no experimental observation of adsorbed hydrogen on beryllium metal. Analysis of the Mulliken populations for the 19 Be atom system indicates that this cluster is too small to model the surface of bulk beryllium. However, the population analysis for $Be_{33}$ gives strong indications that this cluster is an adequate model for surface interactions. Simultaneous oxygenation and cesiation of $Be_{45}$ results in a greater work function lowering than does cesiation alone, while hydrogenation of $Be45Cs_2$ results in a work function increase. The electron population analysis for $Be_{45}O_2Cs_2$ indicates that the emitted electron is predominantly vacating a cesium orbital. In $Be_{45}H_2Cs_2$, however, the Be cylinder is more involved in ionization, donating approximately 40% of the emitted charge.

Two additional graduate students worked on certain aspects of the project. Doctoral student Makoto Sawamura investigated quantum confinement phenomena in the context of lead iodide clusters at the Hartree-Fock level of approximation. The work is described in detail in his doctoral dissertation and in an articles published in The Journal of Physical Chemistry, Physical Review B and Chemical Physics Letters. Masters thesis student Ping Wang completed a project involving a theoretical study of the cesium suboxides and the nature of the large work function lowering (as low as 0.9 eV) from the standpoint of ab initio calculations using the finite cluster model. She completed her degree

requirements in May, 1990 and the results of her study are being published in The Journal of Chemical Physics.

During the third year of the grant permission was obtained from the AFOSR to use certain of the grant funds to assist in the purchase of a scanning tunneling microscope (STM). The instrument was acquired and a laboratory was set up. The initial research was carried out by a third doctoral student, John F. Womelsdorf. He completed benchmark studies on small (~15 Å diameter) gold colloidal particles. The images were striking and the work was published in The Journal of Physical Chemistry. Following this study, it was planned to study a series of cesium suboxides and attempt to measure their work functions. This work, together with a study of the fundamental interaction between the STM tip and substrate, are now underway and are being supported by a one year extension from the AFOSR. A paper describing our findings on tip-surface interactions was published in Surface Science.

Publications 1-5 and 9-13 (Section 4) comprise the remainder of this Final Report. Copies of the three student theses (Publications 6, 7 and 8, Section 4) were sent separate from this Report.

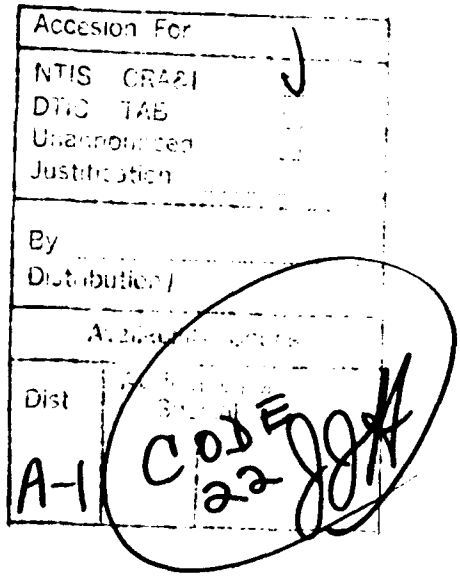

Surface Science 208 (1989) 189–204
North-Holland, Amsterdam



# EFFECTS OF HYDROGEN AND OF CESIUM ADSORPTION ON A BERYLLIUM SURFACE: A THEORETICAL AND EXPERIMENTAL STUDY

M.M. MARINO, W.C. ERMLER

*Department of Chemistry and Chemical Engineering, Stevens Institute of Technology, Hoboken, NJ 07030, USA*

G.S. TOMPA * and M. SEIDL

*Department of Physics and Engineering Physics, Stevens Institute of Technology, Hoboken, NJ 07030, USA*

Received 29 February 1988; accepted for publication 19 September 1988

Cesium and hydrogen adsorption on beryllium clusters containing 19, 33 and 45 atoms are studied using restricted Hartree–Fock (RHF) calculations and ab initio relativistic effective core potentials. The Be clusters are taken as cylindrical plugs from a Be metal wafer. Be–Cs and Be–H internuclear distances are optimized, while Be–Be internuclear distances are frozen at the bulk metal values. For each system, numerous low-lying electronic states are investigated. The calculations are carried out in the context of an experimental study to determine the effects of Cs and of H adsorption on the work function of Be metal. Auger electron spectroscopy and experimental work function measurements indicate that $H_2$ does not adsorb on polycrystalline Be, while photoemission and thick Cs overlayer measurements show a 2.3 eV lowering in the work function of Be metal upon Cs adsorption. RHF calculations indicate that $Be_{19}$, with three layers of atoms, is too small to adequately model the Be surface. Calculations on $Be_{33}$, a five-layered system, and $Be_{45}$, a seven-layered system, show that H does not chemisorb on the surfaces of these clusters, whereas Cs does and lowers the ionization potential of $Be_{33}$ by 1.5 eV. The emitted electron from the $Be_{33}Cs_2$ cluster vacates a molecular orbital which is localized in the surface layer.

## 1. Introduction

It is well known that adsorption of cesium on a metal surface lowers the work function of that metal [1,2]. In particular, the reduction in the work function of beryllium arising from cesium adsorption has been the focus of a very recent study [3]. In the present work, cesium and hydrogen adsorption on a beryllium surface are studied using ab initio quantum mechanical calculations. $H_2$ adsorption on polycrystalline Be is also studied by monitoring the work function and the Be (104 eV) differentiated Auger electron signal intensity.

* Current address: EMCORE Corporation, 35 Elizabeth Avenue, Somerset, NJ 08873, USA.

0039-6028/89/$03.50 

Theoretical studies of the adsorption process yield detailed information about the metal surface which is not easily obtained experimentally. For example, results related to charge distributions and orbital structure are calculated. Many such studies have used clusters as models of the surface [4–7]. A good model of the adsorption process, however, requires the use of clusters large enough to accurately describe the metal surface and its interaction with the substrate, while remaining small enough for application of accurate theoretical methods. In this study, the clusters are taken as cylindrical plugs from a Be wafer having Be–Be internuclear distances equal to those in the bulk hcp metal. Larger spherical clusters were the focus of [illegible] [8]. The use of effective core potentials to describe the core electrons in [illegible] and beryllium allow the calculations to remain tractable while maintaining a well-defined level of theory. The complexity of the calculations is simplified further by preserving full $D_{3h}$ point-group symmetry in each cylindrical cluster.

## 2. Methodology

### 2.1. Theoretical model and calculations

The model systems are taken as cylindrical "plugs" from Be wafers having surfaces corresponding to the (0001) hcp metal faces. A view of this wafer along the $c$ direction is illustrated in fig. 1. Table 1 defines all the cylinders of a given radius which may be formed from a wafer of a given thickness. In this study, three such cylinders are treated. The first has a thickness of three layers and is comprised of 19 Be atoms; the second is five layers thick and contains 33 Be atoms, while the third contains 45 atoms and seven layers. All three cylinders have a radius $R_3$ which includes a one-unit cell step along the $a$ direction. Be–Be internuclear distances are equal to those in the bulk hcp metal ($a = 2.29$ Å, $c = 3.58$ Å) [9]. The resulting cylinders have $D_{3h}$ point-group symmetry, and the adsorption of atomic hydrogen, one on the top surface and one on the bottom surface of all three cylinders, is modeled such that the three-fold symmetry is preserved. The same applies to the adsorption of atomic cesium. In all cases, the Be–adsorbate internuclear distances have been optimized in self-consistent field (SCF) calculations. The 19- and 33-atom cesiated and hydrogenated cylinders are shown in figs. 2 and 3. The 45-atom cylinder is not shown, but it is similar to the one picture in fig. 3, except that it contains seven layers instead of five, and the two surface layers are identical to the surface layers of $Be_{19}$ (fig. 2). Results obtained using these systems are compared to those calculated by treating identical bare Be cylinders.

Calculations were accomplished on a Cray X-MP supercomputer using programs based on the "equal contribution theorem" for two-electron in-

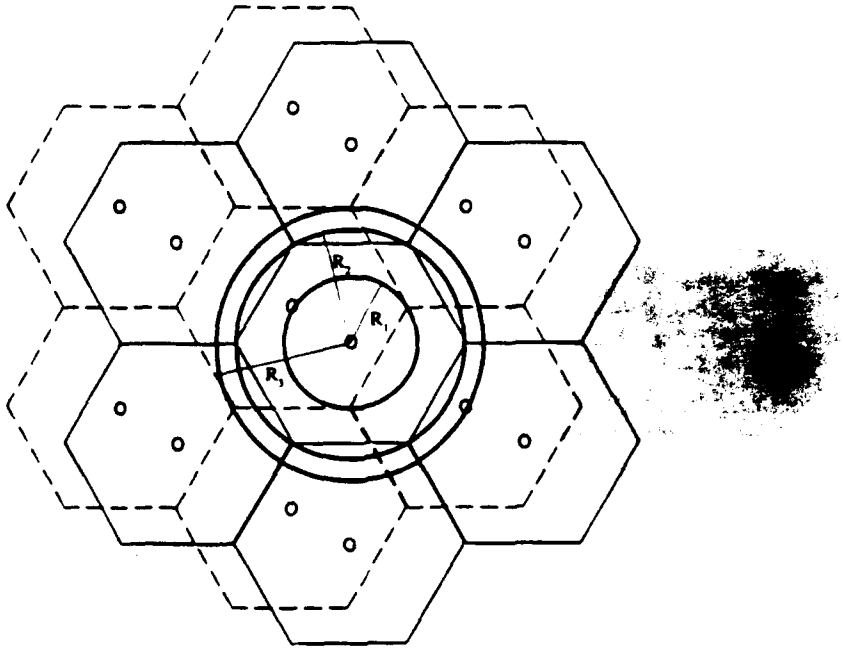


Fig. 1. A view of bulk Be metal along the $c$ direction. Nuclei are situated at the apices of the hexagons, as well as at their centers. Layers represented by dashes lie at $c/2$ on the $c$ axis (see table 1.)

tegrals [10]. Ab initio restricted closed-shell and restricted open-shell Hartree–Fock calculations, each corresponding to an average energy of configuration, were carried out on numerous low-lying states of each cluster. (The

**Table 1**
Be clusters by coordination cylinder and hcp layer

| Cylinder height ($z$-coordinate) | $R_0$ | $R_1$ | $R_2 = a$ | $R_3$ |
|---|---|---|---|---|
| $+\infty c/2$ | | | | |
| ⋮ | | | | |
| $3c/2$ | 0 | 3 | 3 | 6 |
| $c$ | 1 1 | 1 1 | 7 7 | 7 7 |
| $c/2$ | 0 0 0 | 3 3 3 | 3 3 3 | 6 6 6 |
| 0 | 1 1 1 1 | 1 1 1 1 | 7 7 7 7 | 7 7 7 7 |
| $-c/2$ | 0 0 0 | 3 3 3 | 3 3 3 | 6 6 6 |
| $-c$ | 1 1 | 1 1 | 7 7 | 7 7 |
| $-3c/2$ | 0 | 3 | 3 | 6 |
| ⋮ | | | | |
| $-\infty c/2$ | | | | |
| No. atoms | 1 1 3 3 | 1 7 9 15 | 7 13 27 31 | 7 19 33 45 |

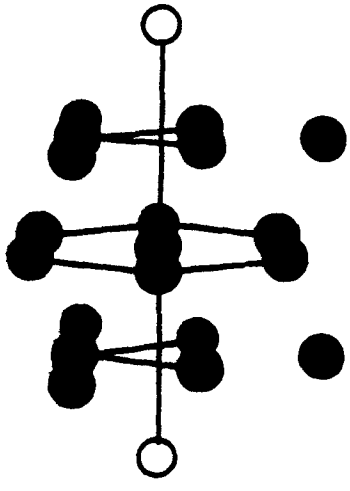

Fig. 2. $Be_{19}X_2$, X = Cs, H.

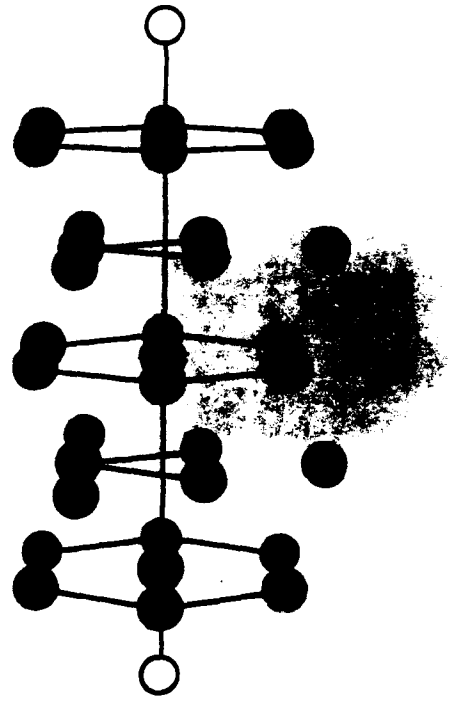

Fig. 3. $Be_{33}X_2$, X = Cs, H.

average energy of configuration is defined as the weighted mean of the energies of all the multiplets for the configuration.) The largest clusters required about one hour of Cray X-MP time for each geometric orientation. The following basis sets of contracted Gaussian-type functions were used for beryllium, cesium and hydrogen, respectively: (3s2p)/[2s1p] [11], (5s5p)/[3s2p] [12], and (4s1p)/[2s1p] [13]. Ab initio effective potentials (EP) [14] were used to represent the 1s core electrons on Be [11] and the 1s–4s, 2p–4p, and 3d–4d core electrons in Cs [12]. In the case of Cs, relativistic effects were incorporated into the EP [14]. Binding energies calculated relative to the completely dissociated clusters are given in table 2. (Valence SCF energies for atomic Be, $Be^+$, Cs, $Cs^+$, H and $H^-$ are −0.95083, −0.65457, −19.84225, −19.72876, −0.49928 and −0.44815 hartrees, respectively, for the basis sets used in this study.) The total adsorption energies given in table 2 for the cesiated and hydrogenated clusters were calculated relative to the SCF energies of the naked clusters plus that of two adsorbate atoms.

Theoretical work functions are given in table 3. The first values in each row were calculated as the difference between the total valence SCF energy of a neutral cluster and that of the ion generated by removing one electron from

Table 2
Restricted Hartree–Fock energies of states of $Be_m$ and $Be_mX_2$ clusters

| Cluster | Occupied MO's [a] | | | | | | Cluster BE (kcal/mol) | Total adsorption energy (kcal/mol·atom) |
|---|---|---|---|---|---|---|---|---|
| | $a_1'$ | $a_2'$ | $a_2''$ | $e'$ | $e''$ | $a_1''$ | | |
| $Be_{19}$ [b,c] | 4 | 1 | 3 | 4 | 2 | 0 | 325.25 | |
| $[Be_{19}]^+$ | 4 | **0** | 3 | 4 | 2 | 0 | 294.70 | |
| $Be_{19}Cs_2$ | 6 | 1 | 5 | 5 | 3 | 0 | 402.99 | 38.87 |
| $[Be_{19}Cs_2]^+$ | 6 | **1** | 5 | 5 | 3 | 0 | 405.37 | |
| $Be_{19}H_2$ [b,d] | 4 | 1 | 3 | 4 | 2 | 1 | 393.76 | 34.25 |
| $[Be_{19}H_2]^+$ | 4 | 1 | 3 | 4 | 2 | **0** | 579.66 | |
| $Be_{33}$ | 6 | 1 | 5 | 6 | 4 | 1 | 724.94 | |
| $[Be_{33}]^+$ | 6 | 1 | 6 | **6** | 4 | 1 | 815.76 | |
| $Be_{33}Cs_2$ [b,e] | 8 | 1 | 7 | 7 | 6 | 1 | 768.46 | 21.76 |
| $[Be_{33}Cs_2]^+$ | 8 | 1 | 7 | 7 | **6** | 1 | 779.74 | |
| $Be_{33}H_2$ [b,f] | 7 | 1 | 5 | 6 | 4 | 1 | 727.32 | 1.19 |
| $[Be_{33}H_2]^+$ [b] | 7 | 1 | 5 | **6** | 4 | 1 | 818.70 | |
| $Be_{45}$ [b,g] | 8 | 2 | 7 | 8 | 6 | 2 | 1078.74 | |
| $[Be_{45}]^+$ | 8 | 2 | 7 | 7 | 6 | 2 | 1196.77 | |
| $Be_{45}H_2$ [b,h] | 8 | 2 | 7 | 8 | 6 | 2 | 1115.07 | 18.16 |
| $[Be_{45}H_2]^+$ | 8 | 2 | 7 | **8** | 6 | 2 | 1228.41 | |

[a] Entries correspond to total number of occupied MO's of each entry. Bold numbers denotes orbital from which the electron was removed.
[b] State corresponds to the weighted average of configuration.
[c] Open-shell state: $(a_2')^1(a_2'')^1$.
[d] Open-shell state: $(a_2')^1(a_1'')^1$.
[e] Open-shell state: $(e'')^2$.
[f] Open-shell state:( $(a_1')^1(a_2'')^1$.
[g] Open-shell state: $(a_2')^1(e')^1$.
[h] Open-shell state: $(a_2')^1(e')^3$.

the highest occupied orbital of that cluster. The values immediately following are due to Koopmans' theorem and correspond to the negative of the energy of the molecular orbital (MO) from which the electron was ionized. Experimental values obtained as discussed below are also shown.

Atomic net electron charge values are given in tables 4–6, as calculated using a Mulliken population analysis [15]. Values of $R$ appearing in these tables correspond to optimum atom-to-surface distances. These distances were calculated from the minimum of a curve fit to SCF energies for three or more distances.

### 2.2. *Experimental procedure*

Experimental measurements were performed in an ultrahigh vacuum system with a base pressure of $5 \times 10^{-11}$ Torr. Pressures were monitored with a nude ionization gauge whose controller allowed calibration for $H_2$. The general

Table 3
Work functions of $Be_m$ and $B_mX_2$ clusters

| Cluster | $\phi$ (eV) [a] |
|---|---|
| $Be_{19}$ | 5.35, 5.04 |
| $Be_{19}Cs_2$ | 3.41, 2.99 |
| $Be_{19}H_2$ | 4.30, 3.96 |
| $Be_{33}$ | 4.41, 4.11 |
| $Be_{33}Cs_2$ | 2.92, 2.60 |
| $Be_{33}H_2$ | 4.37, 4.09 |
| $Be_{45}$ | 3.16, 2.94 |
| $Be_{45}H_2$ | 3.40, 3.15 |
| Be (expt) | 3.92 |
| BeCs (expt) [b] | 1.6 |
| BeH (expt) | 3.92 |
| $\Delta\phi[Be_{19}-Be_{19}Cs_2]$ [c] | 1.94, 2.05 |
| $\Delta\phi[Be_{19}-Be_{19}H_2]$ [c] | 1.05, 1.08 |
| $\Delta\phi[Be_{33}-Be_{33}Cs_2]$ [c] | 1.49, 1.51 |
| $\Delta\phi[Be_{33}-Be_{33}H_2]$ [c] | 0.05, 0.01 |
| $\Delta\phi[Be_{45}-B_{45}H_2]$ [d] | −0.24, −0.21 |
| $\Delta\phi[Be-BeCs]_{expt}$ [c] | 2.3 |
| $\Delta\phi[Be-BeH]_{expt}$ | 0 |

[a] Where two values appear, these are Koopmans' theorem and $\Delta E_{SCF}$ values, respectively.
[b] At optimum Cs coverage.
[c] Values correspond to a work function lowering.
[d] Values correspond to a work function increase.

experimental apparatus was described previously [3,16]. The sample was mounted on a carousel that allowed rotation to either a retarding field electron diode station [17,18], where work function shifts were measured, or to a cylindrical mirror analyzer station having a center-mounted electron gun with which Auger electron spectroscopy (AES) measurements were made. A sputter ion gun was co-focused onto the sample with the AES system and was used to sputter clean the surface.

AES showed that no O or C contaminants were present after sputter cleaning. The only contaminants present were Ar (< 1.1%) and N (< 2.4%), and these were due to the sputter cleaning. After cleaning, AES and work function shifts indicated the Be surface to be free of contaminants for a period in excess of one hour.

The experimental procedure was as follows. The sample was first sputter cleaned. $H_2$ could be introduced into the system at any time before, during or after sputter cleaning. Cs was deposited onto the surface from a low-energy Cs (5 eV) source [3] before or after sputter cleaning at a separate deposition station adjacent to the work function station. The Auger signal was generally monitored during cleaning. After cleaning, the Auger signal either continued to be monitored or the sample was rotated from its position facing the

AES/sputter cleaning station to a new position facing the work function diode, thus allowing the work function shift to be monitored. The repositioning was accomplished in approximately twenty seconds.

## 3. Results and discussion

Total adsorption energies for the cesiated and the hydrogenated [illegible] appear in table 2. As was previously mentioned, the energies were [illegible] relative to the total SCF energies of the naked clusters plus that of [illegible] adsorbate atoms in their ground states. These energies are 38.9, 21.8, 3[illegible] and 18.2 kcal/mol · atom for $Be_{19}Cs_2$, $Be_{33}Cs_2$, $Be_{19}H_2$, $Be_{33}H_2$ and $Be_{45}H_2$ respectively. For $Be_{19}Cs_2$ dissociation to $Be_{19}^- + Cs^+ + Cs$ requires 58.9 kcal/mol · atom. Dissociation of $Be_{19}H_2$ to yield $Be_{19}^+ + H + H^-$ and $Be_{19}^- + H + H^+$ requires 108.6 and 175.3 kcal/mol · atom, respectively. Dissociation of $Be_{33}Cs_2$ to $Be_{33}^- + Cs + Cs^+$ needs 49.4 kcal/mol · atom. Energies of 149.8, and 64.6 kcal/mol · atom are needed to dissociate $Be_{33}H_2$ to $Be_{33}^- + H + H^+$ and $Be_{33}^+ + H + H^-$, respectively. Finally, the dissociation of $Be_{45}H_2$ to yield $Be_{45}^+ + H + H^-$ and $Be_{45}^- + H + H^+$ requires 68.1 and 150.12 kcal/mol · atom, respectively. Therefore, the lowest-energy dissociation limit is of the form $Be_n + 2X$, where X is an adatom in the ground state. This procedure will be named method 1. There are two alternative ways of calculating the adsorption energy, methods 2 and 3. Method 2 involves calculation of the adsorption energy relative to the total energy of the lowest electronic state and MO configuration for the equilibrium geometry of the cluster–adsorbate system and the *same* electronic state for a cluster–adsorbate separation of approximately 10 Å, which is taken as infinite separation. This method assumes no crossings among electronic states.

[illegible] $Be_{19}Cs_2$, $Be_{33}Cs_2$, $Be_{19}H_2$ and $Be_{45}H_2$, this assumption leads to [illegible] errors. In these cases, the lowest energy electronic state corresponding to the calculated equilibrium geometry is not the lowest energy state calculated at infinite cluster–adsorbate separation. This method yields adsorption energies of 53.7, 56.3, 136.4 and 177.0 kcal/mol · atom for $Be_{19}Cs_2$, $Be_{33}Cs_2$, $Be_{19}H_2$ and $Be_{45}H_2$, respectively. Clearly, method 2 overestimates the adsorption energies of $Be_{19}Cs_2$, $Be_{33}Cs_2$, $Be_{19}H_2$ and $Be_{45}H_2$ (by 14.8, 23.8, 102.1 and 158.8 kcal/mol · atom, respectively, relative to method 1). No electronic state crossings were found for $Be_{33}H_2$. However, the ground state of $Be_{33}H_2$ is open-shell and nearly degenerate (0.01 eV lower in energy) with a closed-shell state that is 3.65 eV higher in energy at dissociation than the ground state.

Method 3, the second alternative method for calculation of the adsorption energy, involves taking the energy difference between the lowest electronic state of the cluster–adsorbate system at equilibrium and the lowest electronic

state of the same system at a cluster–adsorbate separation of approximately 10 Å. This method yielded adsorption energies of 43.8, 36.8, 99.0, 47.1 and 64.2 kcal/mol · atom for $Be_{19}Cs_2$, $Be_{33}Cs_2$, $Be_{19}H_2$, $Be_{33}H_2$ and $Be_{45}H_2$, respectively. Relative to method 1, this method overestimates the adsorption energy of $Be_{19}Cs_2$, $Be_{33}Cs_2$, $Be_{19}H_2$, $Be_{33}H_2$ and $Be_{45}H_2$ by 4.9, 15.0, 64.7, 45.9 and 46.0 kcal/mol · atom, respectively. No electronic state crossings were found for $Be_{33}H_2$. Consequently, methods 2 and 3 yield the same value of the adsorption energy for this cluster. Ideally, methods 1 and 3 should agree, provided that the lowest energy electronic state at both the equilibrium geometry and at infinite cluster–adsorbate separation has been found.

There are several problems inherent in using method 3. First of all, the calculations presented here all involve restricted Hartree–Fock theory, which is not generally accurate for the description of systems having geometries far from equilibrium. As was previously stated, method 3 requires calculation of the total energy for the system at a cluster–adsorbate separation of approximately 10 Å. Inspection of the gross atomic populations (GAP) for $Be_{19}Cs_2$ at this distance reveals improper dissociation to neutral atoms. The GAP of cesium for this system should be 18.9 electrons per Cs atom. In this case, the GAP is 17, with approximately 1/2 electron from each cesium 6s orbital being donated to the cluster. There should be no such ionization at this cluster–adsorbate separation, unless an electron is transferred from Cs to Be upon dissociation, yielding $Be_{19}^-$ and $Cs + Cs^+$. However, dissociation to these species requires 40.1 kcal/mole more energy than dissociation to $Be_{19} + 2\ Cs$.

RHF calculations predict a net energy gain of 18.2 and 1.2 kcal/mol upon hydrogen approach to the $Be_{45}$ and $Be_{33}$ surfaces, respectively. The approach of hydrogen on the $Be_{19}$ surface, on the other hand, results in an energy gain of 34.3 kcal/mol. Cesium adsorption on both the $Be_{19}$ and $Be_{33}$ surfaces yields energy gains of 38.9 kcal/mol · atom and 21.8 kcal/mol · atom, respectively. Therefore, while cesium is predicted to adsorb on both $Be_{19}$ and $Be_{33}$ (i.e. at a hole and at a head-on site) at the SCF level of theory, hydrogen adsorbs strongly on $Be_{19}$ and appears to adsorb moderately on $Be_{45}$ (i.e., at a hole site) but only negligibly on $Be_{33}$ (i.e., at a head-on site).

Table 3 contains calculated values for the ionization potentials of all the clusters studied, as well as values for the shift in ionization potential ($\Delta\phi$) resulting from Cs or H adsorption. Experimentally determined values of the work functions due to Cs or $H_2$ adsorption on Be metal are also included. Results for the $Be_{45}$ system indicate a slight rise by 0.2 eV in the ionization potential of the cluster due to H adsorption, while results for the $Be_{33}$ system indicate a lowering by 1.5 eV in the ionization potential of the cluster due to Cs adsorption, and no lowering due to H adsorption. The experimental findings are 2.3 and 0.0 eV lowering in the work function of Be metal due to adsorption of Cs and of $H_2$, respectively. Adsorption of Cs and of H on $Be_{19}$, however, results in ionization potential lowerings of approximately 2.0 and 1.0

Table 4
Electron populations of $Be_{19}$, $Be_{19}Cs_2$ and $Be_{19}H_2$

| Cluster | z-coordinate [a] | Atom label | No. atoms [b] | Net charge per atom | | Total net charge difference ([Cluster]$^+$ − Cluster) |
|---|---|---|---|---|---|---|
| | | | | Cluster | [Cluster]$^+$ | |
| $Be_{19}$ | 0 | BeO | 1 | 1.43 | 1.41 | −0.02 |
| | c/2 | BeA | 6 | −0.08 | −0.07 | 0.06 |
| | c/2 | BeC | 6 | −0.09 | 0.00 | 0.54 |
| | 0 | BeB | 6 | −0.07 | 0.00 | 0.42 |
| $Be_{19}Cs_2$ | 0 | BeO | 1 | 1.36 | 1.35 | −0.01 |
| | c/2 | BeA | 6 | −0.05 | −0.07 | −0.12 |
| | c/2 | BeC | 6 | −0.17 | −0.11 | 0.37 |
| | 0 | BeB | 6 | −0.14 | −0.07 | 0.43 |
| | R [c] | Cs | 2 | 0.39 | 0.55 | 0.33 |
| $Be_{19}H_2$ | 0 | BeO | 1 | 1.38 | 1.33 | −0.05 |
| | c/2 | BeA | 6 | −0.16 | −0.15 | 0.06 |
| | c/2 | BeC | 6 | −0.06 | 0.07 | 0.78 |
| | 0 | BeB | 6 | −0.02 | 0.01 | 0.18 |
| | R [d] | H | 2 | 0.04 | 0.05 | 0.02 |

[a] c = 3.58 Å.
[b] Number of symmetry equivalent atoms.
[c] R = 3.70 Å for Be plane to Cs distance. (Be to Cs distance is 3.93 Å.)
[d] R = 0.85 Å for Be plane to H distance. (Be to H distance is 1.57 Å.)

eV, respectively. Although the first value is in close agreement with experiment, the second is not.

These discrepancies are explained using the electron populations listed in tables 4 and 5. In the case of $Be_{19}$, total net charge differences indicate participation in charge redistribution by both the surface (BeC, z-coordinate = c/2) and middle (BeB, z-coordinate = 0) layers upon ionization of the cluster. In $Be_{19}$, ionization of the cluster results in a contribution of 0.4 electron from Be atoms (BeB) in the middle layer compared to 0.5 electron for Be atoms on the surface. Thus, the middle and surface layers of the cluster are involved almost equally in the electron ionization process. For $Be_{19}Cs_2$, both the surface (BeC) and middle (BeB) layers contribute 0.4 electron, while Cs donates 0.3 electron. Since electron emission is from the surface of the bulk metal, it is concluded that $Be_{19}$ is too small a cluster to model the Be metal surface involved in Cs adsorption.

On the other hand, the middle layer of $Be_{19}H_2$ contributes 0.2 electron, with the surface layers (BeC) being predominantly involved in ionization. H donates only a minimal amount (0.02) of charge. Part of the charge contributed by the middle (BeB) layer is shifted toward the BeC group of atoms in $Be_{19}H_2$. Since the greatest charge perturbation occurs on the surface, this

Table 5
Electron populations of $Be_{33}$, $Be_{33}Cs_2$ and $Be_{33}H_2$

| Cluster | z-coordinate [a] | Atom label | No. atoms [b] | Net charge per atom | | Total net charge difference ([Cluster]$^-$ − Cluster) |
|---|---|---|---|---|---|---|
| | | | | Cluster | [Cluster]$^-$ | |
| $Be_{33}$ | 0 | BeO | 1 | 0.96 | 0.97 | 0.01 |
| | $c/2$ | BeA | 6 | 0.55 | 0.53 | −0.14 |
| | $c/2$ | BeC | 6 | −0.10 | −0.07 | 0.14 |
| | 0 | BeB | 6 | −0.32 | −0.29 | 0.21 |
| | $c$ | BeH | 12 | −0.18 | −0.10 | 0.89 |
| | $c$ | BeD | 2 | 0.20 | 0.14 | −0.11 |
| $Be_{33}Cs_2$ | 0 | BeO | 1 | 0.94 | 0.93 | −0.01 |
| | $c/2$ | BeA | 6 | 0.57 | 0.52 | −0.25 |
| | $c/2$ | BeC | 6 | −0.12 | −0.07 | 0.27 |
| | 0 | BeB | 6 | −0.34 | −0.33 | 0.09 |
| | $c$ | BeH | 12 | −0.28 | −0.22 | 0.67 |
| | $c$ | BeD | 2 | 0.44 | 0.40 | −0.08 |
| | $R$ [c] | Cs | 2 | 0.46 | 0.60 | 0.29 |
| $Be_{33}H_2$ | 0 | BeO | 1 | 1.00 | 1.00 | 0.00 |
| | $c/2$ | BeA | 6 | 0.45 | 0.44 | −0.12 |
| | $c/2$ | BeC | 6 | −0.06 | −0.04 | 0.12 |
| | 0 | BeB | 6 | −0.30 | −0.26 | 0.24 |
| | $c$ | BeH | 12 | −0.23 | −0.16 | 0.84 |
| | $c$ | BeD | 2 | 0.87 | 0.82 | −0.10 |
| | $R$ [d] | H | 2 | −0.24 | −0.23 | −0.02 |

[a] $c = 3.58$ Å.
[b] Number of symmetry equivalent atoms.
[c] $R = 3.77$ Å for Be to Cs distance.
[d] $R = 1.58$ Å for Be to H distance at local minimum (see text).

model appears to be adequate for the description of H adsorption. However, further analysis reveals that this is not the case. As was stated previously, the middle layer (BeB) of $Be_{19}$ participates appreciably (donating 0.4 electron) in the ionization process, indicating that this cluster does not reasonably model the bulk surface. Adsorption of Cs or H onto this surface, therefore, yields information about the interaction of these two species with a Be cluster, but this information cannot be interpreted as also applying to the process whereby a Cs or H atom adsorbs onto the bulk surface. Such an extension may be made only in cases where the bare cluster is a good model of the bulk metal.

$Be_{71}$, a five-layer cluster, and $Be_{45}$, a seven-layer cluster, appear to model the Be metal surface more appropriately. Ionization of these clusters indicates that the surface layers (BeH for $Be_{33}$ and BeG for $Be_{45}$) donate most of the emitted electron. Although the middle layers also contribute charge, the involvement of the surface layers is three to four times as great. The adsorp-

Table 6
Electron populations of $Be_{45}$ and $Be_{45}H_2$

| Cluster | z-coordinate [a] | Atom label | No. atoms [b] | Net charge per atom | | Total net charge difference ([Cluster]$^-$ − Cluster) |
|---|---|---|---|---|---|---|
| | | | | Cluster | [Cluster]$^-$ | |
| $Be_{45}$ | 0 | BeO | 1 | 1.00 | 1.00 | 0.00 |
| | c/2 | BeA | 6 | 0.42 | 0.41 | −0.06 |
| | c/2 | BeC | 6 | −0.18 | −0.16 | 0.12 |
| | 0 | BeB | 6 | −0.34 | −0.30 | 0.24 |
| | c | BeH | 12 | −0.18 | −0.17 | 0.12 |
| | c | BeD | 2 | 1.36 | 1.34 | −0.04 |
| | 3c/2 | BeF | 6 | −0.14 | −0.14 | 0.00 |
| | 3c/2 | BeG | 6 | −0.02 | 0.08 | 0.60 |
| $Be_{45}H_2$ | 0 | BeO | 1 | 0.99 | 0.98 | −0.01 |
| | c/2 | BeA | 6 | 0.43 | 0.41 | −0.12 |
| | c/2 | BeC | 6 | −0.14 | −0.12 | 0.12 |
| | 0 | BeB | 6 | −0.36 | −0.32 | 0.24 |
| | c | BeH | 12 | −0.14 | −0.13 | 0.12 |
| | c | BeD | 2 | 1.32 | 1.30 | −0.04 |
| | 3c/2 | BeF | 6 | −0.18 | −0.18 | 0.00 |
| | 3c/2 | BeG | 6 | −0.06 | 0.04 | 0.60 |
| | R [c] | H | 2 | 0.01 | 0.01 | 0.00 |

[a] $c = 3.58$ Å.
[b] Number of symmetry equivalent atoms.
[c] $R = 0.86$ Å for Be plane to H distance at local minimum (see text). Be to H distance is 1.58 Å.

tion process, then, is represented more reasonably by using $Be_{33}$ or $Be_{45}$ rather than $Be_{19}$ to model the metal surface.

Table 6 shows that the surface (BeG, z-coordinate = $3c/2$) layers of $Be_{45}$ and $Be_{45}H_2$ are most affected during the ionization process, although the other layers of $Be_{45}H_2$ are also involved in ionization, their contribution is minimal compared to the charge donated by the surface (BeG) layers (0.2 versus 0.6). As with the $Be_{19}$ systems, some of the contributed charge is shifted toward several groups of atoms in the $Be_{45}$ clusters, for example, BeA (z-coordinate = $c/2$). However, the largest percentage of the charge involved in ionization is donated by the BeG atoms in the surface layer. It is also interesting to note that the net charge differences for $Be_{45}H_2$ are nearly identical to those for $Be_{45}$, the only difference being 0.06 for the BeA layer. The approach of H on the $Be_{45}$ surface does not affect the ionization process. The same conclusion is reached from an analysis of the electron populations of $Be_{33}$ and $Be_{33}H_2$, which appear in table 5. The values of $\Delta\phi$ appearing in table 3 are another indication that H has no effect on the $Be_{33}$ and $Be_{45}$ surfaces. The greatest shift in ionization potential occurs for the latter surface and is 0.2. $\Delta\phi$ for $Be_{33}$ is practically 0. Therefore, H is not predicted to chemisorb on

the Be surface and, in fact, does not in the case of $Be_{33}$ (the adsorption energy is 1 kcal/mol · atom). The adsorption energy of H on $Be_{45}$, although greater (18 kcal/mol · atom), is attributed to a local minimum since both the population analysis and $\Delta\phi$ values indicate no effect on the $Be_{45}$ surface due to H adsorption.

H approaches the $Be_{33}$ surface directly above a Be atom (directly overhead site) in the present calculations. There are three other possible sites for adsorption. These are the Be–Be midpoint, eclipsed and open sites. The first has the adsorbate approaching the Be surface directly between [illegible] located on the surface. The second involves adsorption [illegible] triangle of Be atoms located on the surface, the center of which [illegible] above a Be atom situated in a layer next to the surface (which is the [illegible] for $Be_{99}$). The open site has the adsorbate approaching the Be surface directly above the center of a triangle of Be atoms located on the surface, directly below which there is no Be atom. According to a study by Bagus et al., the directly overhead site is the least stable for the adsorption of H onto a Be surface [19]. These adsorption energies were obtained in SCF calculations using clusters containing two to three layers. $Be_{33}$ is a five-layer cluster and thus should yield a reasonable value for the adsorption energy associated with the directly overhead approach of an atom to the surface, while adsorption on an eclipsed site is adequately modeled by the seven-layer $Be_{45}$ cylinder. Method 3 yields 47.1 kcal/mol · atom, while method 1 predicts only negligible adsorption for H on $Be_{33}$. For reasons already stated, method 1 is expected to be more accurate. Therefore, H is predicted to adsorb very weakly, if at all on $Be_{33}$. The lowest energy $Be_{33}$–H distance is 1.58 Å, which represents a local minimum since, as discussed above, H does not bind to $Be_{33}$. Bagus et al. reported an SCF adsorption energy of 32 kcal/mol for H on $Be_{36}$ (a three-layer cluster with 14 atoms on the top and bottom layers and 8 atoms in the middle) and a $Be_{36}$–H distance of 1.38 Å [19]. These values also correspond to adsorption on a directly overhead site.

Adsorption of H on $Be_{45}$ amounts to 18.2 kcal/mol · atom. The optimum H-to-Be-plane distance is 0.86 Å, which is also a local minimum since the electron populations of $Be_{45}$ and $Be_{45}H_2$ are nearly identical, indicating that H has no effect on – i.e., does not chemisorb to – the $Be_{45}$ surface. The corresponding values for adsorption onto a $Be_{36}$ cluster reported by Bagus et al. are 42.3 kcal/mol for the adsorption energy and 0.95 Å for the distance from H to the surface.

It is also the surface layers (BeH) of $Be_{33}Cs_2$ that are predominantly involved in electron removal. These layers contribute 0.7 electron, whereas the greatest charge contributed by the inner layers is 0.3. The total net charge differences of $Be_{33}Cs_2$ differ from those of $Be_{33}$, indicating that Cs, unlike H, is affecting electron removal. In fact, Cs donates 0.3 electron to this process. The effects of charge redistribution resulting from ionization are greater for

the inner layers (relative to the surface layers) of $Be_{33}Cs_2$ than for those of $Be_{33}H_2$. The BeC group of atoms contribute 0.3 electron, while the BeA atoms accept 0.3 electron in $Be_{33}Cs_2$. These amounts correspond to less than half of the charge contributed by the surface layers. In $Be_{33}H_2$, the greatest contribution by the inner layers is approximately one fourth of the charge contributed by the surface. The small but non-negligible involvement of the inner layers of $Be_{33}Cs_2$ in the ionization process indicates that the discrepancy between the calculated and measured work function lowering (table 3) may be improved by treating a cluster corresponding to a larger cylinder height: for example, [illegible] atom cylinder of table 1. Another possibility is the treatment of [illegible] having the same height as $Be_{33}$ or $Be_{45}$ but a greater radius (see table 1 and fig. 1). In addition to improvements in $\Delta\phi$, adsorption of Cs on an eclipsed site (for example, Be45) is predicted to be more stable. Unlike the head-on site, this position allows the Cs to interact more closely with the surface triangles of Be since there is no center atom present.

It is noted that the present study contains certain constraints and assumptions. First, no geometry relaxation was attempted for the Be clusters. Although the Be–adatom distances were optimized, the full $D_{3h}$ symmetry of the cluster was maintained, and the Be–Be distances were held fixed at the experimental lattice constants of Be metal. For clusters of this size, it is probable that the optimum geometry may not match precisely that of the bulk metal. Surface geometries do not generally match the corresponding bulk lattice constants. Most materials are known to experience some degree of reconstruction at the surface due to the bending of outward-directed (from the surface) unpaired orbitals. Second, adsorption of Cs and of H was modeled using only one atom above the top and bottom layers of the cluster. Since the shift in the work function of Be metal depends on the degree of surface coverage [3], the results may be altered by adsorption of more than one atom of Cs or H on each cluster.

Third, the calculations do not include electron correlation effects. As previously mentioned, all low-lying electronic states of each cluster were studied. Several of these states were nearly degenerate (within 0.1 eV), making a reordering of states possible upon inclusion of electron correlation. Such effects may be accounted for, at least in part, through the use of local-density-functional approaches. These methods replace the exchange terms in the Hartree–Fock equations by spherical potentials, otherwise known as muffin-tin potentials, through which some electron correlation corrections are introduced into the system. Metal surfaces such as that of tungsten have been studied using these approaches [20]. However, the results presented here are ab initio, unlike those obtained using density-functional theory. Furthermore, correlation energy cancellation is expected between the neutral and cationic cluster systems. Although this cancellation is not complete because the neutral system contains a greater number of electrons, the clusters treated here are large enough (e.g., $Be_{33}Cs_2$ contains 84 electrons) so as to minimize this error.

Fourth, the valence basis sets used in this study were not complete. Additional p-type functions, as well as d-type GTF's may alter the computed adsorption energies to some degree. Finally, no periodic boundary conditions were imposed on the clusters, making the results dependent on cluster size.

Despite these conditions, the work presented here provides useful information about the adsorption process, including a detailed analysis of the nature of the interactions at the surface, the latter of which cannot be obtained via experiment alone. All of the theoretical results are calculated using ab initio procedures; that is, no experimental parameters were used, [illegible] were approximated and all terms in the Hamiltonian were retained. [illegible] tic effects for cesium were incorporated into the calculations through [illegible] initio effective core potential. Despite the neglect of periodic boundary [illegible] tions, the clusters used to model the Be surface were large, containing three layers, five layers and seven layers in the case of $Be_{19}$, $Be_{33}$ and $Be_{45}$, respectively. Energies for numerous low-lying electronic states were studied.

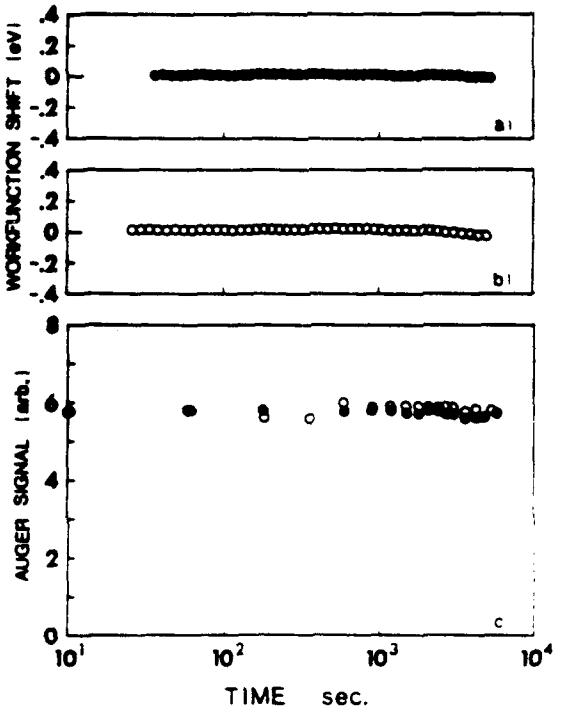


Fig. 4. (a) The work function shift of sputter cleaned Be in time exposed to the residual gas in the chamber ($7.6 \times 10^{-11}$ Torr). (b) The work function shift of sputter cleaned Be exposed to $H_2$ ($2.0 \times 10^{-8}$ Torr) at $t = 50$ s. (c) The change in sputter cleaned Be AES signal in time upon exposure to the residual gas ($7.6 \times 10^{-11}$ Torr) in the chamber (dark curve) and upon exposure to $H_2$ ($3.0 \times 10^{-8}$ Torr)

The states were chosen by analyzing the highest occupied and lowest unoccupied molecular orbitals. Finally, independent SCF calculations were used to determine the ionization potentials of the clusters in addition to the use of Koopmans' theorem.

The experimental findings of Cs adsorption on Be have been presented and discussed elsewhere [3]. Exposure of the surface to $H_2$ yielded no observable change. That is, the Be substrate Auger signal was not attenuated and there was no discernable work function shift. Typical results are shown in fig. 4. In curve a, the change in the work function with time is shown for sputter cleaned polycrystalline Be exposed to the residual gases in the chamber at $7.6 \times 10^{-11}$ Torr. Curve b corresponds to the same sample with the exception that at time $t = 50$ s, $H_2$ was let into the chamber at $2.0 \times 10^{-8}$ Torr. This corresponds to a flux of $3 \times 10^{13}$ molecules/cm$^2$ · s at room temperature. No change in the work function was seen for a period in excess of $10^3$ s, corresponding to a fluence greater than $3 \times 10^{16}$ molecules/cm$^2$. Curve c shows the Be (104 eV) Auger electron signal for a sample first sputter cleaned and exposed to the residual gases in the vacuum (solid symbol curve) and for the same sample sputter cleaned in and maintained in $H_2$ at $3 \times 10^{-8}$ Torr.

## 4. Conclusions

Analysis of the Mulliken populations for $Be_{19}$ indicates that this cluster is too small to model the bulk surface. However, the population analyses for $Be_{33}$ and $Be_{45}$ indicate that these clusters are adequate models of the Be metal surface. The adsorption energy of Cs on $Be_{33}$ is calculated as 21.8 kcal/mol · atom. The decrease in the ionization potential of $Be_{33}Cs_2$ relative to $Be_{33}$ is calculated to be 1.5 eV. The experimental work function lowering resulting from Cs adsorption is measured as 2.3 eV [3]. The adsorption energies of H on $Be_{33}$ and $Be_{45}$ are 1 and 18 kcal/mol · atom, respectively. The first value is negligible, while the latter is attributed to a local minimum since Mulliken population analysis and $\Delta\phi$ values for both $Be_{33}$ and $Be_{45}$ indicate no effect on these clusters due to H adsorption. Experiment reveals no adsorption of $H_2$ on Be metal, thus ruling out dissociative chemisorption.

## Acknowledgments

This research was supported in part by the National Science Foundation under grant No. CHE-8712315, which included supercomputer time at the Pittsburgh Supercomputing Center, and by the Air Force Office of Scientific Research. The Newark Remote Access Center and the New Jersey Commission on Science and Technology are acknowledged for providing computing

equipment and network access to Pittsburgh. We thank N.W. Winter and J.M. Powers for their assistance and advice regarding the construction of the figures.

## References

[1] L.W. Swanson and R.W. Strayer, J. Chem. Phys. 48 (1968) 2421.
[2] R.E. Weber and W.T. Peria, Surface Sci. 14 (1969) 13.
[3] G.S. Tompa, M. Seidl, W.C. Ermler and W.E. Carr, Surface Sci. 185 (1987) L453.
[4] J. Rubio, F. Illas and J.M. Ricart, J. Chem. Phys. 84 (1986) 3311.
[5] G. Pacchioni, W. Pewesdorf and J. Koutecky, Chem. Phys. 83 (1984) 201.
[6] C.W. Bauschlicher, D.H. Liskow, C.F. Bender and H.F. Schaefer III, J. Chem. Phys. (1975) 4815.
[7] C.W. Bauschlicher, Chem. Phys. Letters 117 (1985) 33.
[8] R.B. Ross, W.C. Ermler, C.W. Kern and R.M. Pitzer, Chem. Phys. Letters 134 (1987) 115; W.C. Ermler, R.B. Ross, C.W. Kern, R.M. Pitzer and N.W. Winter, J. Phys. Chem. 92 (1988) 3042.
[9] R.G. Wyckoff, *Crystal Structures*, 2nd ed. (Interscience, New York, 1974).
[10] R.M. Pitzer, J. Chem. Phys. 58 (1973) 3111; private communication.
[11] W.C. Ermler, C.W. Kern, R.M. Pitzer and N.W. Winter, J. Chem. Phys. 84 (1986) 3937.
[12] R.B. Ross, T. Atashroo, J.M. Powers, W.C. Ermler, L.A. LaJohn and P.A. Christiansen, to be published.
[13] T.H. Dunning, Jr., J. Chem. Phys. 53 (1970) 2823; 55 (1971) 3958.
[14] P.A. Christuansen, W.C. Ermler and K.S. Pitzer, Ann. Rev. Phys. Chem. 36 (1985) 407; W.C. Ermler, R.B. Ross and P.A. Christuansen, Advan. Quantum Chem. 19 (1988) 139
[15] R.S. Mulliken, J. Chem. Phys. 23 (1955) 1833.
[16] G.S. Tompa, W.E. Carr and M. Seidl, Surface Sci. 198 (1988) 431.
[17] A.G. Knapp, Surface Sci. 34 (1983) 289.
[18] F.H. Haaves, M.F. Hill, S.M.A. Lecchini and B.A. Pethica, J. Chem. Phys. 42 (1965) 2919.
[19] P.S. Bagus, H.F. Schaefer and C.W. Bauschlicher, J. Chem. Phys. 78 (1983) 1390.
[20] S. Ohnishi, A.J. Freeman and E. Wimmer, Phys. Rev. B 29 (1984) 5267.

# AB INITIO STUDY OF THE LAYERED SEMICONDUCTOR CLUSTER $Bi_6I_{18}$

M.M. MARINO [a], M. SAWAMURA [b], W.C. ERMLER [a] and C.J. SANDROFF [c]

[a] *Department of Chemistry and Chemical Engineering, Stevens Institute of Technology, Hoboken, NJ 07*

[b] *Department of Physics and Engineering Physics, Stevens Institute of Technology, Hoboken, NJ 07*

[c] *Bellcore, Red Bank, NJ 07701, USA*

Received 26 June 1989; in final form 11 August 1989

$Bi_6I_{18}$ is studied using ab initio Hartree–Fock calculations including relativistic effects. Electronic spectra, geometric parameters and net atomic charges are reported. Blue-shifts in the optical absorption spectra relative to bulk $BiI_3$ are observed. Increases in interlayer distances result in shortened Bi–Bi separations. Results are consistent with quantum size effects in small semiconductor clusters and with scanning tunneling microscope images.

The properties of clusters are attracting increased attention because they represent an intermediate physical regime where neither atomic nor solid-state descriptions are independently appropriate [1–3]. Although numerous experimental techniques to synthesize clusters both in gaseous and condensed phases are in use [4–9], there is no generally available experimental procedure to determine the structure and spectra of the clusters produced. Hence, theoretical insights into cluster structure as a function of cluster size takes on a major role.

The computational difficulty inherent in treating large systems comprised of heavy elements, however, has precluded rigorous ab initio studies on such clusters. Theoretical treatments on systems of this type have largely neglected relativistic effects, as well as certain exchange interactions among electrons. Consequently, the majority of ab initio work in semiconductor systems has been limited to small clusters of light elements such as silicon [10,11]. In such strongly covalent systems, it is found that small isolated clusters tend to reconstruct to form tightly bound symmetrical structures with a high degree of coordination. Moreover, the tendency to minimize the number of exposed dangling bonds means that the bulk silicon structure is recovered only for very large clusters.

The structure of the layered semiconductor investigated here exhibits a radically different dependence on cluster size than do those of isotropic silicon. Unlike clusters of Si, $Bi_6I_{18}$ essentially retains the structure of the bulk crystalline lattice in the lateral direction for the range of geometries studied. We find, however, that there can be significant electronic coupling between interlayer perturbations and intralayers lattice dimensions in this cluster. Indeed, for large increases in the Bi–I interlayer spacings, we see in-plane lattice constants decrease by as much as 10%. With these results, it might be possible to explain recent compelling scanning tunneling images of $BiI_3$ clusters [12].

The $Bi_6I_{18}$ cluster model studied is shown in fig. 1. It has the layer symmetry of the bulk crystal and is comprised of a plane of bismuth atoms, above and below which is situated a triangular layer of iodine atoms. This model was chosen based on experimental data on small clusters of the layered semiconductors $PbI_2$ and $BiI_3$ grown as colloidal suspensions. Clusters of the type $BiI_3$ were found to be comprised of two hexagonally closed-packed layers of iodines between which was sandwiched a layer of metal atoms in a honeycombed arrangement [8]. $Bi_6I_{18}$ has $D_{3d}$ point group symmetry (cubic close-packing) and represents a fragment of the bulk crystalline solid (one unit cell thick) having iodine layers slightly perturbed from the bulk arrangement to preserve the symmetry of the cluster. The coordination numbers for our cluster and for the bulk crys-



0 009-2614/89/$ 03.50 

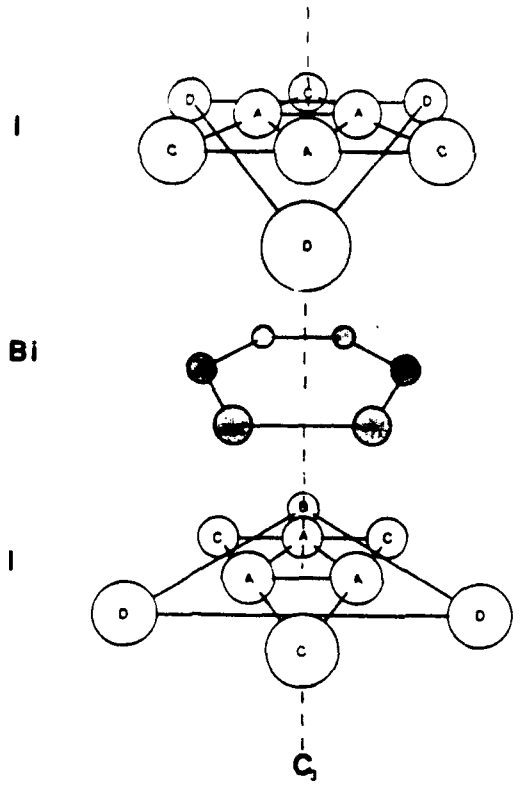


Fig. 1. $Bi_6I_{18}$ cluster having $D_{3d}$ point group symmetry. (The threefold rotation axis is indicated by $C_3$.) Three symmetry-distinct I atoms are indicated. All interatomic distances correspond to bulk lattice constants. The positions of the ID atoms, however, are rotated by 49.2° relative to the bulk.

Table 1
Coordination numbers

| | Atom | I | Bi | Total |
|---|---|---|---|---|
| bulk [a] | Bi | 6 | 0 | 6 |
| | I | 6 | 2 | 8 |
| cluster [b] | Bi | 6 | 0 | 6 |
| | IA | 5 | 2 | 7 |
| | IC | 2 | 2 | 4 |
| | ID | 3 | 2 | 5 |

[a] Ref. [13]. [b] See fig. [1].

tal are given in table 1. It is interesting to note that these values are equal for Bi. This results from the fact that our model cluster was constructed such that each bismuth lies at the center of a distorted octahedron. (Bi–ID distances are 38.5% longer than Bi–I distances in crystalline $BiI_3$.) This arrangement is similar to that of bulk $BiI_3$, where each bismuth lies at the center of a nearly perfect octahedron of iodines. Bi–Bi, I–I and Bi–I internuclear distances were initially determined from the lattice constants of crystalline $BiI_3$ [13]. However, the ID group of atoms (see fig. 1) were rotated by 49.2° counterclockwise with respect to the original bulk arrangement to obtain a cluster of $D_{3d}$ symmetry. This results in IC–ID separations which are 41.4% [illegible] than the corresponding bulk crystal values. [illegible] nuclear distances were then optimized in ab [illegible] Hartree–Fock calculations, consistent with the variation principle and preserving the cylindrical structure of the cluster. All initial and optimum nearest-neighbor interatomic distances in $Bi_6I_{18}$ are given in table 2. This table also contains the corresponding bulk crystal values, where applicable.

Ab initio effective core potentials which include relativistic effects [14] were used to represent the 1s–4s, 2p–4p and 3d–4d core electrons in I [15] and the 1s–5s, 2p–5p, 3d–5d and 4f core electrons in Bi [16]. Basis sets of contracted Gaussian-type functions were used to represent the valence orbitals of Bi and I [15,16]. Self-consistent field (SCF) energies for the lowest-lying molecular orbital electron configurations were calculated for each geometric orientation of the cluster. These ab initio restricted closed-shell and restricted open-shell Hartree–Fock linear combination of atomic orbital – molecular orbital (LCAO-MO) calculations were accomplished using programs based on the "equal contribution theorem" for two-electron symmetry orbital integrals [17]. The lowest unoccupied MOs (LUMOs) of all the electron configurations studied for neutral $Bi_6I_{18}$ were quite low-lying. For example, the six

Table 2
$Bi_6I_{18}$ nearest-neighbor interaction distances (Å)

| Atom pair | Bulk [a] | Initial | Optimum |
|---|---|---|---|
| Bi–IA | 3.09 | 3.09 | 3.20 |
| Bi–IC | 3.09 | 3.09 | 3.20 |
| Bi–ID | – | 4.20 | 4.28 |
| IA–IA | 4.37 | 4.37 | 4.35 |
| IA–IC | 4.37 | 4.37 | 4.35 |
| IA–ID | – | 4.37 | 4.35 |
| IC–ID | – | 6.18 | 6.15 |
| Bi–Bi | 4.37 | 4.37 | 4.35 |

[a] Ref. [13].

LUMOs for the lowest-energy electron configuration studied had energies below −2.75 eV, indicating that the neutral system is electron deficient.

This conclusion is supported by Koopmans' theorem [18]. If the cluster wavefunction $\Psi(2N)$, a $2N$-electron antisymmetrized product of MOs $\{\phi_m\}$, is stationary and $\phi_m$ is an eigenfunction of the Fock operator, then $\Psi(2N+1)$, where an electron is added to $\phi_m$, is also stationary with respect to any further variations in the orbitals to first order. This indicates that systems possessing very low-lying LUMOs are electron deficient, in that addition of one or more electrons to these orbitals will increase the overall stability.

To satisfy this electron deficiency, we studied a doubly charged anionic $Bi_6I_{18}$ cluster. We also believe that the anion is the most natural cluster to consider from the experimental point of view since clusters of this type are prepared in solution as colloidal particles in the presence of excess iodide ion [19]. The total energy of $Bi_6I_{18}^{2-}$ was found to be more than 10 eV lower than the corresponding neutral species. In this case, nearly all the LUMOs have energies greater than zero, indicating that the system's electrophilicity has been quenched. A geometry optimization of $Bi_6I_{18}^{2-}$ indicated that the equilibrium interlayer distances were expanded vertically by 9.5% relative to bulk $BiI_3$. This vertical expansion leads to a 3.6% increase in Bi–IA and Bi–IC distances and to a 1.9% increase in Bi–ID interatomic separations (table 2). Intralayer distances, however, were contracted by only 0.5% relative to those in the bulk. This system tends to contract laterally as the interlayer separations are increased. For example, expansion of the interlayer separation by 60% results in a 10% contraction in metal layer lateral dimensions.

A total of sixteen low-lying MO electron configurations of the cluster were studied at both the calculated equilibrium interatomic distances and at a geometry corresponding to a 60% expansion in the interlayer distance and a 10% contraction in lateral dimensions. These percentages were chosen from the results of a series of calculations at geometries ranging from 10% contraction to 60% expansion of the lattice constants in the vertical direction and 20% contraction to 10% expansion in the lateral direction. All of these configurations, with the exception of states 13, 15, 16, 17, 19 and 20, possessed two unpaired electrons and were treated as pure spin triplet states, i.e. the cluster wavefunctions are spin eigenfunctions having total spin quantum number $S=1$. States 13, 17 and 20 correspond to the same electron configuration comprised of four open-shell electrons coupled to form pure triplet states. The same applies to states 15, 16 and 19.

Since the heavy elements [redacted] involve appreciable relativistic effects [redacted] spin–orbit splitting, a precise definition of [redacted] metry for an MO configuration of a given [redacted] able 3) is somewhat ambiguous. The calculations reported here are based on $L$–$S$ atomic coupling in the context of averaged relativistic effective core potentials (REPs) [14]. More extensive calculations that make us of REP-based spin–orbit operators and explicit electron correlation are required to specify the electronic states more precisely [14]. However, the present calculations provide an accurate representation of cluster electronic states in terms of $L$–$S$ coupled separated atomic states. Note that for large clusters the dependence of electronic properties on specific total orbital and spin angular momentum coupling is reduced considerably due to the presence of bands of adjacent states [20].

Excitation energies are given in table 3. Each value is the difference between the total SCF energy of the ground state and that of an excited state. State 11 at 1.28 eV is the only closed-shell state lying within 4 eV of the ground state. Table 4 reports electron charge per atom values based on a Mulliken population analysis [21] for the lowest-lying state at each of the aforementioned geometries. The energy separations for equilibrium $Bi_6I_{18}^{2-}$ listed in table 3 are band-like. States 1 through 12 exhibit a nearly monotonic rise in energy and lie considerably below the experimental band gap of bulk crystalline $BiI_3$ at 2.1 eV [22]. States 13 through 20 are, however, considerably blue-shifted relative to this band gap. This may be attributed to quantum confinement effects, as suggested by recent $PbI_2$ cluster studies [8,23]. A total of 65 single electron transitions among 190 possible transitions among the low-lying triplet states were examined. Fig. 2 shows that these transitions peak at 0.3, 2.9 and 3.7 eV. The higher-lying peaks are blue-shifted by 0.8 and 1.6 eV with respect to the energy band gap of the bulk crystal. On the other hand, the

Table 3
Electronic states of $Bi_6I_{18}^{2-}$ (eV)

| State No. | Term symbol | MO configuration [a] | | | | | | | | ΔE (equil.) [b] |
|---|---|---|---|---|---|---|---|---|---|---|
| | | $10a_{1g}$ | $11a_{1g}$ | $10a_{2u}$ | $13e_g$ | $14e_g$ | $14e_u$ | $5a_{1u}$ | $4a_{2g}$ | |
| 1 | $^3E_u$ | 2 | 0 | 0 | 4 | 1 | 0 | 1 | 0 | 0.00 |
| 2 | $^3A_{2g}$ | 2 | 0 | 0 | 4 | 2 | 0 | 0 | 0 | 0.20 |
| 3 | $^3A_{1g}$, $^3A_{2g}$, $^3E_g$ [c] | 2 | 0 | 0 | 4 | 1 | 1 | 0 | 0 | 0.23 |
| 4 | $^3E_g$ | 2 | 1 | 0 | 4 | 1 | 0 | 0 | 0 | 0.50 |
| 5 | $^3A_{1g}$, $^3A_{2g}$, $^3E_g$ [c] | 2 | 0 | 0 | 4 | 0 | 2 | 0 | 0 | 0.64 |
| 6 | $^3E_g$ | 2 | 0 | 0 | 4 | 0 | 1 | 1 | 0 | 0.69 |
| 7 | $^3E_u$ | 2 | 0 | 1 | 4 | 1 | 0 | 0 | 0 | 0.83 |
| 8 | $^3A_{1g}$ | 2 | 1 | 0 | 4 | 0 | 0 | 1 | 0 | 0.89 |
| 9 | $^3E_g$ | 2 | 0 | 0 | 4 | 1 | 0 | 0 | 1 | 0.95 |
| 10 | $^3A_{2g}$ | 2 | 0 | 0 | 4 | 0 | 0 | 1 | 1 | 1.20 |
| 11 [d] | $^1A_{1g}$ | 2 | 0 | 0 | 4 | 0 | 0 | 2 | 0 | 1.28 |
| 12 | $^3A_{2g}$ | 2 | 0 | 1 | 4 | 0 | 0 | 1 | 0 | 1.35 |
| 13 | $^3E_u$ | 1 | 0 | 0 | 4 | 2 | 0 | 1 | 0 | 2.67 |
| 14 | $^3E_g$ | 1 | 0 | 0 | 4 | 3 | 0 | 0 | 0 | 2.87 |
| 15 | $^3E_u$ | 1 | 0 | 0 | 4 | 2 | 1 | 0 | 0 | 2.93 |
| 16 | $^3A_{2g}$ | 1 | 0 | 0 | 4 | 2 | 0 | 1 | 0 | 3.09 |
| 17 | $^3A_{2g}$ | 1 | 0 | 0 | 4 | 2 | 1 | 0 | 0 | 3.39 |
| 18 | $^3A_{1g}$, $^3A_{2g}$, $^3E_g$ [c] | 2 | 0 | 0 | 3 | 0 | 3 | 0 | 0 | 3.61 |
| 19 | $^3A_{1g}$ | 1 | 0 | 0 | 4 | 2 | 1 | 0 | 0 | 3.81 |
| 20 | $^3A_{1g}$ | 1 | 0 | 0 | 4 | 2 | 0 | 1 | 0 | 3.99 |

[a] Occupations of the outermost MOs are shown. [b] See text and table 2.
[c] Average of these triplet states. [d] Lowest-lying closed-shell singlet state found.

transitions due to two or more electron excitations peak at 2.[illegible] eV and at lower energies (approximately 0.3 and [illegible] eV).

Charge/atom values appearing in table 4 indicate that the predominant interlayer interactions occur between the atoms comprising the Bi hexagon and the largest I triangle (BiB and ID in fig. 1) for the lowest energy state of $Bi_6I_{18}^{2-}$ at both geometries treated. This was also observed for the other fifteen electron configurations of $Bi_6I_{18}^{2-}$ listed in table 3. No differences were seen between charge/atom val-

Table 4
Population analysis for the lowest energy states of $Bi_6I_{18}^{2-}$ [a]

| Atom [b] | Charge/atom [c] (equil.) | Charge/atom [c] (expanded Z) |
|---|---|---|
| Bi | 0.89 | 0.67 |
| IA | −0.26 | −0.18 |
| IC | −0.29 | −0.32 |
| ID | −0.67 | −0.51 |

[a] Ref. [21]. [b] See fig. 1. [c] Electron units.

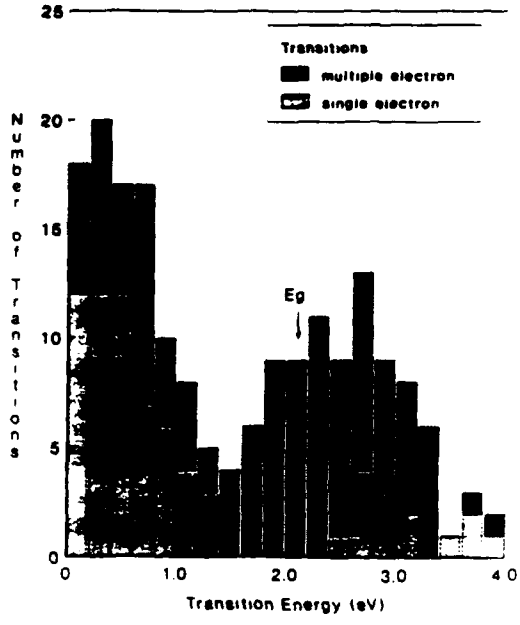


Fig. 2. Distribution of transition energies of $Bi_6I_{18}^{2-}$. The arrow marks the position of the bulk band gap.

ues for the ground state and the corresponding values for states 2 through 12 at the equilibrium geometry, indicating that the electronic transitions are predominantly intralayer in nature and occur among symmetry related atoms. A more detailed analysis of the Mulliken populations revealed that these electron excitations correspond to metal–metal transitions. Differences in charge/atom values between states 13 through 20 of $Bi_6I_{18}^{2-}$ shown in table 3 (also relative to the equilibrium geometry) and those of the ground state are as large as 0.07, which compares to 0.02 for states 2–12. In these cases, the transitions involve both Bi and I atoms.

We expect that a less restricted geometry optimization, i.e. one where the Bi and I layers are optimized independently, will lead to a cluster having even shorter metal–metal separations. Such was the case for $Pb_7I_{14}^{2-}$, a layered semiconductor very similar to $BiI_3$. Calculations on this representative fragment of the bulk $PbI_2$ crystal indicate a 10% reduction in metal–metal separations relative to crystalline $PbI_2$, while I–I distances essentially remained at the bulk lattice constants [23].

Our findings regarding the reduction of in-plane lattice constants when interlayer distances are expanded from their equilibrium values aid the understanding of recent scanning tunneling microscope (STM) images of layered $BiI_3$ clusters [12]. In that study, atomically resolved images showed structures having honeycombed symmetry after colloidal suspensions of $BiI_3$ were evaporated onto graphite surfaces. Since the central bismuth plane in $BiI_3$ has honeycombed symmetry (in contrast to the hexagonal symmetry of the iodine planes), the STM images are most likely individual bismuth atoms. Interestingly, the lattice constant of these putative $Bi_{10}I_{30}$ clusters was measured to be 0.65 nm, roughly 20% smaller than the bulk in-plane lattice constant, which is consistent with the present calculations. Hence, these STM images could be revealing clusters whose topmost layer of iodine has been removed or displaced from its underlying bismuth plane. Chemical oxidation or cluster–tip interactions could be among the phenomena responsible for these large perturbations.

The research at Stevens was supported in part by Bellcore, the National Science Foundation under Grant No. CHE-8712315, which included an allocation of supercomputer time at the Pittsburgh Supercomputing Center, and the Air Force Office of Scientific Research. We are grateful to the referee for helpful comments and suggestions.

## References

[1] J. Stapelfeldt, J. Woerner and T. Moeller, Phys. Rev. Letters 62 (1989) 98.
[2] C. Hayashi, Phys. Today 40 (1987) 44.
[3] T. Inoshita, S. Ohnishi and A. Oshiyama, Phys. Rev. Letters 57 (1986) 2560.
[4] J.R. Heath, S.C. O'Brian, Q.-L. Zhang, R.F. Curl, F.K. Tittle and R.E. Smalley, J. Chem. Phys. 83 (1985) 5520.
[5] A. Fojtik, H. Weller, U. Koch and A. Henglein, Ber. Bunsenges. Physik. Chem. 88 (1984) 969.
[6] R.L. Whetten, D.M. Cox, D.J. Trevor and A. Kaldor, J. Phys. Chem. 89 (1985) 566.
[7] R. Rossetti, R. Hull, J.M. Gibson and L.E. Brus, J. Chem. Phys. 82 (1985) 552.
[8] C.J. Sandroff, S.P. Kelty and D.M. Hwang, J. Chem. Phys. 85 (1986) 5337.
[9] O.I. Micic, M.T. Nenadovic, M.T. Peterson and A.J. Nozik, J. Phys. Chem. 91 (1987) 1295.
[10] K. Ragavachari, J. Chem. Phys. 84 (1986) 5672.
[11] J.R. Chelikowsky, J.C. Philips, M. Kamal and M. Strauss, Phys.Rev. Letters 62 (1989) 292.
[12] D. Sarid, T. Hensen, L.S. Bell and C.J. Sandroff, J. Vacuum Sci. Technol. A 6 (1988) 424.
[13] R.G. Wyckoff, Crystal structures, 2nd Ed. (Interscience, New York, 1960).
[14] W.C. Ermler, R.B. Ross and P.A. Christiansen, Advan. Quantum Chem. 19 (1989) 139.
[15] L.A. LaJohn, P.A. Christiansen, T. Atashroo and W.C. Ermler, J. Chem. Phys. 87 (1987) 2812.
[16] R.B. Ross, J.M. Powers, T. Atashroo, W.C. Ermler, L.A. LaJohn and P.A. Christiansen, to be published.
[17] R.M. Pitzer, J. Chem. Phys. 58 (1973) 3111.
[18] T. Koopmans, Physica 1 (1933) 104.
[19] C.J. Sandroff, D.M. Hwang and W.M. Chung, Phys. Rev. B. 33 (1986) 5953.
[20] R.B. Ross, W.R. Ermler, C.W. Kern and R.M. Pitzer, Chem. Phys. Letters 134 (1987) 115.
[21] R.S. Mulliken, J. Chem. Phys. 23 (1955) 1833.
[22] G. Harbeke and E. Tosatti, RCA Rev. 36 (1975) 40.
[23] M.M. Marino, M. Sawamura, W.C. Ermler and C.J. Sandroff, to be published.

# Structure and Properties of Cesium-Coated Surfaces and the Effects of Hydrogen and Oxygen Implantation*

Walter C. Ermler and Maria M. Marino

Stevens Institute of Technology, Department of Chemistry and Chemical Engineering, Hoboken, New Jersey 07030

## ABSTRACT

Cesium, hydrogen and oxygen adsorption on beryllium clusters are studied using restricted Hartree-Fock (RHF) calculations and ab initio relativistic effective core potentials. The clusters are taken as cylindrical plugs from Be wafers. Cs-, H- and O-to-substrate internuclear distances are optimized. For each system numerous low-lying electronic states are investigated, and the Mulliken electron populations are analyzed. The calculations are carried out in the context of an experimental study to determine the effects of various adsorbates on the work function of the substrate. Auger electron spectroscopy and experimental work function measurements indicate that $H_2$ does not adsorb on polycrystalline Be, while photoemission and thick Cs overlayer measurements show a 2.3 eV lowering in the work function of Be metal upon Cs adsorption. The continuous oxidation of Cs has been studied using ultraviolet photoelectron spectroscopy and electron spectroscopy by deexcitation of metastable noble gas atoms. Results indicate that the work function of Cs is lowered upon exposure of the surface to small doses of oxygen. RHF calculations show that a 19 atom Be cluster, with three layers of atoms, is too small to adequately model the Be surface, while the 33 atom cluster, a five-layered system, and the 45 atom cluster, a seven-layered system, are more accurate representations of the bulk metal. The emitted electron is clearly seen as vacating a molecular orbital which is localized in the surface layer of the cluster, thereby giving further credence to the model.

## 1. INTRODUCTION

Adsorption of cesium on a metal surface lowers the work function of that metal by amounts generally in the neighborhood of two electron volts[1]. In addition, the work function of cesium itself is depressed by about 0.5 eV upon selective exposure to $O_2$ to form $Cs_{11}O_3$ [2]. In particular, the reduction in the work function of beryllium arising from cesium adsorption has been the focus of recent studies[3]. Cesium, hydrogen and oxygen adsorption on a beryllium surface are studied here using ab initio quantum mechanical procedures. Such theoretical studies of the adsorption process yield detailed information about the metal surface which is neither straightforwardly nor accurately obtained from experimental data. For example, charge distributions and orbital structure result from ab initio calculations. Many such studies have used clusters as models of the surface[4-7]. A good model of adsorption processes, however, requires the use of clusters large enough to accurately describe the surface interactions as well as those involving substrate, while remaining small enough for application of accurate theoretical methods.

In this study, the model systems are defined as cylindrical "plugs" from Be wafers having surfaces corresponding to the (0001) hcp metal faces. A view of this wafer along the c-direction is illustrated in Figure 1. All cylinders of a given radius which may be formed from a wafer of a given thickness are defined in Table 1.

Three such cylinders are treated here. The first has a thickness of three layers and is comprised of 19 Be atoms; the second is five layers thick and contains 33 Be

*Proceedings of the SPIE OE/LASE '89 Conference on Microwave and Particle Beam Sources and Directed Energy Concepts, January 16-20, 1989, Los Angeles, CA.

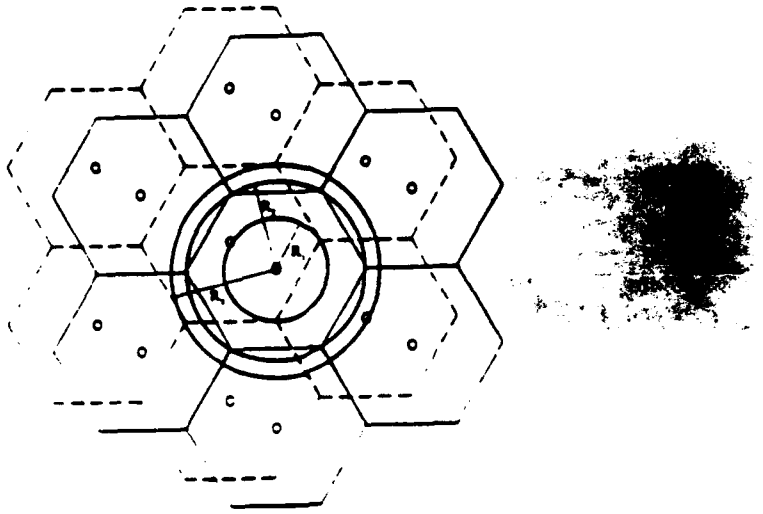

Figure 1. A view of Bulk Be metal along the c direction. Nuclei are situated at the apices of the hexagons, as well as at their centers. Layers represented by dashes lie at c/2 on the c axis (see Table 1).

Table 1. Be Clusters by Coordination Cylinder and hcp Layer

| Cylinder Height (z-coord.) | $R_0$ | | | | $R_1$ | | | | $R_2$=a | | | | $R_3$ | | | |
|---|---|---|---|---|---|---|---|---|---|---|---|---|---|---|---|---|
| -c/2 | | | | | | | | | | | | | | | | |
| . | | | | | | | | | | | | | | | | |
| . | | | | | | | | | | | | | | | | |
| 3c/2 | | | | 0 | | | | 3 | | | | 3 | | | | 6 |
| c | | | 1 | 1 | | | 1 | 1 | | | 7 | 7 | | | 7 | 7 |
| c/2 | | 0 | 0 | 0 | | 3 | 3 | 3 | | 3 | 3 | 3 | | 6 | 6 | 6 |
| 0 | 1 | 1 | 1 | 1 | 1 | 1 | 1 | 1 | 7 | 7 | 7 | 7 | 7 | 7 | 7 | 7 |
| - c/2 | | 0 | 0 | 0 | | 3 | 3 | 3 | | 3 | 3 | 3 | | 6 | 6 | 6 |
| - c | | | 1 | 1 | | | 1 | 1 | | | 7 | 7 | | | 7 | 7 |
| -3c/2 | | | | 0 | | | | 3 | | | | 3 | | | | 6 |
| . | | | | | | | | | | | | | | | | |
| . | | | | | | | | | | | | | | | | |
| -∞c/2 | | | | | | | | | | | | | | | | |
| No. Atoms | 1 | 1 | 3 | 3 | 1 | 7 | 9 | 15 | 7 | 13 | 27 | 31 | 7 | 19 | 33 | 45 |

atoms, while the third contains 45 atoms and seven layers. All three cylinders have a radius $R_3$ which includes a one unit cell step along the a-direction. Be-Be internuclear distances are taken as the same as the bulk hcp metal (a=2.29Å, c=3.58Å)[8]. The resulting cylinders have $D_{3h}$ point-group symmetry, and the

adsorption of atomic hydrogen, one on the top surface and one on the bottom surface of all three cylinders, is modeled such that the three-fold symmetry is preserved. The same applies to the adsorption of atomic cesium and oxygen. The Be-adsorbate internuclear distances are optimized in self-consistent field (SCF) calculations. The 19- and 33-atom cesiated and hydrogenated cylinders are shown in Figures 2 and 3.

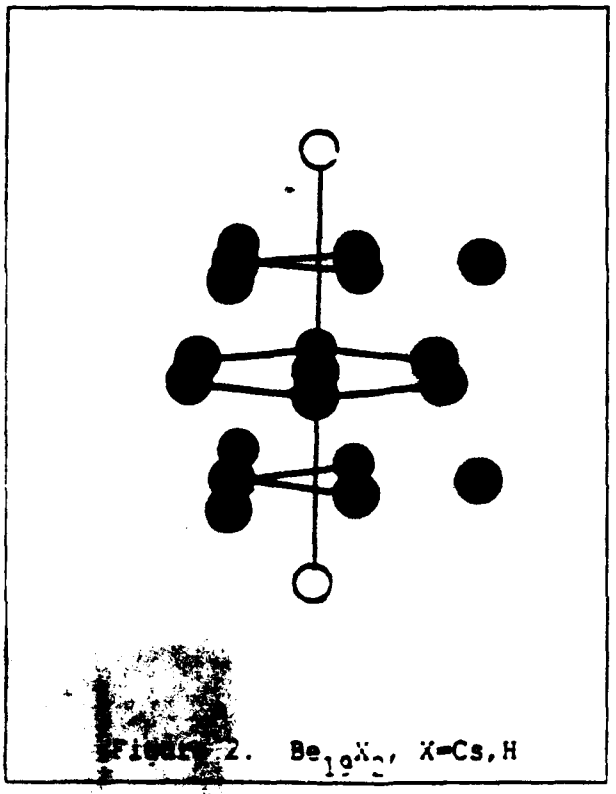

Figure 2. $Be_{19}X_2$, X=Cs,H

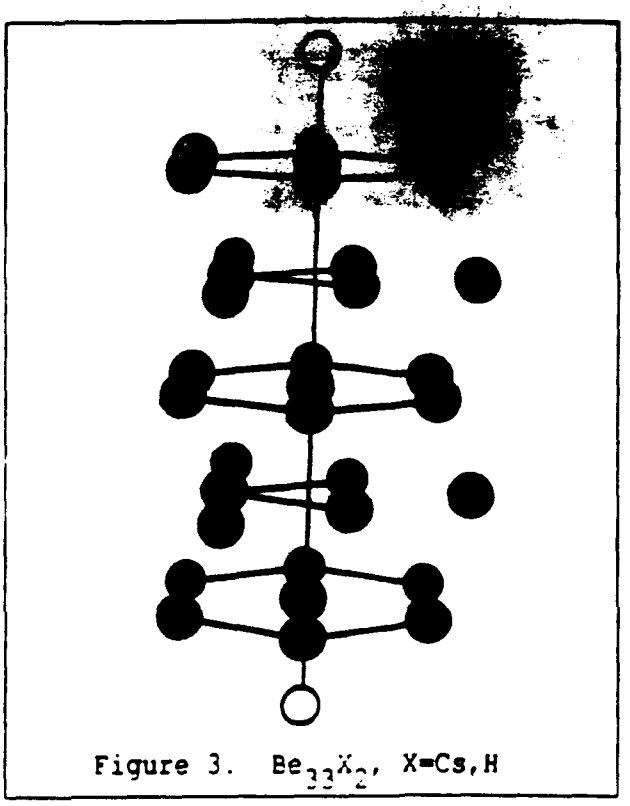

Figure 3. $Be_{33}X_2$, X=Cs,H

The 45-atom cylinder is not shown, but it is similar to the one pictured in Figure 3, except that it contains seven layers instead of five, with the two surface layers identical to the surface layers of the 19 atom cluster (Figure 2). Finally, the simultaneous interaction of oxygen atoms and hydrogen atoms and a cesium overlayer are modelled by the addition of either H or O to the top and bottom layers of $Be_{45}$ between "capping" Cs atoms. That is, $CsHBe_{45}HCs$ or $CsOBe_{45}OCs$ (see Figure 2). Results obtained using these systems are compared to those calculated by treating identical bare and cesiated Be cylinders.

Calculations were accomplished on a Cray X-MP supercomputer using point-group symmetry optimized programs based on the "equal contribution theorem" for two-electron integrals[9]. Ab initio restricted closed-shell and restricted open-shell Hartree-Fock calculations, each corresponding to an average energy of configuration, were carried out on numerous low-lying states of each cluster. (The average energy of configuration is defined as the weighted mean of the energies of all the multiplets for the designated configuration.) The largest clusters required about two to three hours of Cray X-MP time for each geometric orientation. The following basis sets of contracted Gaussian-type functions were used for beryllium, cesium, hydrogen, and oxygen, respectively: (3s2p)/<2s1p>[10], (5s5p)/<3s2p>[11], (4s1p)/<2s1p>[12], and (4s4p)/<2s2p>[13]. Ab initio effective potentials (EP)[14] were used to represent the 1s core electrons in Be[10] and O[13], and the 1s-4s,

2p-4p, and 3d-4d core electrons in Cs[11]. Relativistic effects, especially important for Cs, were incorporated into the EP's[14]. Cluster binding energies calculated relative to the completely dissociated clusters are given in Table 2. Total adsorption energies given for the cesiated and hydrogenated clusters were calculated relative to the SCF energies of the naked clusters plus that of two adsorbate atoms. For O and H plus $Be_{45}Cs_2$, energies are relative to this cluster.

Table 2. Restricted Hartree-Fock Energies of $Be_m$ and $Be_mX_2$ Clusters

| Cluster | Occupied MO's[a] $a_1'$ | $a_2'$ | $a_2''$ | $e'$ | $e''$ | $a_1''$ | B.E. (kcal/mole) | Adsorption Energy (kcal/mole) |
|---|---|---|---|---|---|---|---|---|
| $Be_{19}$[b,c] | 4 | 1 | 3 | 4 | 2 | 0 | 325.25 | |
| $[Be_{19}]^+$ | 4 | 0 | 3 | 4 | 2 | 0 | 394.70 | |
| $Be_{19}Cs_2$ | 6 | 1 | 5 | 5 | 3 | 0 | 402.99 | 38.87 |
| $[Be_{19}Cs_2]^+$ | 6 | 1 | 5 | 5 | 3 | 0 | 405.37 | |
| $[Be_{19}H_2]$[b,d] | 4 | 1 | 3 | 4 | 2 | 1 | 393.76 | 34.25 |
| $[Be_{19}H_2]^+$ | 4 | 1 | 3 | 4 | 2 | 0 | 579.66 | |
| $Be_{33}$ | 6 | 1 | 5 | 6 | 4 | 1 | 724.94 | |
| $[Be_{33}]^+$ | 6 | 1 | 5 | 6 | 4 | 1 | 815.76 | |
| $Be_{33}Cs_2$[b,e] | 8 | 1 | 7 | 7 | 6 | 1 | 768.46 | 21.76 |
| $[Be_{33}Cs_2]^+$ | 8 | 1 | 7 | 7 | 6 | 1 | 779.74 | |
| $Be_{33}H_2$[b,f] | 7 | 1 | 5 | 6 | 4 | 1 | 727.32 | 1.19 |
| $[Be_{33}H_2]^+$[b] | 7 | 1 | 5 | 6 | 4 | 1 | 818.70 | |
| $Be_{45}$[b,g] | 8 | 2 | 7 | 8 | 6 | 2 | 1078.74 | |
| $[Be_{45}]^+$ | 8 | 2 | 7 | 7 | 6 | 2 | 1196.77 | |
| $Be_{45}Cs_2$[b,h] | 10 | 2 | 9 | 9 | 7 | 2 | 1108.95 | 15.11 |
| $[Be_{45}Cs_2]^+$[b] | 10 | 2 | 9 | 9 | 7 | 2 | 1151.78 | |
| $Be_{45}H_2$[b,i] | 8 | 2 | 7 | 8 | 6 | 2 | 1115.07 | 18.16 |
| $[Be_{45}H_2]^+$ | 8 | 2 | 7 | 8 | 6 | 2 | 1228.41 | |
| $Be_{45}O_2Cs_2$[b,j] | 12 | 2 | 11 | 9 | 8 | 2 | 1214.17 | 52.61[k] |
| $[Be_{45}O_2Cs_2]^+$[b] | 12 | 2 | 10 | 9 | 8 | 2 | 1263.79 | |
| $[Be_{45}H_2Cs_2]$[b] | 11 | 2 | 10 | 8 | 7 | 2 | 1058.49 | -50.46 |
| $[Be_{45}H_2Cs_2]^+$[b] | 11 | 2 | 10 | 8 | 7 | 2 | 1090.06 | |

Table 2. (continued)

[a] Underline denotes orbital from which the electron was removed.
[b] State corresponds to the weighted average of configuration.
[c] Open-shell state: $(a_2')^1(a_2'')^1$
[d] Open-shell state: $(a_2')^1(a_1'')^1$
[e] Open-shell state: $(e'')^2$
[f] Open-shell state: $(a_1')^1(a_2'')^1$
[g] Open-shell state: $(a_2')^1(e')^1$
[h] Open-shell state: $(e')^2$
[i] Open-shell state: $(a_2')^1(E')^3$
[j] open-shell state: $(a_1')^1(a_2'')^1$
[k] Adsorption energy of O on Cs-coated $Be_{45}$

Calculated work functions are reported in Table 3. The first values in each row were obtained as the difference between the total valence SCF energy of a neutral cluster and that of the ion generated by removing one electron from the highest occupied orbital of that cluster. The values immediately following are due to Koopmans' theorem and correspond to the negative of the energy of the molecular orbital (MO) from which the electron was ionized. Experimental values are also shown.

Table 3. Work Functions of $Be_m$ and $B_mX_2$ Clusters

| Cluster | $\Phi$(ev)[a] |
|---|---|
| $Be_{19}$ | 5.35,5.04 |
| $Be_{19}Cs_2$ | 3.41,2.99 |
| $Be_{19}H_2$ | 4.30,3.96 |
| $Be_{33}$ | 4.41,4.11 |
| $Be_{33}Cs_2$ | 2.92,2.60 |
| $Be_{33}H_2$ | 4.37,4.09 |
| $Be_{45}$ | 3.16,2.94 |
| $Be_{45}Cs_2$ | 2.40,2.18 |
| $Be_{45}H_2$ | 3.40,3.15 |
| $Be_{45}O_2Cs_2$ | 1.97,1.89 |
| $Be_{45}H_2Cs_2$ | 2.96,2.67 |
| Be (expt.) | 3.92 |
| BeCs (expt.)[b] | 1.6 |
| BeH (expt.) | 3.92 |

Table 3. (continued)

| | |
|---|---|
| $\Delta\Phi[Be_{19}\text{-}Be_{19}Cs_2]^c$ | 1.94,2.05 |
| $\Delta\Phi[Be_{19}\text{-}Be19H_2]^c$ | 1.05,1.08 |
| $\Delta\Phi[Be_{33}\text{-}Be_{33}Cs_2]^c$ | 1.49,1.51 |
| $\Delta\Phi[Be_{33}\text{-}Be_{33}H_2]^c$ | 0.05,0.01 |
| $\Delta\Phi[Be_{45}\text{-}Be_{45}Cs_2]^c$ | 0.76,0.76 |
| $\Delta\Phi[Be_{45}\text{-}Be_{45}H_2]^d$ | -0.24,-0.21 |
| $\Delta\Phi[Be_{45}Cs_2\text{-}Be_{45}O_2Cs_2]^c$ | 0.43,0.29 |
| $\Delta\Phi[Be_{45}Cs_2\text{-}Be_{45}H_2Cs_2]^d$ | -0.56,-0.49 |
| $\Delta\Phi[Be\text{-}BeCs]^c_{expt.}$ | 2.3 |
| $\Delta\Phi[Be\text{-}BeH]_{expt.}$ | 0 |

[a]Where two values appear, these are Koopmans' theorem and ΔE(SCF) values, respectively.
[b]At optimum Cs coverage.
[c]Values correspond to a work function lowering.
[d]Values correspond to a work function increase.

Atomic net electron charge values are given in Tables 4, 5, 6 and 7, as calculated using a Mulliken population analysis[15]. Values of R appearing in these tables correspond to optimum atom-to-surface distances. These distances were calculated from the minimum of a curve fit to SCF energies for three or more distances.

Table 4. Electron Populations of $Be_{19}$, $Be_{19}Cs_2$ and $Be_{19}H_2$

| Cluster | Z-coord[a] | Atom Label | No. Atoms[b] | Cluster Net Charge per Atom | [Cluster]$^+$ Net Charge per Atom | Total Net Charge Difference ([Cluster]$^+$ - Cluster) |
|---|---|---|---|---|---|---|
| $Be_{19}$ | 0 | BeO | 1 | 1.43 | 1.41 | -0.02 |
| | c/2 | BeA | 6 | -0.08 | -0.07 | 0.06 |
| | c/2 | BeC | 6 | -0.09 | 0.00 | 0.54 |
| | 0 | BeB | 6 | -0.07 | 0.00 | 0.42 |
| $Be_{19}Cs_2$ | 0 | BeO | 1 | 1.36 | 1.35 | -0.01 |
| | c/2 | BeA | 6 | -0.05 | -0.07 | -0.12 |
| | c/2 | BeC | 6 | -0.17 | -0.11 | 0.37 |
| | 0 | BeB | 6 | -0.14 | -0.07 | 0.43 |
| | R[c] | Cs | 2 | 0.39 | 0.55 | 0.33 |

Table 4. (continued)

| | | | | | | |
|---|---|---|---|---|---|---|
| $Be_{19}H_2$ | 0 | BeO | 1 | 1.38 | 1.33 | -0.05 |
| | c/2 | BeA | 6 | -0.16 | -0.15 | 0.06 |
| | c/2 | BeC | 6 | -0.06 | 0.07 | 0.78 |
| | 0 | BeB | 6 | -0.02 | 0.01 | 0.18 |
| | R[d] | H | 2 | 0.04 | 0.05 | **0.02** |

[a] c=3.58Å

[b] No. of symmetry equivalent atoms.

[c] R=3.70Å for Be plane to Cs distance. (Be to Cs distance is 3.93 Å.)

[d] R=0.85Å for Be plane to H distance. (Be to H distance is 1.57 Å.)

Table 5. Electron Populations of $Be_{33}$, $Be_{33}Cs_2$ and $Be_{33}H_2$

| Cluster | Z-coord[a] | Atom Label | No. Atoms[b] | Cluster Net Charge per Atom | $[Cluster]^+$ Net Charge per Atom | Total Net Charge Difference ($[Cluster]^+$ - Cluster) |
|---|---|---|---|---|---|---|
| $Be_{33}$ | 0 | BeO | 1 | 0.96 | 0.97 | 0.01 |
| | c/2 | BeA | 6 | 0.55 | 0.53 | -0.14 |
| | c/2 | BeC | 6 | -0.10 | -0.07 | 0.14 |
| | 0 | BeB | 6 | -0.32 | -0.29 | 0.21 |
| | c | BeH | 12 | -0.18 | -0.10 | 0.89 |
| | c | BeD | 2 | 0.20 | 0.14 | -0.11 |
| $Be_{33}Cs_2$ | 0 | BeO | 1 | 0.94 | 0.93 | -0.01 |
| | c/2 | BeA | 6 | 0.57 | 0.52 | -0.25 |
| | c/2 | BeC | 6 | -0.12 | -0.07 | 0.27 |
| | 0 | BeB | 6 | -0.34 | -0.33 | 0.09 |
| | c | BeH | 12 | -0.28 | -0.22 | 0.67 |
| | c | BeD | 2 | 0.44 | 0.40 | -0.08 |
| | R[c] | Cs | 2 | 0.46 | 0.60 | 0.29 |
| $Be_{33}H_2$ | 0 | BeO | 1 | 1.00 | 1.00 | 0.00 |
| | c/2 | BeA | 6 | 0.45 | 0.44 | -0.12 |
| | c/2 | BeC | 6 | -0.06 | -0.04 | 0.12 |
| | 0 | BeB | 6 | -0.30 | -0.26 | 0.24 |
| | c | BeH | 12 | -0.23 | -0.16 | 0.84 |
| | c | BeD | 2 | 0.87 | 0.82 | -0.10 |
| | R[d] | H | 2 | -0.24 | -0.23 | -0.02 |

[a] c=3.58Å

[b] No. of symmetry equivalent atoms

[c] R=3.77Å for Be to Cs distance.

[d] R=1.58Å for Be to H distance at local minimum (see text).

Table 6. Electron Populations of $Be_{45}$ and $Be_{45}H_2$

| Cluster | Z-coord[a] | Atom Label | No. Atoms[b] | Cluster Net Charge per Atom | $[Cluster]^+$ Net Charge per Atom | Total Net Charge Difference ($[Cluster]^+$ - Cluster) |
|---|---|---|---|---|---|---|
| $Be_{45}$ | 0 | BeO | 1 | 1.00 | 1.00 | [illegible] |
| | c/2 | BeA | 6 | 0.42 | 0.41 | |
| | c/2 | BeC | 6 | -0.18 | -0.16 | |
| | 0 | BeB | 6 | -0.34 | -0.30 | 0.[illegible] |
| | c | BeH | 12 | -0.18 | -0.17 | 0.12 |
| | c | BeD | 2 | 1.36 | 1.34 | -0.04 |
| | 3c/2 | BeF | 6 | -0.14 | -0.14 | 0.00 |
| | 3c/2 | BeG | 6 | -0.02 | 0.08 | 0.60 |
| $Be_{45}Cs_2$ | 0 | BeO | 1 | 0.97 | 0.97 | 0.00 |
| | c/2 | BeA | 6 | 0.46 | 0.45 | -0.06 |
| | c/2 | BeC | 6 | -0.19 | -0.17 | 0.12 |
| | 0 | BeB | 6 | -0.37 | -0.34 | 0.18 |
| | c | BeH | 12 | -0.23 | -0.21 | 0.24 |
| | c | BeD | 2 | 1.22 | 1.21 | -0.02 |
| | 3c/2 | BeF | 6 | -0.06 | -0.09 | -0.18 |
| | 3c/2 | BeG | 6 | -0.05 | 0.00 | 0.30 |
| | R[c] | Cs | 2 | 0.29 | 0.51 | 0.44 |
| $Be_{45}H_2$ | [illegible] | BeO | 1 | 0.99 | 0.98 | -0.01 |
| | [illegible] | BeA | 6 | 0.43 | 0.41 | -0.12 |
| | [illegible] | BeC | 6 | -0.14 | -0.12 | 0.12 |
| | [illegible] | BeB | 6 | -0.36 | -0.32 | 0.24 |
| | [illegible] | BeH | 12 | -0.14 | -0.13 | 0.12 |
| | [illegible] | BeD | 2 | 1.32 | 1.30 | -0.04 |
| | 3c/2 | BeF | 6 | -0.18 | -0.18 | 0.00 |
| | 3c/2 | BeG | 6 | -0.06 | 0.04 | 0.60 |
| | R[d] | H | 2 | 0.01 | 0.01 | 0.00 |

[a] c=1.58Å

[b] No. of symmetry equivalent atoms

[c] R=3.70Å for Be plane to Cs distance. (Be to Cs distance is 3.93 Å.)

[d] R=0.86Å for Be plane to H distance at local minimum (see text). Be to H distance is 1.58Å.

Table 7. Electron Populations of $Be_{45}O_2Cs_2$ and $Be_{45}H_2Cs_2$

| Cluster | Z-coord[a] | Atom Label | No. Atoms[b] | Cluster Net Charge per Atom | $[Cluster]^+$ Net Charge per Atom | Total Net Charge Difference ($[Cluster]^+$ - Cluster) |
|---|---|---|---|---|---|---|
| $Be_{45}O_2Cs_2$ | 0 | BeO | 1 | 1.01 | 1.02 | [illegible] |
| | c/2 | BeA | 6 | 0.48 | 0.48 | |
| | c/2 | BeC | 6 | -0.19 | -0.18 | |
| | 0 | BeB | 6 | -0.36 | -0.35 | 0.[illegible] |
| | c | BeH | 12 | -0.22 | -0.21 | 0.12 |
| | c | BeD | 2 | 1.15 | 1.14 | -0.02 |
| | 3c/2 | BeF | 6 | 0.18 | 0.16 | -0.12 |
| | 3c/2 | BeG | 6 | -0.02 | -0.03 | -0.06 |
| | R | O | 2 | -0.98 | -1.00 | -0.04 |
| | R'[d] | Cs | 2 | 0.34 | 0.86 | 1.04 |
| $Be_{45}H_2Cs_2$ | 0 | BeO | 1 | 0.96 | 0.93 | -0.03 |
| | c/2 | BeA | 6 | 0.51 | 0.49 | -0.12 |
| | c/2 | BeC | 6 | -0.15 | -0.12 | 0.18 |
| | 0 | BeB | 6 | -0.33 | -0.31 | 0.12 |
| | c | BeH | 12 | -0.26 | -0.24 | 0.24 |
| | c | BeD | 2 | 1.10 | 1.09 | -0.02 |
| | 3c/2 | BeF | 6 | -0.01 | -0.04 | -0.18 |
| | 3c/2 | BeG | 6 | 0.02 | 0.05 | 0.18 |
| | [illegible] | H | 2 | -0.16 | -0.15 | 0.02 |
| | [illegible] | Cs | 2 | 0.04 | 0.33 | 0.58 |

[illegible]=1.80Å[f]

[b] No. of symmetry equivalent atoms

[c] R=1.50Å for Be plane to O distance. (Be to O distance is 2.0Å.)

[d] R'=3.1Å for O to Cs distance.

[e] R=0.86Å for Be plane to H distance. (Be to H distance is 1.58Å.)

[f] R'=3.2Å for H to Cs distance.

## 2. RESULTS AND DISCUSSION

RHF calculations predict a net energy gain of 18.2 and 1.2 kcal/mole·atom upon hydrogen approach to the $Be_{45}$ and $Be_{33}$ surfaces, respectively. The approach of hydrogen on the $Be_{19}$ surface, on the other hand, results in an energy gain of 34.3 kcal/mole·atom. Cesium adsorption on the $Be_{19}$ and $Be_{33}$ surfaces leads to energy gains of 38.9 kcal/mole·atom and 21.8 kcal/mole·atom, respectively. Therefore, while cesium is predicted to adsorb on both $Be_{19}$ and $Be_{33}$ (i.e. at a hole and at a head-on site), at the SCF level of theory, hydrogen adsorbs strongly on $Be_{19}$ and appears to adsorb moderately on $Be_{45}$ (i.e., at a hole site) but only negligibly on $Be_{33}$ (i.e., at a head-on site).

Table 3 contains calculated values for the ionization potentials of all the clusters studied, as well as values for the shift in ionization potential ($\Delta\Phi$) resulting from Cs or H adsorption. Experimentally determined values of the work functions due to Cs or $H_2$ adsorption on Be metal are also included[3].

Results for the 45 atom system indicate a slight rise by 0.2 eV in the ionization potential of the cluster due to H adsorption, while results for the $Be_{33}$ system indicate a lowering by 1.5 eV in the ionization potential of the cluster due to Cs adsorption, and no lowering due to H adsorption. The experimental findings are 2.3 eV and 0.0 eV lowering in the work function of Be metal due to adsorption of Cs and of $H_2$, respectively. Adsorption of Cs and of H on $Be_{19}$, however, results in ionization potential lowerings of approximatley 2.0 eV and 1.0 eV, respectively. Although the first value is in close agreement with experiment, the second is not.

These discrepancies are explained by referring to the electron populations listed in Tables 4 and 5. Total net charge differences, in the case of $Be_{19}$, indicate participation in charge redistribution by both the surface (BeC, z-coord.=c/2) and middle (BeB, z-coord.=0) layers upon ionization of the cluster. In $Be_{19}$, ionization of the cluster results in a contribution of 0.4 electron from Be atoms (BeB) in the middle layer compared to 0.5 electron for Be atoms on the surface. Thus, the middle and surface layers of the cluster are involved almost equally in the electron ionization process. For $Be_{19}Cs_2$, both the surface (BeC) and middle (BeB) layers contribute 0.4 electron, while $Cs_2$ donates 0.3 electron. Since electron emission is from the surface of the bulk metal, it is concluded that $Be_{19}$ is too small a cluster to model the Be metal surface involved in Cs adsorption.

On the other hand, the middle layer of $Be_{19}H_2$ contributes 0.2 electron, with the surface layers (BeC) being predominantly involved in ionization. H donates only a minimal amount (0.02 electron) of charge. Part of the charge contributed by the middle (BeB) layer is shifted toward the BeC group of atoms in $Be_{19}H_2$. Since the greatest charge perturbation occurs on the surface, this model at first appears to be adequate for the description of H adsorption. However, further analysis reveals that this is not the case. As was stated previously, the middle layer (BeB) of $Be_{19}$ participates appreciably (donating 0.4 electron) in the ionization process, indicating that this cluster does not reasonably model the bulk surface. Adsorption of Cs or H onto this surface, therefore, yields information about the interaction of these two species with a finite 19 atom Be cluster, but this information cannot be interpreted as also applying to the process whereby a Cs or H atom adsorbs onto the bulk Be surface. Such an extension may be made only in cases where the bare cluster is a good model of the bulk metal.

$Be_{33}$, a five-layer cluster, and $Be_{45}$, a seven-layer cluster, appear to model the Be metal surface more appropriately. Ionization of these clusters indicates that the surface layers (BeH for $Be_{33}$ and BeG for $Be_{45}$) donate the emitted electron. Although the middle layers also contribute, the involvement of the surface layers is three to four times as great. The adsorption process, then, is represented more reasonably by using $Be_{33}$ or $Be_{45}$ clusters rather than $Be_{19}$ to model the metal surface.

Table 6 shows that the surface (BeG, z-coord.=3c/2) layers of $Be_{45}$ and $Be_{45}H_2$ are most affected during the ionization process. Although the inner layers of $Be_{45}H_2$ are also involved in ionization, their contribution is minimal compared to the charge donated by the surface (BeG) layers (0.2 electron vs 0.6). As with the $Be_{19}$ systems, some of the contributed charge is shifted toward several groups of atoms in the $Be_{45}$ clusters: for example, BeA (z-coord.=c/2). However, the largest percentage of the charge involved in ionization is donated by the BeG atoms in the surface layer. It is also noted that the net charge differences for $Be_{45}H_2$ are nearly identical to

those for $Be_{45}$, the only difference being 0.06 for the BeA layer. The approach of H to the $Be_{45}$ surface does not affect the ionization process. The same conlusion is reached from an analysis of the electron populations of $Be_{33}$ and $Be_{33}H_2$, which appear in Table 5.

The values of $\Delta\Phi$ appearing in Table 3 are another indication that H has no effect on the $Be_{33}$ and $Be_{45}$ surfaces. The greatest shift in ionization potential occurs for the latter surface and is 0.2. $\Delta\Phi$ for $Be_{33}$ is practically zero. Therefore, H is not predicted to chemisorb on the Be surface and, in fact, clearly [illegible] in the case of the head-on approach, as modelled by $Be_{33}$ (the [illegible] energy is 1 kcal/mol·atom). Adsorption of H on $Be_{45}$, as shown in Table 2, is favored by 18.2 kcal/mol·atom. The optimum H-to-Be-plane distance is 0.86Å. The corresponding values for adsorption onto a $Be_{36}$ cluster reported by Bagus et al. are 42.3 kcal/mol for the adsorption energy and 0.95Å for the distance from H to the surface. The adsorption energy of H on $Be_{45}$, although greater (18 kcal/mol·atom), is attributed to a local minimum due to state crossing and is akin to physisorption since both the population analysis and $\Delta\Phi$ values indicate no effect on the $Be_{45}$ surface due to adsorption of atomic hydrogen.

Hydrogen approaches the $Be_{33}$ surface above a Be atom (directly overhead site) in the present calculations. There are three other possible sites for adsorption. These are the Be-Be midpoint, eclipsed and open sites. The adsorbate approaches the Be surface directly between two Be atoms located on the surface in the first case. The second involves adsorption over a triangle of Be atoms located on the surface, the center of which is directly above a Be atom situated in a layer next to the surface (which is the case for $Be_{45}$). The open site has the adsorbate approaching the Be surface directly above the center of a triangle of Be atoms located on the surface. However, in this case, there is no Be atom directly below. According to a study by Bagus et al., based on SCF calculations using clusters containing two to three layers, the directly overhead site is the least stable for the adsorption of H onto a Be surface[19]. $Be_{33}$ is a five-layer cluster and thus should yield a reasonable value for the adsorption energy associated with the directly overhead approach of an atom to the surface, while adsorption on an eclipsed site is adequately modeled by the seven-layer $Be_{45}$ cylinder.

It is clear that the surface layers (BeH) of $Be_{33}Cs_2$ are predominantly involved in electron removal. These layers contribute 0.7 electron, whereas the greatest charge contributed by the inner layers is 0.3 (see Table 5). The total net charge differences of $Be_{33}Cs_2$ differ from those of $Be_{33}$, indicating that Cs, unlike H, is affecting electron removal. In fact, Cs donates 0.3 electron to this process. The effects of charge redistribution resulting from ionization are greater for the inner layers (relative to the surface layers) of $Be_{33}Cs_2$ than for those of $Be_{33}H_2$. The BeC group of atoms contribute 0.3 electron, while the BeA atoms accept 0.3 electron in $Be_{33}Cs_2$. The sum of these amounts still corresponds to less than half of the charge contributed by the surface layers. In $Be_{33}H_2$, the greatest contribution by the inner layers is approximately one fourth of the charge contributed by the surface. The surface layers of $Be_{45}Cs_2$ are also predominantly involved in the ionization process. However, the atoms in the inner layers, particularly those on the outer edges of the cylinder, are involved significantly (see Table 6). In this case, as opposed to $Be_{33}$, the cesium interacts more closely with the $Be_{45}$ surface, thus making edge effects more apparent. In the hydrogenated case, these edge effects were not present since H is much smaller than Cesium (0.5 vs. 1.67 for the ionic radius of H and Cs, respectively). The small but non-negligible contribution of the inner layers of $Be_{33}Cs_2$ and $Be_{45}Cs_2$ to the ionization process indicates that the discrepency between the calculated and measured workfunction lowering (Table 3) may be improved by treating a cluster corresponding to a model based on cylinders having the same height

as $Be_{19}$ or $Be_{45}$ but a greater radius (see Table 1 and Figure 1). In addition to improvements in $\Delta\Phi$, adsorption of Cs on an eclipsed site is predicted to be more stable, providing that the cluster model has a surface large enough to minimize the edge effects. Unlike the head-on site, this position allows the Cs to interact more closely with the surface triangles of Be since there is no center atom present.

Both oxygenation and cesiation of $Be_{45}$ results in a greater work function lowering than does cesiation alone, while hydrogenation of $Be_{45}Cs_2$ results in a work function increase (see Table 3). The electron population analysis for $Be_{45}O_2Cs_2$ indicates that the emmitted electron is predominantly vacating a cesium orbital. In $Be_{45}H_2Cs_2$, however, the Be cylinder is more invovled in ionization, donating approximately 40% of the emitted charge (see Table 7).

Experimentally Cs adsorption on Be results in work a function lowering of 2.3 eV, whereas exposure of a Be surface to $H_2$ yielded no observable change[3]. That is, the Be substrate Auger signal was not attenuated in the case of $H_2$ and there was no discernable work function shift.

## 3. CONCLUSIONS

Analysis of the Mulliken populations for $Be_{19}$ indicates that this cluster is too small to model the bulk surface. However, the population analyses for $Be_{19}$ and $Be_{45}$ indicate that these clusters are adequate models of the Be metal surface involved in hydrogen adsorption. A wider cylinder is needed for the adequate modelling of cesium adsorption. The adsorption energy of Cs on the $Be_{19}$ cluster is 21.8 kcal/mol·atom. The decrease in the ionization potential of $Be_{19}Cs_2$ relative to $Be_{19}$ is calculated to be 1.5 eV. The experimental work function lowering resulting from Cs adsorption is measured as 2.3 eV.[3] The adsorption energies of H on $Be_{19}$ and $Be_{45}$ are 1 and 18 kcal/mol·atom, respectively. The first value is negligible, while the latter is attributed to a local minimum since the population analysis and $\Delta\Phi$ values for both $Be_{19}$ and $Be_{45}$ indicate no effect on these clusters due to H adsorption. Experiment reveals no adsorption of $H_2$ on Be metal, thus ruling out dissociative chemisorption.

## 4. ACKNOWLEDGMENTS

This research was supported in part by the Air Force Office of Scientific Research and by the National Science Foundation under grant No. CHE-8712315, which included supercomputer time at the Pittsburgh Supercomputing Center.

## 5. REFERENCES

1. L.W. Swanson and R.W. Strayer, J. Chem. Phys. 48, 2421 (1968); R.E. Weber and W.T. Peria, Surf. Sci. 14, 13 (1969).
2. B. Woratschek, G. Ertl, J. Kuppers, W. Sesselmann and H. Haberland, Phys. Rev. Lett. 57, 1484 (1986); B. Woratschek, W. Sesselmann, J. Kuppers, G. Ertl and H. Haberland, J. Chem. Phys. 86, 2411 (1987).
3. G.S. Tompa, M. Seidl, W.C. Ermler and W.E. Carr, Surf. Sci. 185 L453, (1987); M.M. Marino, W.C. Ermler, G.S. Tompa, and M. Seidl, Surf. Sci. 186, 1 (1989).
4. J. Rubio, F. Illas and J.M. Ricart, J.Chem. Phys. 84, 3311 (1986).
5. G. Pacchioni, W. Pewesdorf and J. Koutecky, Chem. Phys. 83, 201 (1984).
6. C.W. Bauschlicher, D.H. Liskow, C.F. Bender and H.F. Schaefer III, J. Chem. Phys. 62, 4815 (1975).
7. C.W. Bauschlicher, Chem. Phys. Let. 117 33, (1985).
8. R.G. Wyckoff, Crystal Structures, 2nd ed., Interscience, New York (1974).
9. R.M. Pitzer, J. Chem. Phys. 58, 3111 (1973), and private communication.
10. W.C. Ermler, C.W. Kern, R.M. Pitzer and N.W. Winter, J. Chem. Phys. 84, 3937

(1986).
11. R.B. Ross, T. Atashroo, J.M. Powers, W.C. Ermler, L.A. LaJohn and P.A. Christiansen, to be published.
12. T.H. Dunning, Jr. J. Chem. Phys. 53, 2823 (1970); ibid. 55, 3958 (1971).
13. L.F. Pacios and P.A. Christiansen, J. Chem. Phys. 82, 2665 (1985).
14. P.A. Christiansen, W.C. Ermler and K.S. Pitzer, Annu. Rev. Phys. Chem. 36, 407 (1985); W.C. Ermler, R.B. Ross and P.A. Christiansen, Adv. Quantum Chem. 19, 139 (1988).
15. R.S. Mulliken, J. Chem. Phys. 23, 1833 (1955).
16. P.S. Bagus, H.F. Schaefer and C.W. Bauschlicher, J. [redacted]ys. 78, 1390 (1983).

# *Ab initio* study of the geometry and electronic structure of lead iodide semiconductor clusters

M. M. Marino,* M. Sawamura,† and W. C. Ermler*†
*Stevens Institute of Technology, Hoboken, New Jersey 07030*

C. J. Sandroff
*Bellcore, Red Bank, New Jersey 07701*
(Received 16 October 1989)

Layered anisotropic semiconductor clusters of the type $Pb_xI_{2x}$ are studied in *ab initio* Hartree-Fock calculations that include relativistic effects. Total energies, internuclear distances, and net atomic charges are calculated. Large increases in the equilibrium iodine-lead interlayer distance result in as much as a 10% reduction of the in-plane internuclear separations and blueshifts in the electronic spectra, which are attributed to quantum size effects observed in recent experimental studies.

The properties of clusters are attracting increased attention because they represent an intermediate physical regime where neither atomic nor solid-state descriptions seem totally adequate.[1-3] Besides interest in fundamental questions such as how electronic structure evolves as a function of size, there is also the possibility of using finite-size effects to create new materials having unique electronic and optical properties.[4,5] In modern semiconductor research, for example, it is commonplace to fabricate structures whose physical dimensions are considerably smaller than carrier wavelengths, which leads to physical phenomena that cannot be observed in bulk matter.[6] Clusters containing from about 10 to 1000 atoms are particularly noteworthy because their properties set the ultimate limits on the use of physical size to alter the behavior of matter.

Many experimental techniques are now available to synthesize clusters both in gas and condensed phases,[7-12] but as yet there is no generally available experimental procedure to determine the structure and spectra of the clusters produced. Hence, theoretical insight into cluster structure as a function of cluster size takes on a major role. The computational difficulty inherent in treating large systems comprised of heavy elements, however, has precluded rigorous *ab initio* studies on such clusters. Up to now, theoretical treatments on systems of this type have largely neglected relativistic effects, as well as certain exchange interactions among electrons.[13] Consequently, the majority of *ab initio* work in semiconductor systems has appeared on small clusters of light elements such as silicon.[14,15] In such strongly covalent systems, it is found that small isolated clusters tend to reconstruct and to form tightly bound symmetrical structures with a high degree of coordination. Moreover, this tendency to minimize the number of exposed dangling bonds has the consequence that the bulk silicon structure is recovered only for very large clusters.

In this Rapid Communication, we report the results of rigorous *ab initio* quantum-mechanical calculations on semiconductor clusters containing as many as 21 heavy atoms. All of the theoretical results presented here were calculated using fully *ab initio* procedures; that is, no experimental parameters were used and all of the terms in the Hamiltonian were retained. Since no integrals were approximated or disregarded, all Coulomb and exchange interactions among electrons were explicitly evaluated for each cluster. Furthermore, relativistic effects, which are significant in these heavy-element systems,[16] were also included in the calculations.

The structures of the layered semiconductors investigated here exhibit a radically different dependence on cluster size than do those of isotropic silicon. Unlike clusters of Si, layered semiconductors of the type $Pb_xI_{2x}$ essentially retain the structure of the bulk crystalline lattice in the lateral direction for the range of geometries studied. We find, however, that there can be significant electronic coupling between interlayer perturbations and intralayer lattice constants in these clusters. Indeed, for very large increases in the Pb-I interlayer spacings, we see in-plane lattice constants decrease by as much as 20%. With these results, it might be possible to explain recent compelling scanning tunneling images of structurally related $BiI_3$ clusters.[17]

Two cluster models are studied, one of $Pb_6I_{12}$ and two of $Pb_7I_{14}$ stoichiometry. These are shown in Fig. 1. Each has the layer symmetry of the bulk crystal and is comprised of a plane of lead atoms above which are situated two triangular layers of iodine atoms. $Pb_6I_{12}$ has $D_{3h}$ point-group symmetry (hexagonal close packing), while both $Pb_7I_{14}$ clusters have $D_{3d}$ point-group symmetry (cubic close packing). All three represent fragments of the bulk crystalline solid (one unit cell thick) having iodine layers slightly perturbed from the bulk arrangement to preserve the symmetry of each cluster. Pb-Pb, I-I, and

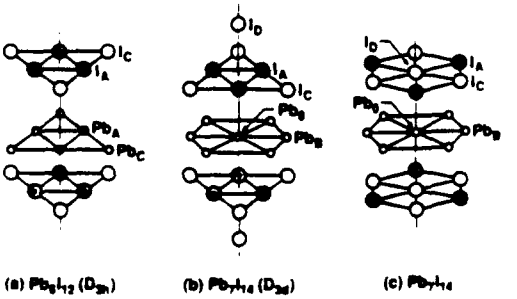


FIG. 1. $Pb_xI_{2x}$ clusters ($x=6,7$).

 

Pb-I internuclear distances were initially determined from the lattice constants of crystalline $PbI_2$.[18] All internuclear distances were then optimized in *ab initio* Hartree-Fock calculations, consistent with the variation principle and within the symmetry constraints. Self-consistent field (SCF) energies for the lowest-lying molecular-orbital electron configurations were calculated for each geometric orientation of the clusters. SCF calculations on heavy-element systems based on relativistic effective core potentials (REP's) have been shown to yield reliable geometric parameters.[16] In addition, this method yields fully optimized molecular orbitals for each electronic state treated, in contrast to many standard methods based on band theory. REP's (Ref. 19) were used to represent the $1s$-$4s$ $2p$-$4p$, and $3d$-$4d$ core electrons in I [Ref. 20(a)] and the $1s$-$5s$, $2p$-$5p$, $3d$-$5d$, and $4f$ core electrons in Pb.[20(b)] Relativistic effects cannot be ignored for systems containing heavy elements such as Pb and I.[16] Basis sets of contracted Gaussian-type functions were used to represent the valence orbitals of Pb and I.[20] Calculations were accomplished on a Cray X-MP supercomputer using programs based on the "equal contribution theorem" for two-electron symmetry orbital integrals.[21] These *ab initio* restricted closed-shell and restricted open-shell Hartree-Fock linear combination of atomic-orbital–molecular-orbital (LCAO-MO) calculations consumed approximately 20 min of Cray X-MP time for each nuclear configuration. The geometry optimizations required a minimum of ten orientations per cluster.

Energy-optimized interlayer and intralayer distances of $Pb_6I_{12}$ were found to be 11% expanded and 1% contracted, respectively, relative to bulk $PbI_2$. This swollen interlayer distance is not unexpected for a $Pb_6I_{12}$ cluster having $D_{3h}$ point-group symmetry because the electron-rich I atoms of the top layer are arranged in "head-on" positions relative to those in the bottom layer. This is in contrast to bulk $PbI_2$, where each iodine atom in a top layer is positioned directly above the midpoint between two iodine atoms located in a bottom layer. This system tends to contract laterally as the interlayer separations expand. For example, expansion of the interlayer separation by 40% results in a 7% contraction in metal-layer lateral dimensions.

A total of five MO electron configurations were studied for neutral $Pb_6I_{12}$. Four of these states were nearly degenerate and lay 1.6 eV higher in energy than the ground state. The electronic excitations involved orbitals associated with both iodine and lead atoms. Furthermore, five of the six lowest unoccupied MO's (LUMO's) for each electron configuration have energies lower than $-2.7$ eV, indicating that the neutral system is electron deficient. This conclusion is supported by means of Koopmans' theorem.[22]

If the cluster wave function $\Psi(2N)$, a $2N$-electron antisymmetrized product of MO's $\{\phi_m\}$, is stationary and $\phi_m$ is an eigenfunction of the Fock operator, then $\Psi(2N+1)$, whereby an electron is added to $\phi_m$, is also stationary with respect to any further variations in the orbitals. This means that the orbital energy $\varepsilon_m$ corresponds to the electron affinity of the neutral system, providing that $\varepsilon_m$ is unoccupied. Therefore, systems possessing very low-lying LUMO's are electron deficient; i.e., the addition of one or more electrons to these orbitals will increase the overall stability of the system.

To satisfy this electron deficiency, we studied a doubly charged anionic $Pb_6I_{12}$ cluster. We also believe that the anion is the most natural cluster to consider from the experimental point of view since clusters of this type are prepared in solution as colloidal particles in the presence of excess iodide ions.[23] The total energy of $Pb_6I_{12}^{2-}$ is more than 6 eV lower than the corresponding neutral species. In this case, nearly all of the LUMO's have energies greater than zero ($\sim$2.7 eV), indicating a quenching of the system's electrophilicity.

A geometry optimization was also carried out for $Pb_6I_{12}^{2-}$. The equilibrium interlayer and intralayer distances were found to be expanded by 14% and 1%, respectively, relative to bulk $PbI_2$. This cluster is also slightly swollen with respect to neutral $Pb_6I_{12}$, but this is expected due to the increased ionicity. As with the neutral cluster, expansion of the interlayer separation results in a contraction of intralayer distances, although not as pronounced as for the neutral system; that is, a 40% expansion in interlayer separation results in a 3% contraction in lateral dimensions relative to the bulk crystal. As previously mentioned, results of SCF calculations on heavy-element systems have been shown to be reliable, with the accuracy of the method increasing as the number of electrons treated explicitly increases.[16] Therefore, SCF results for $Pb_6I_{12}^{2-}$, a 110-valence-electron system, are expected to be reliable, and any structural differences between our models and those of bulk $PbI_2$ are attributable to cluster effects.

A total of ten low-lying electron configurations of the cluster were studied at both the calculated equilibrium interatomic distances and at a geometry corresponding to a 60% expansion in the interlayer distance and a 10% contraction in lateral dimensions. These percentages were chosen from the results of a series of calculations at geometries ranging from 30% contraction to 100% expansion of the lattice constants in the vertical direction and 30% contraction to 20% expansion in the lateral direction. All of the open-shell configurations were treated as pure spin triplet states; i.e., the cluster wave functions are spin eigenfunctions having total spin quantum number $S=1$. Excitation energies relative to the lowest state found are given in Table I, while Table II reports electron charge/atom values calculated based on a Mulliken population analysis[24] for the lowest-lying state at each of the aforementioned two geometries.

The energy separations for equilibrium $Pb_6I_{12}^{2-}$ listed in Table I are clearly bandlike, with the two lowest-lying states nearly degenerate in energy and states 3 through 8 lying at or near the band gap of bulk crystalline $PbI_2$ at 2.5 eV.[25] The last state corresponding to $Pb_6I_{12}^{2-}$ listed in Table I is considerably blueshifted relative to the band gap of the bulk. The same type of energy separations occur at an expanded interlayer distance, the only exception being for state 4, which has an energy value between three essentially degenerate low-lying states and four states grouped near the band gap of the bulk solid. A total of 45 electron transitions among the ten lowest-lying states found were examined. The density of states shown in Fig. 2 indicates that these transitions are peaked at 0.2

TABLE I. Electronic states of $Pb_xI_{2x}$ clusters (eV).

| Cluster | State No. | $\Delta E$ (Equil.)[a] | $\Delta E$ (Expanded $Z$)[a] |
|---|---|---|---|
| $Pb_6I_{12}^{2-}$[b] | 1 | 0.00 | 0.00 |
| | 2 | 0.03 | 0.14 |
| | 3 | 2.14[c] | 0.47 |
| | 4 | 2.21 | 1.19[c] |
| | 5 | 2.25 | 1.31 |
| | 6 | 2.36 | 2.05 |
| | 7 | 2.41 | 2.12 |
| | 8 | 2.49 | 2.39 |
| | 9 | 2.53 | 2.47 |
| | 10 | 4.84 | 3.06 |
| $Pb_7I_{14}^{2-}$[d] | 1 | 0.00 | 0.00 |
| | 2 | 0.26 | 0.35 |
| (five layers) | 3 | 0.28 | 0.76 |
| | 4 | 0.35 | 0.95 |
| | 5 | 0.59 | 1.11 |
| | 6 | 0.63 | 2.14 |
| | 7 | 0.75 | 2.71 |
| | 8 | 0.76 | 2.90 |
| | 9 | 0.99 | 3.29 |
| | 10 | 1.01 | 3.49 |
| | 11 | 1.26 | 3.99 |
| $Pb_7I_{14}^{2-}$[e] | 1 | 0.00 | 0.00 |
| | 2 | 0.68 | 1.71 |
| (three layers) | 3 | 1.54 | 1.99 |
| | 4 | 1.80 | 2.39 |
| | 5 | 1.83 | 3.17 |
| | 6 | 2.19 | 4.29 |
| | 7 | 2.39 | 4.67 |
| | 8 | 3.27 | 4.75 |
| | 9 | 3.31 | ... |
| | 10 | 4.97 | ... |

[a]See text.
[b]See Fig. 1(a).
[c]Lowest-lying closed-shell singlet state.
[d]See Fig. 1(b).
[e]See Fig. 1(c).

2.5, and 4.9 eV, with the second peak lying near the experimental bulk band gap of $PbI_2$ and the third blueshifted relative to the band gap by 2.3 eV.

Charge/atom values appearing in Table II indicate that the predominant interlayer interactions occur between the atoms comprising the smaller Pb and I triangles [$Pb_A$ and $I_A$ in Fig. 1(a)] for the lowest-energy state of $Pb_6I_{12}^{2-}$ at both geometries treated. This is also the case for the other eight-electron configurations of $Pb_6I_{12}^{2-}$ listed in Table I, with the exception of the highest-energy state (state 10). Comparison between charge/atom values for this state at the equilibrium geometry and at an expanded interlayer separation shows that the interlayer interactions predominantly involve both types of Pb and I atoms [Fig. 1(a)]. No differences are seen between charge/atom values for the ground state and the corresponding values for each of the higher-energy states (states 2–9 in Table I) at both geometries treated, indicating that the electronic transitions are predominantly intralayer and occur among symmetry-related atoms. A more detailed analysis of the Mulliken populations reveals that these electron excitations correspond to metal-metal transitions. Differences in charge/atom values between the highest-energy state of $Pb_6I_{12}^{2-}$ (state 10) listed in Table I and the ground state are as high as 0.2 (compared to −0.02 for states 2–9). In this case, the transition involves both Pb and I atoms.

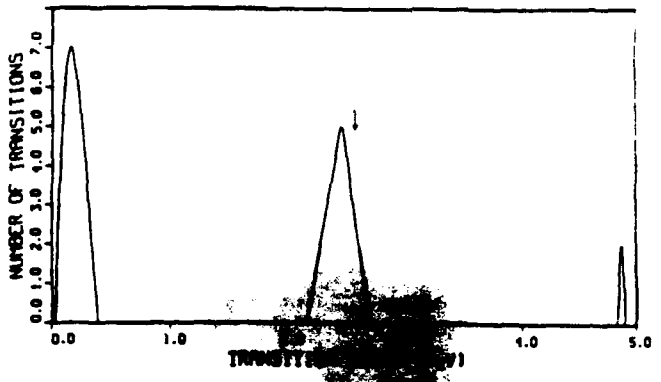


FIG. 2. Density of calcula[illegible] states. The arrow marks the position of the bulk band gap.

As noted above, two cluster orientations were studied for $Pb_7I_{14}$ [Figs. 1(b) and 1(c)]. Since the neutral system was found to be electron deficient, analogous to $Pb_6I_{12}$, two electrons were added to the cluster. A geometry and electronic state optimization of the first [Fig. 1(b)] resulted in a 20% contraction and 10% expansion of interlayer and intralayer distances, respectively, relative to bulk $PbI_2$. The lowest 11 states (the energy for each of which corresponds to the weighted mean of the energies of all the pure spin multiplets for that particular electron configuration) are nearly monotonically distributed for the five-layered cluster, as shown in Table I. On the other hand, bandlike behavior is observed when the interlayer distances are expanded by 60% and lateral dimensions are contracted by 10% relative to the bulk crystal. Energy gaps of 2.7 eV and higher may be attributed to quantum

TABLE II. Population analysis for the lowest-energy states of $Pb_xI_{2x}$ clusters (Ref. 22).

| Cluster | Atom | Charge/atom[a] (Equil.) | Charge/atom[a] (Expanded $Z$) |
|---|---|---|---|
| $Pb_6I_{12}^{2-}$[b] | $Pb_A$ | 0.81 | 0.57 |
| | $Pb_C$ | 0.69 | 0.67 |
| | $I_A$ | −0.44 | −0.33 |
| | $I_C$ | −0.64 | −0.62 |
| $Pb_7I_{14}^{2-}$[c] | $Pb_0$ | 1.01 | −0.29 |
| (five layers) | $Pb_B$ | 0.80 | 0.55 |
| | $I_A$ | −0.41 | −0.15 |
| | $I_C$ | −0.59 | −0.51 |
| | $I_D$ | −0.93 | −0.53 |
| $Pb_7I_{14}^{2-}$[d] | $Pb_0$ | 0.08 | −0.49 |
| (three layers) | $Pb_B$ | 0.80 | 0.67 |
| | $I_A$ | −0.53 | −0.45 |
| | $I_C$ | −0.53 | −0.45 |
| | $I_D$ | −0.26 | −0.05 |

[a]Electron units.
[b]See Fig. 1(a)
[c]See Fig. 1(b).
[d]See Fig. 1(c).

size effects, which are responsible for blueshifts in the spectrum. The predominant interlayer interactions occur among the Pb layer, $I_A$ and $I_D$ [Table II and Fig. 1(b)], and a comparison of charge/atom values for the ground state and the corresponding values for each of the excited states at both geometries indicates that all of the transitions involve both Pb and I orbitals.

The second $Pb_7I_{14}$ cluster studied, which contains three layers [Fig. 1(c)], was also found to be electron deficient. Consequently, a doubly charged anion was investigated. Initial intralayer atomic distances for this cluster corresponded to those in the bulk crystal,[18] although interlayer atomic distances differed from those of the bulk due to the positioning of the hexagonal layers. Upon optimization it was found that the lowest-energy geometry of $Pb_7I_{14}^{2-}$ corresponds to a 2.2% lateral contraction and a 38.7% vertical expansion relative to the bulk lattice constants. The cluster was also studied at a geometry corresponding to a 60% vertical elongation and a 20% lateral contraction. These percentages were chosen from a series of calculations analogous to those on $Pb_6I_{12}^{2-}$. A total of ten electron configurations were studied for the anion at both the equilibrium geometry and at an expanded interlayer separation. The energies of these states appear in Table I (dashed lines indicate energies greater than 5 eV). As for the five-layered cluster, the states correspond to the weighted mean of all the multiplets for a particular electron configuration. Clearly, the system exhibits a band-like behavior (Table I). The first excited state at 0.68 eV corresponds to a single electron transition. The next three states (1.54–1.83 eV) are double excitations from the ground state, while states 6 and 7 (2.19–2.39) correspond to single excitations. The remaining states (3.29 eV and higher), which are higher lying than the bulk-energy band gap, correspond to double excitations from the ground state. It is noteworthy that elongated $Pb_7I_{14}^{2-}$ exhibits energy gaps of 3.17, 4.67, and 4.75 eV, which may be attributed to quantum size effects, as suggested by Sandroff, Hwang, and Chung (3.42, 3.95, and 4.80 eV).[23]

Charge/atom values for all $Pb_7I_{14}$ clusters studied (Table II) indicate that the interlayer interactions involve both types of Pb and I atoms in each layer [Figs. 1(b) and 1(c)]. The center lead ($Pb_0$) and the center iodines ($I_D$) are especially affected by interlayer perturbations since the charge on these shifts by as much as 1.3 electrons (for $Pb_0$) in the case of five-layered $Pb_7I_{14}^{2-}$. The largest perturbations are expected for these atoms, however, since they lie along a symmetry axis and therefore experience the greatest number of nearest-neighbor interactions. $Pb_0$, in fact, is positioned at the center of symmetry. Although not tabulated, there are also significant differences (as large as 0.6) between charge/atom values for the lowest-energy state and the corresponding values for each of the higher-energy states of the $Pb_7I_{14}$ anionic cluster at the two geometries listed in Table II, further indicating that the electron excitations in these clusters involve both the Pb and I layers.

Our findings regarding the reduction of in-plane lattice constants when interlayer distances are expanded from their equilibrium values aid in the understanding of recent scanning tunneling microscope (STM) images of layered $BiI_3$ clusters.[17] (These layered semiconductors are very similar chemically to those of $PbI_2$ and both systems have been studied experimentally.[11]) In that study, atomically resolved images showed structures having honeycombed symmetry after colloidal suspensions of $BiI_3$ were evaporated onto graphite surfaces. Since the central bismuth plane in $BiI_3$ has honeycombed symmetry (in contrast to the hexagonal symmetry of the iodine planes), the STM images are most likely individual bismuth atoms. Interestingly, the lattice constant of these putative $Bi_{10}I_{30}$ clusters was measured to be 0.65 nm, roughly 20% smaller than the bulk in-plane lattice constant. Hence, these STM images could be revealing clusters whose topmost layer of iodine has been removed or displaced from its underlying bismuth plane. Chemical oxidation or cluster-tip interactions could be responsible for these large perturbations.

The research at Stevens was supported in part by Bellcore, the National Science Foundation under Grant No. CHE-8912674, an allocation of supercomputer time at the Pittsburgh Supercomputing Center, and the Air Force Office of Scientific Research.

*Department of Chemistry and Chemical Engineering.
†Department of Physics and Engineering Physics.

[1] J. Stapelfeldt, J. Woermer, and T. Moeller, Phys. Rev. Lett. **62**, 98 (1989).
[2] C. Hayashi, Phys. Today, **40** (No. 12), 44 (1987).
[3] T. Inoshita, S. Ohnishi, and A. Oshiyama, Phys. Rev. Lett. **57**, 2560 (1986).
[4] D. S. Chemla and D. A. B. Miller, Opt. Lett. **11**, 522 (1986).
[5] T. Takagahara, Phys. Rev. B **36**, 9293 (1987).
[6] R. Dingle, W. Wiegmann, and C. H. Henry, Phys. Rev. Lett. **33**, 827 (1974).
[7] J. R. Heath *et al.*, J. Chem. Phys. **83**, 5520 (1985).
[8] A. Fojtik *et al.*, Ber. Bunsenges. Phys. Chem. **88**, 969 (1984).
[9] R. L. Whetten *et al.*, J. Phys. Chem. **89**, 566 (1985).
[10] R. Rossetti *et al.*, J. Chem. Phys. **82**, 552 (1985).
[11] C. J. Sandroff, S. P. Kelty, and D. M. Hwang, J. Chem. Phys. **85**, 5337 (1986).
[12] O. I. Micic *et al.*, J. Phys. Chem. **91**, 1295 (1987).
[13] See, for example, R. Rossetti *et al.*, J. Chem. Phys. **82**, 552 (1985); L. E. Brus, *ibid.* **79**, 5566 (1983).
[14] K. Ragavachari, J. Chem. Phys. **84**, 5672 (1986).
[15] J. R. Chelikowsky *et al.*, Phys. Rev. Lett. **62**, 292 (1989).
[16] P. A. Christiansen, W. C. Ermler, and K. S. Pitzer, Annu. Rev. Phys. Chem. **36**, 409 (1985).
[17] D. Sarid *et al.*, J. Vac. Sci. Technol. A **6**, 424 (1988).
[18] R. G. Wyckoff, *Crystal Structures* (Interscience, New York, 1960), 2nd. ed.
[19] W. C. Ermler, R. B. Ross, and P. A. Christiansen, Adv. Quantum Chem. **19**, 139 (1988).
[20] (a) L. A. LaJohn *et al.*, J. Chem. Phys. **87**, 2812 (1987); (b) R. B. Ross *et al.* (unpublished).
[21] R. M. Pitzer, J. Chem. Phys. **58**, 3111 (1973).
[22] T. Koopmans, Physica (Utrecht) **1**, 104 (1933).
[23] C. J. Sandroff, D. M. Hwang, and W. M. Chung, Phys. Rev. B **33**, 5953 (1986).
[24] R. S. Mulliken, J. Chem. Phys. **23**, 1833 (1955).
[25] G. Harbeke and E. Tosatti, RCA Rev. **36**, 40 (1975).

# Ab Initio Study of Quantum Confinement Effects in $(PbI_2)_7$ Semiconductor Clusters

Makoto Sawamura[†] and Walter C. Ermler*[,†,‡]

*Department of Physics and Engineering Physics and Department of Chemistry and Chemical Engineering, Stevens Institute of Technology, Hoboken, New Jersey 07030* *(Received: December 27, 1989)*

Molecular orbital theory is used in the context of ab initio Hartree–Fock calculations to study the origin of quantum confinement effects in layered $Pb_7I_{14}$ clusters. As the cluster geometry is energy optimized in several steps, the structure distends into two quasi-hemispherical iodine layers sandwiching a hexagonal lead layer. At the equilibrium geometry for the lowest electronic state, Pb–Pb in-plane interatomic distances are contracted by 11.3% compared to the experimental bulk $PbI_2$ values. Optical spectra are observed to be blue-shifted by 0.3–2.1 eV relative to the energy band gap of crystalline $PbI_2$.

## Introduction

There is increasing interest in exploiting the unique properties attributable to quantum size or quantum confinement effects in the design of optoelectronic devices.[1-5] In fact, it is currently within the limits of technology to synthesize semiconductor cluster systems that have volumes and surface areas that are of the same order of magnitude as carrier wavelengths.[7,9] These size-dependent phenomena typically yield blue-shifted optical spectra,[2,3] exciton confinement,[4,5] depressed ionization energies,[6,7] and nonbulk fragment structures[3,8] compared to bulk properties.

In this article, we address the origin of quantum confinement phenomena in semiconductor clusters from the perspective of rigorous ab initio molecular orbital theory.

In recent years, cluster studies involving geometry optimizations and electronic structure determinations have been made possible by the availability of supercomputers.[8-11] Yet, the intermediate regime between molecules and solids, where certain quantum size effects emerge, is not fully understood. However, that threshold may require clusters containing as many as 1000 atoms,[12,13] where rigorous ab initio calculations are still not feasible. Even for smaller clusters, geometry optimizations employing gradient methods require enormous computational effort.[9] However, the advent of scanning tunneling microscopy (STM) has provided useful information about cluster geometry[14,15] although tip–surface interactions may perturb the surface and absorbed clusters.[16] Transmission electron microscopy (TEM) is also used to directly measure the size and geometry of larger clusters.[2,17,18] Information derived by using these approaches may be used as a starting point

**TABLE I: Energy-Optimized Interatomic Distances (Å)**

| atomic pair | geometry[a] | | | | |
|---|---|---|---|---|---|
| | o[b] | a | b | c | d |
| Pb–Pb | 4.56 | 4.56 | 4.46 | 4.04 | 4.04 |
| $I_A$–$I_A$ | 4.56 | 4.56 | 4.46 | 4.61 | 4.61 |
| $I_A$–$I_O$ | 4.56 | 4.56 | 4.46 | 4.61 | 4.64 |
| $Pb_A$–$I_A$ | 3.22 | 3.00 | 3.46 | 3.44 | 3.44 |
| $Pb_O$–$I_O$ | 3.22 | 1.85 | 2.57 | 2.56 | 3.07 |
| Pb–I[c] | 1.85 | 1.85 | 2.57 | 2.56 | |

[a] See Figure 1. [b] Bulk geometry (see ref 21). [c] Interlayer distance.

[†] Department of Physics and Engineering Physics
[‡] Department of Chemistry and Chemical Engineering

(1) Hayashi, C. *Phys. Today* **1987**, No. 12, 44.
(2) Sandroff, C. J.; Hwang, D. M.; Chung, W. M. *Appl. Phys. Lett.* **1988**, *53*, 104.
(3) Ermler, W. C.; Ross, R. B.; Sawamura M. In *Proceedings of the Supercomputing Symposium, 1988*; University of Alberta: Edmonton, 1988.
(4) Brus, L. E. *J. Chem. Phys.* **1984**, *80*, 4403.
(5) Itoh, T.; Iwabuchi, Y.; Kataoka, M. *Physica B* **1988**, *145*, 567.
(6) Burt, M. G.; Heine, V. *J. Phys. C* **1978**, *11*, 961.
(7) Woratschek, B.; Ertl, G.; Küppers, J.; Sesselman, W. *Phys. Rev. Lett.* **1986**, *57*, 1484.
(8) Raghavachari, K. *J. Chem. Phys.* **1986**, *84*, 5672.
(9) Jena, P. In *Microclusters*; Sugano, S., Nishina, Y. N., Ohnishi, S., Eds.; Springer-Verlag: Berlin, 1987.
(10) Ross, R. B.; Ermler, W. C.; Kern, C. W.; Pitzer, R. M. *Chem. Phys. Lett.* **1987**, *134*, 115.
(11) Inoshita, T.; Ohnishi, S.; Oshiyama, A. *Phys. Rev. Lett.* **1986**, *57*, 2560.

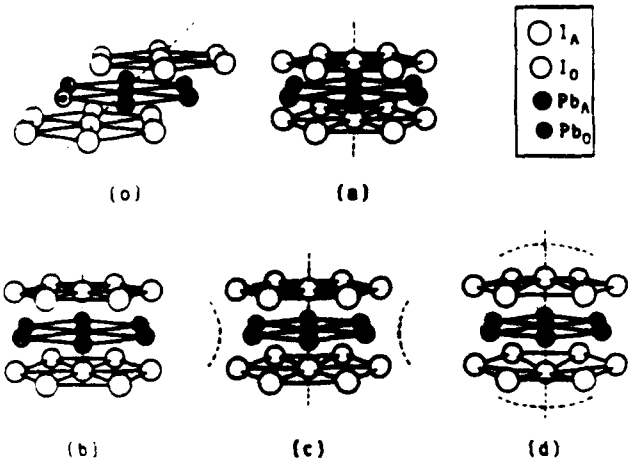


Figure 1. $Pb_7I_{14}$ cluster geometries: (o) a fragment of bulk $PbI_2$, (a) the initial geometry, (b) optimization in two degrees of freedom, (c) optimization in three degrees of freedom, (d) optimization of $z$ coordinates of $I_O$ atoms in addition to (c).

for the computational determination of cluster geometry. Recent STM studies on metal–iodine semiconductor clusters suggested the existence of microclusters having a layered structure, which appear to be cylindrical fragments of the bulk.[19]

Spherical microclusters of metals and semiconductors that have been investigated in recent years have been called supermolecules[10,20] and superatoms[11] (shell models). The supermolecules are spherical or cylindrical bulk fragments for which cluster properties were derived through ab initio calculations, while the superatoms are based on jellium models with spherical boundaries. However, in either case, surface and internal geometric reconstructions due to the size of the microclusters were not treated. In the regime of microclusters of small to intermediate size (ten to several hundred atoms), nonbulk characteristics may emerge.

## Calculations

A recent TEM study on $PbI_2$ microclusters indicated the size distributions of surface physisorbed clusters peaked at 12, 18, and 29 Å.[2,19] In the present ab initio study a cylindrical structure for a gas-phase $Pb_7I_{14}$ cluster is assumed. A combination of hexagonal lead and iodine planes is fixed at bulk lattice positions and used as the initial cluster geometry (Figure 1a). A portion of crystalline lead iodide appears in Figure 1o ($a$ = 4.56 Å, $c$ = 6.96 Å).[21] Interlayer distance and in-plane interatomic distances were initially set at their bulk values, 1.85 and 4.56 Å, respectively (Table I, column o). The central atoms on the hexagonal layers were in head-on positions, leading to $Pb_A$–$I_A$ and $Pb_O$–$I_O$ atomic distances that are shortened in comparison to the bulk (Table I, column o). The diameter of this cylindrical cluster corresponds to the lowest peak in the experimental size distribution.[2] The coordination numbers of the cluster are 2 ($Pb_O$), 4 ($Pb_A$), 1 ($I_O$), and 2 ($I_A$), while in bulk $PbI_2$ they are 6 and 3 for lead and iodine atoms, respectively. Ab initio studies on nonstoichiometric lattice matched clusters can be found elsewhere.[3,22,23]

TABLE II: Molecular Orbital Electron Configurations of $Pb_7I_{14}^{2-}$

| state no. | MO configuration[a] | | | | | |
|---|---|---|---|---|---|---|
| | $a_{1g}$ | $a_{2u}$ | $e_g$ | $e_u$ | $a_{1u}$ | $a_{2g}$[b] |
| 1 | 2 | 0 | 0 | 2 | 0 | 0 |
| 2 | 1 | 0 | 0 | 3 | 0 | 0 |
| 3 | 2 | 0 | 1 | 1 | 0 | 0 |
| 4 | 2 | 1 | 0 | 1 | 0 | 0 |
| 5 | 0 | 0 | 1 | 3 | 0 | 0 |
| 6 | 2 | 0 | 0 | 1 | 0 | 1 |
| 7 | 2 | 0 | 2 | 0 | 0 | 0 |
| 8 | 0 | 0 | 0 | 3 | 1 | 0 |
| 9 | 2 | 1 | 1 | 0 | 0 | 0 |
| 10 | 0 | 0 | 0 | 2 | 2 | 0 |
| 11 | 2 | 1 | 0 | 2 | 0 | 1 |
| 0[c] | 18 | 16 | 8 | 8 | 6 | 4 |

[a] Number of electrons in diamond[illegible] shell. [b] Irreducible representations of MO's in $D_{3d}$ point group symmetry. [c] Number of electrons in inner valence MO's.

Ab initio restricted closed-shell and restricted open-shell Hartree–Fock linear combination of atomic orbitals molecular orbitals (LCAO–MO) calculations were carried out for $Pb_7I_{14}$ clusters that explicitly included the valence electrons of each atom (6s and 6p for Pb, 5s and 5p for I). Basis sets of contracted Gaussian-type functions were used to represent valence orbitals of Pb[24] and I.[25] The core electrons (1s–5s, 2p–5p, 3d–5d, and 4f for Pb,[24] 1s–4s, 2p–4p, and 3d–4d for I[25]) were represented by ab initio effective core potentials that include relativistic effects, which are not negligible for heavy elements such as lead and iodine.[26]

All of the energies of the highest occupied molecular orbitals (HOMO's) and lowest unoccupied molecular orbitals (LUMO's) were observed to be negative for the low-lying states of neutral $Pb_7I_{14}$ clusters. To compensate for this electron deficiency, two extra electrons were added to the valence MO's ($Pb_7I_{14}^{2-}$) throughout the calculations. This procedure is consistent with Koopmans' theorem[27] and was used in earlier studies on $Pb_7I_{12}$,[3] $Bi_6I_{18}$,[22] and $Pb_6I_{12}$[23] in which geometries were frozen at near-bulk values.

Geometry optimizations based on total valence energy calculations required 60 independent geometries. The computer programs employed here take advantage of the cluster symmetry to significantly decrease the number of two-electron integrals that must be calculated.[28] The cluster was treated by using its full $D_{3d}$ point group symmetry. Total valence energies and partial and gross atomic populations[29] for 11 singlet and 11 triplet states including the ground state were calculated for each geometry (Table II). From these states, 55 singlet and 55 triplet transition energies were obtained as differences in total energies of initial and final states. This procedure is more rigorous than conventional HOMO–LUMO gap approximations for transition energies. LUMO's are merely virtual orbitals due to the self-consistent-field (SCF) procedure and are deficient in the sense that certain two-electron self-interactions are present.[30] In addition, if they are used as a final state of a transition, cluster orbital relaxations that accompany the transition are ignored.[31] These orbital relaxations, as well as the proper inclusion of all two-electron in-

(12) Kappes, M. M. *Chem. Rev.* **1988**, *88*, 369.
(13) Stapelfeldt, J.; Wörmer, J.; Möller, T. *Phys. Rev. Lett.* **1989**, *62*, 98.
(14) Sarid, D.; Hansen, T.; Bell, L. S.; Sandroff, C. J. *J. Vac. Sci. Technol. A* **1988**, *6*, 424.
(15) Ganz, E.; Sattler, K.; Clark, J. *Phys. Rev. Lett* **1988**, *60*, 1856.
(16) Mamin, H. J.; Ganz, E.; Abraham, D. W. *Phys. Rev. B* **1986**, *34*, 9015.
(17) Giorgio, S.; Urban, J. *J. Phys. F* **1988**, *18*, 147.
(18) Iijima, S. In ref 9.
(19) Jing, T. W.; Ong, N. P.; Sandroff, C. J. *Appl. Phys. Lett.* **1988**, *53*, 104.
(20) Ermler, W. C.; Kern, C. W.; Pitzer, R. M.; Winter, N. W. *J. Chem. Phys.* **1986**, *84*, 3937.
(21) Donnay, J. D. H.; Donnay, G.; Cox, E. G.; Kennard, O.; King, M. V. *Crystal Data Determinative Tables*; American Crystallographic Association: Washington, DC, 1963.
(22) Marino, M. M.; Sawamura, M.; Ermler, W. C.; Sandroff, C. J. *Chem. Phys. Lett.* **1989**, *163*, 202.
(23) Marino, M. M.; Sawamura, M.; Ermler, W. C.; Sandroff, C. J. *Phys. Rev. B* **1990**, *41*, 1270.
(24) Ross, R. B.; Powers, J. M.; Atashroo, T. A.; Ermler, W. C.; Lajohn, L. A.; Christiansen, P. A. *J. Chem. Phys.*, in press.
(25) Lajohn, L. A.; Christiansen, P. A.; Atashroo, T.; Ermler, W. C. *J. Chem. Phys.* **1987**, *87*, 2812.
(26) Christiansen, P. A.; Ermler, W. C.; Pitzer, K. S. *Annu. Rev. Phys. Chem.* **1985**, *36*, 407.
(27) Koopmans, T. *Physica* **1933**, *1*, 104.
(28) Pitzer, R. M. *J. Chem. Phys.* **1973**, *58*, 3111.
(29) Mulliken, R. S. *J. Chem. Phys.* **1955**, *23*, 1833.
(30) Hunt, W. J.; Goddard III, W. A. *Chem. Phys. Lett.* **1969**, *3*, 414.
(31) Martin, T. P. In *Elementary and Molecular Clusters*; Benedek, G., Martin, T. P., Pacchioni, G., Eds.; Springer-Verlag: Berlin, 1988.

TABLE III: Single-Electron Transition Energies (eV)

| trans[a] | spin[b] | geometry[c] a | b | c | d |
|---|---|---|---|---|---|
| 1-2 | T | -0.65 | 0.05 | -0.17 | 0.23 |
| | S | -0.11 | 0.06 | 0.00 | 0.01 |
| 1-3 | T | 0.08 | 0.73 | 1.73 | 1.95 |
| | S | 0.42 | 1.00 | 1.89 | 1.99 |
| 1-4 | T | 2.70 | 2.46 | 3.07 | 3.21 |
| | S | 2.11 | 2.07 | 2.69 | 2.82 |
| 1-6 | T | 4.53 | 2.68 | 4.25 | 4.36 |
| | S | 3.98 | 2.28 | 3.88 | 3.97 |
| 2-5 | T | -0.38 | 1.60 | 2.31 | 3.59 |
| | S | -0.97 | 1.69 | 2.22 | 3.88 |
| 2-8 | T | -0.48 | 1.93 | 3.17 | 4.45 |
| | S | -1.12 | 1.95 | 3.03 | 4.67 |

[a] Transition $i$-$j$; $i$ and $j$ are the initial and final states, respectively (see Table II). [b] Spin multiplicity; T = triplet and S = singlet. [c] See Figure 1.

teractions, were explicitly included in the present calculations.

The transitions are characterized by an analysis of the dominant electron population shifts. Comparison of atomic orbital populations for initial and final states of a transition represent changes due to the transition (population shifts). Electronic charge is considered to have exited from the orbitals with the most negative population shifts and entered those orbitals with the most positive shifts. These characteristics may be denoted by, for example, "Pb–Pb in-plane transition", "I–Pb interlayer transition", etc.

## Results and Discussion

The geometry was optimized adiabatically (viz., the lowest electronic state was found at each geometry) with respect to the total valence energy at three levels (Table II). First, two parameters, the interlayer and intralayer atomic distances (height and diameter of the cylindrical cluster), were varied (Figure 1b). The in-plane interatomic distances in the lead and iodine layers were assumed to be equal at this level. This process resulted in an estimate of approximate cluster size. The in-plane atomic distance on each layer decreased by 2.2% relative to the bulk lattice constant (Table I, column b). The $Pb_A$–$I_A$ atomic distance and Pb–I interlayer distance were larger than the bulk values by 7.3% and 38.7%, respectively. This vertical expansion of the cluster is attributed to the choice of a compressed initial geometry.

Single-electron transitions from low-lying states (states 1 and 2), chosen from among 110 possible transitions, are tabulated in column b of Table III for this case. Compared to the states for the initially chosen geometry, many state crossings were observed (Table III, column a). States 1 and 2 were found nearly degenerate. Transition energies from states 1 to 4 and to 6 (transitions 1–4 and 1–6), 2.07–2.68 eV, are comparable to the experimental energy band gap in crystalline $PbI_2$ of 2.57 eV.[32] Since the population shifts in both transitions were small in comparison to all the others, it is concluded that the wave functions of the initial and final states were very similar. As a result, it is expected that their transition probabilities are higher. The other transitions (0.05–1.95 eV) were found to lie below the band gap. At this stage, the in-plane atomic distances and optical properties are seen to still be bulklike.

Second, three geometric parameters were varied: the interlayer distance, diameter of the middle layer (lead layer), and the diameter of the top and bottom layers (iodine layers) (Figure 1c). The in-plane interatomic distances in the lead layer contracted by 11.3% while the intralayer iodine distances stayed essentially the same (1.2% elongated) compared to the initial geometry (bulk lattice). The interlayer distance was found to be nearly equal to that of geometry b of Figure 1 (contracted by 0.01 Å). This result showing a contraction of the lead layer is consistent with the experimental STM studies on surface metal clusters of Bi[14] and of Au and Ag.[15] In all of these cases, the metal–metal interatomic distances were observed to be contracted relative to bulk values.

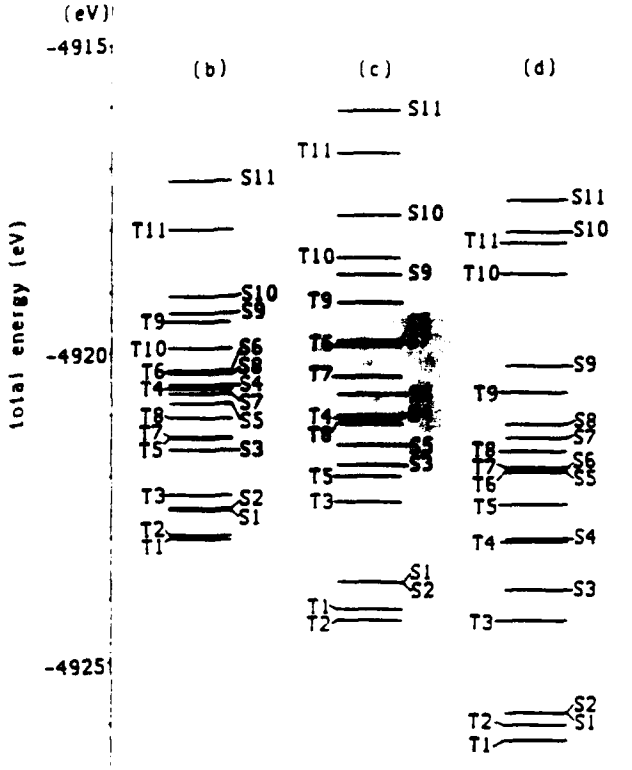


Figure 2. Electronic states of $Pb_7I_{14}^{2-}$ clusters at each level of geometry optimization. T and S indicate triplet and singlet states, respectively. Numbers correspond to Table II.

Figure 2 shows that this geometry deformation resulted in a large spreading of energy states. Total energies were lowered by 1.14–1.36 eV in the low-lying states 1 and 2. However, energies were lowered by only 0.12–0.68 eV in states 3, 4, 5, and 8 and even increased in the remaining states by 0.28–1.46 eV relative to geometry b of Figure 1. As suggested by the spreading of states shown in Figure 2, vibronic properties of the clusters appear to be emerging at this level of geometry optimization. That is, each state has its unique equilibrium geometry with a deep and narrow potential well. However, consistent with the Franck–Condon principle, vertical electronic transitions with no simultaneous geometry shifts are expected. As a result, the energies of singlet electron transitions 1–4, 1–6, and 2–8 are blue-shifted from 0.12 to 1.68 eV relative to the energy band gap (Table III, column c).

The emergence of a blue-shifted ultraviolet (UV) spectrum for geometry c, but not for geometry b, indicates that quantum confinement effects in cluster systems cannot be discussed unambiguously without first determining the optimized geometries. Since both systems had an identical ground-state electron configuration, and were nearly of equal-size nuclear frameworks, the blue-shifted optical spectrum must be due mainly to geometric reconstruction in the lead layer.

This reconstruction leads to difficulties in using a-particle-in-a-box model with accompanying effective mass approximation in microcluster theory.[2] In this model quantum size effects arise from the finite boundary conditions. However, this method may not be able to correctly estimate effects due to internal reconstruction, which are observed to cause large perturbations in transition energies in the present calculations. For example, the following equation for the energy rise due to confinement in layered $PbI_2$ clusters within an effective mass approximation has been used:[2]

$$E\ (\text{eV}) = 235/L_r^2 + 26.85/L_z^2 \qquad (1)$$

$L_r$ is the diameter and $L_z$ the height (both in angstroms) of the cylindrical cluster. The dimensions of geometry b of Figure 1 can be estimated as $L_r = 13.38$ Å and $L_z = 9.60$ Å by assuming the in-plane interatomic distance as the atomic diameter and the circumscribing cylinder as the dimensions of the potential wel

[32] Harbeke, G.; Tosatti, E. *RCA Rev.* **1975**, *36*, 610.

Those of geometry c in Figure 1 are $L_{zz}$ = 13.26 Å (average diameter) and $L_r$ = 9.73 Å. Substitution of these values into eq 1 gives energy increases for geometries b and c of Figure 1, 1.60 and 1.62 eV, respectively. The increment in transition energies due to variation from geometry b to c results in only 0.02 eV, while the average increment in single-electron transition energies between geometries b and c is 0.80 eV in the rigorous ab initio calculations (Table III).

Finally, geometry c of Figure 1 was frozen, except for the central iodine atoms on the top and bottom layers ($I_O$ atoms). The $z$ coordinates of these atoms alone were optimized (Figure 1d, Table I, column d). The equilibrium geometry in this scheme corresponds to the lowest total valence energy of all $PbI_2$ clusters studied. (The system was not fully optimized in all four degrees of freedom because of computational limitations.) The final optimum geometry is quasi-spherical. Variation from geometries c to d of Figure 1 resulted in state crossings, blue-shifted UV spectra (Table III, column d) and the further energy spreading shown in Figure 2d. Transitions 1–3, 1–4, and 1–6 (1.95–4.36 eV) are seen to be predominantly $Pb_O$–$Pb_A$ in-plane transitions. The transition energies increased by only 0.09–0.22 eV from cluster c to cluster d (Table III, columns c and d), because these transitions are largely Pb–Pb inplane transitions and are unperturbed by the changed positions of the $I_O$ atoms. On the other hand, large increases in transition energies in transitions 2–5 and 2–8 (1.28–1.66 eV) are attributable to the $I_O$ locations. In these cases, $I_O$–$Pb_A$ electron transfer is predominant. The transition energies 2.82–4.67 eV in transitions 1–4, 1–6, 2–5, and 2–8 (Table III) agree well with the experimentally observed optical peaks at 3.42, 3.95, and 4.80 eV[10] or 3.1, 3.6, and 4 eV.[33]

## Conclusions

Geometric and optical properties of layered $Pb_7I_{14}$ clusters, reported here at several levels of geometry optimization, indicate an evolution of quantum confinement effects. Surface and internal geometric reconstructions are important components in understanding the nature of such effects. A carefully optimized geometry for layered $Pb_7I_{14}$ indicated a drastic contraction in the Pb–Pb in-plane interatomic distances and blue-shifted UV spectra compared to crystalline $PbI_2$. Bulk fragments treated by using ab initio procedures without full geometry optimization[22,23] or a-particle-in-a-box models (with effective mass approximations)[2] are not sufficiently rigorous for the unambiguous treatment of quantum size effects in semiconductor [illegible] clusters. Surface and internal geometric reconstructions cause increases in transition energies resulting in blue-shifted optical absorption spectra. Complete geometry optimization is expected to result in even larger blue shifts.

*Acknowledgment.* We thank Peter Figliozzi for assisting with the construction of Figure 1 and Maria Marino for helpful discussions. This research was supported in part by the National Science Foundation under Grant CHE-8912674 and the Air Force Office of Scientific Research. The Pittsburgh Supercomputing Center is acknowledged for a grant of Cray supercomputer time.

**Registry No.** $PbI_2$, 10101-63-8.

(33) Nozue, Y. Private communication.

# Ab initio study of the effects of cesium, hydrogen and oxygen adsorption on the work function of beryllium

M.M. Marino
*Department of Chemistry and Chemical Engineering, Stevens Institute of Technology, Hoboken, NJ 07030, USA*

and

W.C. Ermler [1]
*Department of Chemistry, The Ohio State University, Columbus, OH 43210, USA*

Received 12 October 1990

Hydrogen, oxygen and cesium adsorption on beryllium metal were modelled using a $Be_{45}$ cluster containing seven layers. The ab initio Hartree–Fock calculations employ effective core potentials and full $D_{3h}$ point-group symmetry. Cesiation of the surface is found to lower the work function by 2.2 eV, in good agreement with the experimental value of 2.3 eV. Adsorption of oxygen on the cesiated surface lowers the work function by an additional 0.3 eV over the 2.2 eV lowering due to cesiation alone, whereas hydrogenation raises it by 0.48 eV.

It is well known that the work function of a metal can be lowered by the adsorption of cesium [1–4]. Co-adsorption of $O_2$ has been found to lower the work function even further [5]. Studies of this type are important because of the many technical applications of low work function surfaces, one example of which is in the generation of $H^-$ and $D^-$ sources in thermonuclear fusion research [6]. For many years, the lowering of the work function due to alkali-metal adsorption has been explained by way of a mechanism involving charge transfer from adsorbate to substrate [7]. Recently, however, a more covalent interaction between the two has been proposed [8,9].

In this work, the effects of cesium, hydrogen and oxygen adsorption on the work function of beryllium are investigated using a 45-atom cluster to model the Be (0001) surface. The use of clusters as models for surfaces is common [10,11]. Beryllium was chosen as the metal substrate for several reasons. First, Be has a closed-shell ground electronic state and is the smallest such atom to exhibit metallic character. Second, the theoretical results may be compared to experimental work involving Cs adsorption on Be metal [4]. Finally, the $Be_{45}$ cluster used in this study has previously been determined to provide an accurate model of the bulk surface involved in adsorption [12,13]. All of the calculations are carried out at the Hartree–Fock level of theory.

The model systems are taken as cylindrical "plugs" from Be wafers having surfaces corresponding to the (0001) hcp metal face [13]. The cylinder chosen for this study contains 45 atoms and seven layers and has a radius which includes a one-unit cell step along the $a$-direction. Be–Be internuclear distances are equal to those in the bulk hcp metal ($a=2.29$ Å, $c=3.58$ Å) [14]. This cylinder has $D_{3h}$ point-group symmetry, and the adsorption of cesium and oxygen/hydrogen, one on the top surface and one on the bottom surface is modeled such that the threefold symmetry and horizontal mirror plane are preserved. In the case where only one type of adsorbate is involved, the Be-adsorbate internuclear distances have been optimized in self-consistent-field (SCF) calculations. The 45-atom cylinder-plus-adsorbates

[1] Permanent address: Department of Chemistry and Chemical Engineering, Stevens Institute of Technology, Hoboken, NJ 07030, USA.

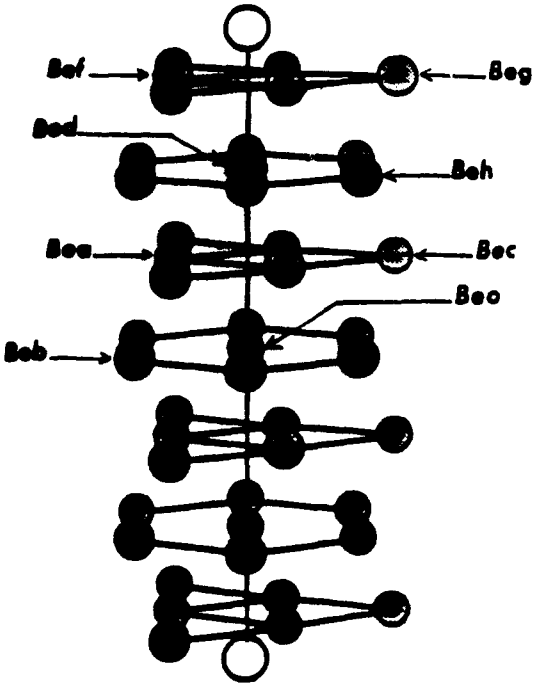


Fig. 1. $Be_{45}X_2$, X = Cs, OCs, HCs.

is shown in fig. 1. Results obtained using these systems are compared to those calculated by treating an identical bare Be cylinder. For cases where two types of adsorbates are involved (i.e., $Be_{45}O_2Cs_2$ and $Be_{45}H_2Cs_2$), no geometry optimization was performed due to the computational expense. Instead, Be–adsorbate and adsorbate–adsorbate internuclear separations correspond to van der Waals radii. Results for these systems are compared to those obtained by treating identical bare Be cylinders which have been cesiated.

Calculations were carried out on a Cray Y-MP supercomputer using [illegible] on the "equal-contribution theorem" [illegible] electron integrals [15]. Ab initio restricted [illegible] and restricted open-shell Hartree–Fock [illegible], each corresponding to an average energy [illegible] single molecular-orbital (MO) configuration, were carried out on numerous low-lying states of each cluster. (The average energy of configuration is defined as the weighted mean of the energies of all the multiplets for the configuration [16].) The calculations for the largest clusters consumed about one hour of Cray Y-MP time for each geometric orientation. The following basis sets of contracted Gaussian-type functions were used for beryllium, cesium, oxygen and hydrogen, respectively: (3s2p)/[2s1p] [17], (5s5p)/[3s2p] [18], (4s4p)/[2s2p] [19] and (4s1p)/[2s1p] [20]. Ab initio effective potentials (EP) [21] were used to represent the 1s core electrons in Be [17] and O [19] and the 1s–4s, 2p–4p, and 3d–4d core electrons in Cs [18]. Relativistic effects, especially important in Cs, were incorporated into the EPs [21].

Binding energies (BE) calculated relative to the completely dissociated clusters are given in table 1. (Valence SCF energies for atomic Be, $Be^+$, Cs, $Cs^+$, O, H and $H^-$ are −0.95083, −0.65457, −19.84225,

Table 1
Restricted Hartree–Fock energies of $Be_{45}$ and $Be_{45}X_2$ clusters

| Cluster | Occupied MOs [a] | | | | | | BE (kcal/mol) | Adsorption energy (kcal/mol atom) |
|---|---|---|---|---|---|---|---|---|
| | $a_1'$ | $a_2'$ | $a_2''$ | e' | e'' | $a_1''$ | | |
| $Be_{45}$ [b] | 8 | 2 | 7 | 7 | 6 | 2 | 1120.00 | |
| $[Be_{45}]^+$ | 8 | 2 | 7 | 7 | 6 | 2 | 1203.66 | |
| $Be_{45}Cs_2$ [b,c] | 10 | 2 | 9 | 9 | 7 | 2 | 1131.02 | 5.51 |
| $[Be_{45}Cs_2]^+$ [b] | 10 | 2 | 9 | 9 | 7 | 2 | 1266.52 | |
| $Be_{45}O_2Cs_2$ [b,d] | 12 | 2 | 11 | 9 | 8 | 2 | 1378.68 | 123.83 [e] |
| $[Be_{45}O_2Cs_2]^+$ [b] | 12 | 2 | 10 | 9 | 8 | 2 | 1520.99 | |
| $[Be_{45}H_2Cs_2]$ | 10 | 2 | 9 | 9 | 7 | 2 | 1272.94 | 70.96 [f] |
| $[Be_{45}H_2Cs_2]^+$ [b] | 10 | 2 | 9 | 9 | 7 | 2 | 1397.62 | |

[a] Underline denotes orbital from which the electron was removed. [b] State corresponds to the weighted average of configuration.
[c] Open-shell state: $(e')^1$. [d] Open-shell state: $(a_1')^1(a_2'')^1$.
[e] Adsorption energy of O on Cs-coated $Be_{45}$. [f] Adsorption energy of H on Cs-coated $Be_{45}$.

−19.72876, −15.64121, −0.49928 and −0.44815 hartree, respectively, for the basis sets used in this study.) The total adsorption energies given in table 1 for the cesiated cluster was calculated relative to the SCF energies of the naked cluster plus that of two adsorbate atoms. For $Be_{45}OCs_2$ and $Be_{45}H_2Cs_2$, energies are relative to H and O adsorbed on $Be_{45}Cs_2$.

Theoretical work function are given in table 2. The first values in each row were calculated as the difference between the total valence SCF energy of a neutral cluster and that of the ion generated by removing one electron from the highest occupied orbital of that cluster. The values immediately following are due to Koopmans' theorem and correspond to the negative of the energy of the molecular orbital (MO) from which the electron was ionized.

Atomic net electron-charge values are given in table 3 as calculated using a Mulliken population analysis [22]. Value of $R$ appearing in these tables correspond to optimum atom-to-surface distances. These distances were calculated from a curve fitted to SCF energies for at least three surface–adsorbate separations corresponding to the lowest-lying electron configuration.

The total adsorption energy for cesiated $Be_{45}$ appears in table 1 as 5.5 kcal/mol atom. As previously mentioned, this energy was calculated relative to the total SCF energies of the naked cluster plus that of the two adsorbate atoms in their ground states, and the value corresponds to an average energy of configuration. Therefore, cesium is predicted to adsorb weakly on $Be_{45}$ (i.e. at a hole site on the Be (0001) surface) at the SCF level of theory. Table 2 contains calculated values for the ionization potentials of $Be_{45}$, as well as values for the shift in ionization potential ($\Delta\Phi$) resulting from Cs, H and/or O adsorption. Experimentally determined values of the work functions due to Cs adsorption on Be metal are also included [4]. Results indicate a lowering by 2.2 eV in the ionization potential of the cluster due to Cs and H adsorption. The experimental finding is a 2.3 eV lowering in the work function of Be metal due to adsorption of Cs.

Table 2
Work functions of $Be_{45}$ and $Be_{45}X_2$ clusters

| Cluster | $\Phi$ (eV) [a] |
|---|---|
| $Be_{45}$ | 4.62, 4.43 |
| $Be_{45}Cs_2$ | 2.41, 2.19 |
| $Be_{45}O_2Cs_2$ | 1.81, 1.89 |
| $Be_{45}H_2Cs_2$ | 2.95, 2.67 |
| Be (expt.) | 3.92 |
| BeCs (expt.) [b] | 1.6 |
| $\Delta\Phi[Be_{45} - Be_{45}Cs_2]$ [c] | 2.21, 2.24 |
| $\Delta\Phi[Be_{45}Cs_2 - Be_{45}O_2Cs_2]$ [c] | 0.60, 0.30 |
| $\Delta\Phi[Be_{45}Cs_2 - Be_{45}H_2Cs_2]$ [d] | −0.54, −0.48 |
| $\Delta\Phi$[Be − BeCs]expt. | 2.3 |

[a] Where two values appear, these are Koopmans' theorem and $\Delta E$(SCF) values, respectively.
[b] Ref. [4].
[c] Values correspond to a work function lowering.
[d] Values correspond to a work function increase.

It is the surface layer of $Be_{45}$ which is predominantly involved in ionization. This layer (BeG in fig. 1) contributes 0.3 electron to the process (table 3), with Cs contributing 0.4 electron. The greatest change contributed by the inner layers is 0.2 electron (BeH in fig. 1). However, comparison of the net charge differences between $Be_{45}Cs_2$ and $Be_{45}$ indicates that the group of atoms most affected by Cs adsorption are on the surface of the cluster (BeG, fig. 1). Cs adsorption shifts the electron contributions of this layer by about 0.2 eV.

Combined oxygenation and cesiation of $Be_{45}$ result in a greater work function lowering than does cesiation alone. Oxygenation of the cesiated cluster further lowers the ionization potential by 0.3 eV for a total ionization potential lowering of 2.5 eV relative to bare $Be_{45}$ (table 2). O adsorbs strongly on cesiated $Be_{45}$, the adsorption energy being 123.8 kcal/mol atom (table 1). Net charge differences for $Be_{45}O_2Cs_2$ (table 3) indicate that cesium contributes significantly to the ionization process. In fact, cesium is donating 1.0 electron to the process, while the role of the surface layers is substantially reduced relative to cesiated $Be_{45}$. The BeG and BeF group of atoms on the surface of $Be_{45}Cs_2$ have a charge of 0.30, while the charge on the same layer in $Be_{45}O_2Cs_2$ is −0.06.

Hydrogenation and cesiation of $Be_{45}$, on the other hand, result in a rise of about 0.5 eV in the ionization potential of $Be_{45}Cs_2$ (table 2). Since cesiation of $Be_{45}$ lowers the ionization potential of the cluster by 2.2 eV, there is still a total lowering of 1.7 eV in the ionization potential of $Be_{45}H_2Cs_2$ relative to bare $Be_{45}$. The adsorption energy of H on cesiated $Be_{45}$ is 70.96 kcal/mol atom (table 1). Therefore, H ad-

Table 3
Atomic populations of $Be_{45}$, $Be_{45}Cs_2$, $Be_{45}O_2Cs_2$ and $Be_{45}H_2Cs_2$

| Cluster | Z-coord. [a] | Atom label | No. atoms [b] | Cluster net charge per atom | {Cluster}$^+$ net charge per atom | Total net charge difference ({cluster}$^+$ − cluster) |
|---|---|---|---|---|---|---|
| $Be_{45}$ | 0 | BeO | 1 | 1.01 | 1.00 | −0.01 |
| | $c/2$ | BeA | 6 | 0.42 | 0.40 | −0.12 |
| | $c/2$ | BeC | 6 | −0.20 | −0.15 | 0.30 |
| | 0 | BeB | 6 | −0.33 | −0.31 | 0.12 |
| | $c$ | BeH | 12 | −0.19 | −0.17 | 0.24 |
| | $c$ | BeD | 2 | 1.36 | 1.34 | −0.04 |
| | $3c/2$ | BeF | 6 | −0.14 | −0.14 | 0.00 |
| | $3c/2$ | BeG | 6 | 0.01 | 0.09 | 0.48 |
| $Be_{45}Cs_2$ | 0 | BeO | 1 | 0.97 | 0.97 | 0.00 |
| | $c/2$ | BeA | 6 | 0.46 | 0.45 | −0.06 |
| | $c/2$ | BeC | 6 | −0.19 | −0.17 | 0.12 |
| | 0 | BeB | 6 | −0.37 | −0.34 | 0.18 |
| | $c$ | BeH | 12 | −0.23 | −0.21 | 0.24 |
| | $c$ | BeD | 2 | 1.22 | 1.21 | −0.02 |
| | $3c/2$ | BeF | 6 | −0.06 | −0.09 | −0.18 |
| | $3c/2$ | BeG | 6 | −0.05 | 0.00 | 0.30 |
| | $R$ [c] | Cs | 2 | 0.29 | 0.51 | 0.44 |
| $Be_{45}O_2Cs_2$ | 0 | BeO | 1 | 1.01 | 1.02 | 0.01 |
| | $c/2$ | BeA | 6 | 0.48 | 0.48 | 0.00 |
| | $c/2$ | BeC | 6 | −0.19 | −0.18 | 0.06 |
| | 0 | BeB | 6 | −0.36 | −0.35 | 0.06 |
| | $c$ | BeH | 12 | −0.22 | −0.21 | 0.12 |
| | $c$ | BeD | 2 | 1.15 | 1.14 | −0.02 |
| | $3c/2$ | BeF | 6 | 0.18 | 0.16 | −0.12 |
| | $3c/2$ | BeG | 6 | −0.02 | −0.03 | −0.06 |
| | $R$ [d] | O | 2 | −0.98 | −1.00 | −0.04 |
| | $R'$ [e] | Cs | 2 | 0.34 | 0.86 | 1.04 |
| $Be_{45}H_2Cs_2$ | 0 | BeO | 1 | 0.93 | 0.94 | 0.01 |
| | $c/2$ | BeA | 6 | 0.46 | 0.45 | −0.07 |
| | $c/2$ | BeC | 6 | −0.15 | −0.12 | 0.13 |
| | 0 | BeB | 6 | −0.38 | −0.36 | 0.17 |
| | $c$ | BeH | 12 | −0.19 | −0.18 | 0.20 |
| | $c$ | BeD | 2 | 0.14 | 0.13 | −0.04 |
| | $3c/2$ | BeF | 6 | −0.08 | −0.11 | −0.17 |
| | $3c/2$ | BeG | 6 | −0.04 | 0.02 | 0.38 |
| | $R$ [f] | H | 2 | −0.11 | −0.12 | −0.02 |
| | $R'$ [g] | Cs | 2 | 0.23 | 0.44 | 0.42 |

[a] $c = 3.58$ Å. [b] No. of symmetry equivalent atoms. [c] $R = 3.70$ Å for Be plane to Cs distance. (Be to Cs distance is 3.93 Å.)
[d] $R = 1.50$ Å for Be plane to O distance. (Be to O distance is 2.0 Å.) [e] $R' = 3.1$ Å for O to Cs distance.
[f] $R = 0.86$ Å for Be plane to H distance. (Be to H distance is 1.58 Å.) [g] $R' = 2.2$ Å for H to Cs distance.

sorbs more than twice as strongly on cesiated $Be_{45}$ than on bare $Be_{45}$. Net charge differences appearing in table 3 indicate that hydrogenation of $Be_{45}Cs_2$ has little effect on the ionization process. The net charges on hydrogenated $Be_{45}$ are nearly the same as those on cesiated $Be_{45}$, with the greatest change occurring for the BeG group of atoms on the surface (0.30 electron versus 0.38 for $Be_{45}Cs_2$ versus $Be_{45}H_2Cs_2$, respectively).

Net-charge per atom values shown in table 3 for

each Cs of neutral $Be_{45}Cs_2$ ($Be_{45}O_2Cs_2$) indicate that the interaction between these atoms and the naked (oxygenated) surface is more covalent in nature, with the charge polarized inward toward the surface. This is in agreement with previous theoretical [8] and recent experimental [9] data for alkali adsorption on metal surfaces. This polarization is more pronounced for the interaction of Cs with the oxygenated surface. The same phenomenon prevails for the charged systems. However, in these cases it is more pronounced, especially for the oxygenated surface, where the net charge per atom value of 0.9 indicates an ionic interaction between the Cs and the oxygenated surface. As expected, the oxygen atoms on both the neutral and charged species are highly electronegative. The smallest dipole between the cesium atoms and the surface of both the neutral and ionized system exists for the hydrogenated surface, although the difference is quite small. It is noteworthy that the dipole interaction between Cs and the surface is greatest for the system having the lowest work function, namely the $Be_{45}O_2$ surface, and smallest for the system having the highest work function, i.e. the hydrogenated $Be_{45}$ surface.

This research was supported in part by a grant from the National Science Foundation under Grant No. CHE-8712674 and by a grant from the Air Force Office of Scientific Research. Grants of Cray Y-MP time at the Ohio State Supercomputer Center and the Pittsburg Supercomputer Center are acknowledged.

## References

[1] J.B. Taylor and I. Langmuir, Phys. Rev. 44 (1933) 423.
[2] L.W. Swanson and R.W. Strayer, J. Chem. Phys. 48 (1968) 2421.
[3] R.E. Weber and W.T. Peria, Surface Sci. 14 (1969) 13.
[4] G.S. Tompa, M. Seidl, W.C. Ermler and W.E. Carr, Surface Sci. 185 (1987) L453.
[5] M. Kiskinova, G. Rangelov and L. Surnev, Surface Sci. 172 (1986) 57.
[6] M. Seidl and A. Pargellis, Phys. Rev. B 26 (1982) 1.
[7] I. Langmuir, J. Am. Chem. Soc. 54 (1932) [illegible].
[8] E. Wimmer, A.J. Freeman, J.R. Hiskes, [illegible], Karo, Phys. Rev. B 28 (1983) 3074.
[9] D.M. Riffe, G.K. Wertheim and P.H. Citrin, Phys. Rev. Letters 64 (1989) 574.
[10] I. Panas, P. Seigbahn and U. Wahlgren, in: ACS Symp. Ser. 394, The challenge of d and f electrons, theory and computations, eds. D.R. Salahub and M.C. Zerner (Am. Chem. Soc., Washington, 1989);
W. Ravenek and F.M.M. Geurts, J. Chem. Phys. 84 (1986) 1613.
[11] G. Angonoa, J. Koutecký, A.N. Ermoshkin and C. Pisani, Surface Sci. 138 (1984) 51;
P.S. Bagus, H.F. Schaefer III and C.W. Bauschlicher Jr., J. Chem. Phys. 78 (1983) 1390.
[12] M.M. Marino and W.C. Ermler, unpublished results.
[13] M.M. Marino, W.C. Ermler, G.S. Tompa and M. Seidl, Surface Sci. 208 (1989) 189.
[14] R.G. Wyckoff, Crystal structures, 2nd Ed. (Interscience, New York, 1974).
[15] R.M. Pitzer, J. Chem. Phys. 58 (1973) 3111, and private communication.
[16] J.C. Slater, Quantum theory of atomic structure, Vol. I (McGraw-Hill, New York, 1960).
[17] W.C. Ermler, C.W. Kern, R.M. Pitzer and N.W. Winter, J. Chem. Phys. 84 (1986) 3937.
[18] R.B. Ross, T. Atashroo, J.M. Powers, W.C. Ermler, L.A. LaJohn and P.A. Christiansen, J. Chem. Phys., in press.
[19] L.F. Pacios and P.A. Christiansen, J. Chem. Phys. 82 (1985) 2665.
[20] T.H. Dunning Jr., J. Chem. Phys. 53 (1970) 2823; 55 (1971) 3958.
[21] W.C. Ermler, R.B. Ross and P.A. Christiansen, Advan. Quantum Chem. 19 (1988) 139.
[22] R.S. Mulliken, J. Chem. Phys. 23 (1955) 1833.

# Imaging of Colloidal Gold on Graphite by Scanning Tunneling Microscopy: Isolated Particles, Aggregates, and Ordered Arrays

**J. F. Womeldorf,* W. C. Ermler,***

*Department of Chemistry and Chemical Engineering and Department of Physics and Engineering Physics, Stevens Institute of Technology, Hoboken, New Jersey 07030*

**and C. J. Sandroff***

*Bellcore, Red Bank, New Jersey 07701* *(Received: August 7, 1990; In Final Form: November 16, 1990)*

Gold colloidal suspensions have been deposited onto highly oriented pyrrolitic graphite and analyzed by using a scanning tunneling microscope (STM). The size distribution of individual particles measured with the STM (16 ± 1.5 nm) agreed well with measurements made by transmission electron microscopy. STM images of colloidal aggregates containing up to 15 individual particles could be obtained under a wide variety of experimental conditions. The quality of these images was extremely sensitive to the type of aggregating agent used, with ionic salts giving better results than molecular species. Under our colloidal deposition conditions we often observed highly ordered hexagonal patterns with a periodicity of 75–150 nm, extending over areas as large as 150 × 150 nm$^2$. Preliminary evidence suggests that this hexagonal lattice is associated with the graphite substrate itself, and not with an ordered, two-dimensional array of colloidal particles.

Perhaps the most significant advantage of the scanning tunneling microscope (STM) over other surface science tools is its ability to scan large areas of a surface and to probe local, nonperiodic structures with atomic scale resolution. This feature is of great utility in searching for adsorbed chemical species ranging from molecules[1] to metallic and semiconductor clusters.[2-6] Metallic clusters adsorbed on graphite have had a special appeal for STM workers[2-4] because they are easily produced, are relatively robust, and are readily differentiated from the graphite substrate through their tunneling characteristics.

Encouraged by the STM results on small metal clusters, we began to explore the properties of larger metallic systems—colloidal particles—deposited on the surface of highly ordered pyrolytic graphite (HOPG). In principle, many important features of colloids could be understood by exploiting the atomic resolution achievable with the STM. For example, local variation of the electrical double layer surrounding colloidal particles, and the geometry of adsorbed molecular species on colloidal surfaces, are

(1) Hallmark, V. M.; Chiang, S.; Rabolt, J. F.; Swalen, J. D.; Wilson, R. J. *Phys. Rev. Lett.* **1987**, *59*, 2879.
(2) Abraham, D. W.; Sayyler, K.; Ganz, E.; Mamin, H. J.; Thomson, R. E.; Clarke, J. *J. Appl. Phys. Lett.* **1986**, *49*, 853.
(3) Ganz, E.; K. Sattler, K.; Clarke, J. *J. Vac. Sci. Technol.* **1988**, *A6*, 419.
(4) Baro, A. M.; Bartolome, A.; Vazquez, L.; Garcia, N.; Reifenberger, R.; Choi, E.; Andres, R. P. *Appl. Phys. Lett.* **1987**, *51*, 1594.
(5) Sarid, D.; Henson, T.; Bell, L. S.; Sandroff, C. J. *J. Vac. Sci. Technol.* **1988**, *A6*, 426.
(6) Jing, T. W.; Ong, N. P.; Sandroff, C. J. *Appl. Phys. Lett.* **1988**, *53*, 1104.

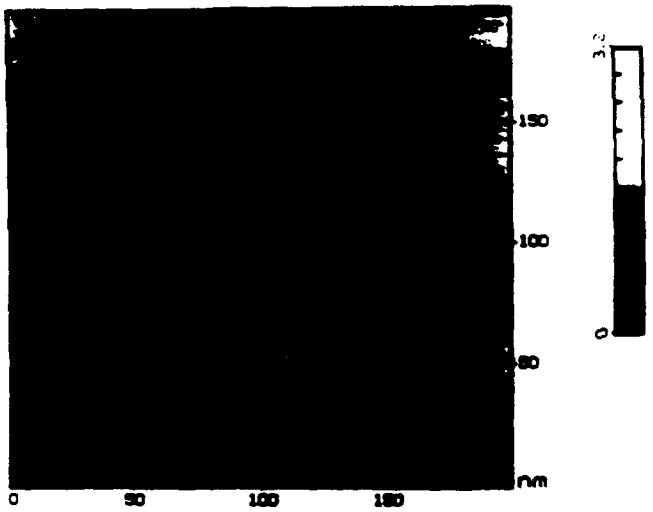


**Figure 1.** STM image of isolated colloidal gold particles on a HOPG surface. The average size of the colloids is 15 nm. The spiky noise in the image is believed to come from salts which precipitate on the graphite surface during the deposition of the colloids.

particularly relevant in the science and technology of dispersed systems.

In this Letter we report some initial STM results from colloidal gold deposited onto HOPG. For a number of reasons, the gold system is an ideal starting point for determining the utility of the STM in colloid science. Not only do simple chemical syntheses produce small particles with a narrow size distribution,[7] but both the aggregation behavior and surface chemistry of the gold particles have been explored in considerable detail.[8-10]

Our aqueous gold colloids were prepared through the chemical reduction of sodium tetrachloroaurate using trisodium citrate according to a modified synthesis[8] first reported by Hillier et al.[7] This recipe results in the formation of stable gold particles with a mean diameter of ~15 nm. These colloidal suspensions remain dispersed for many months, presumably stabilized by citrate ions strongly chemisorbed to the colloid surface.

Because the aqueous gold suspension does not wet the graphite, we found it necessary to modify the HOPG surface in order to obtain a sample surface which was uniformly coated with isolated, unaggregated colloidal particles. This modification was achieved by placing a small drop of 1-propanol on the graphite surface prior to depositing the gold sol. We found that surfaces treated with the alcohol could be partially dried under vacuum with no apparent loss in wetting efficiency.

All of our tunneling images were obtained with an STM operating in air at room temperature.[11] To isolate the system from low-frequency vibrations, the sample head was placed on a 50-kg anvil suspended by rubber cords stretched to approximately twice their equilibrium length. We used Pt/Ir STM tips, and operated the microscope at biases of −500 mV to +500 mV and tunneling currents of ~1 nA in the constant height mode. To ensure that the STM was operating optimally, we would first scan the graphite surface under conditions which allowed us to resolve atomic features on the graphite surface. We would then scan over the surface in search of gold particles.

Figure 1 displays the typical appearance of a colloid-covered HOPG surface scanned by the STM under these conditions. The scan reveals a high density of particles on a flat HOPG background. The stability and brightness of the STM images indicate the presence of conductive metallic particles strongly adsorbed on the HOPG substrate.

To confirm that these images were of gold colloids and not random adsorbed impurities or graphite artifacts, we measured the dimensions of the particles in the $xy$ direction (parallel to the graphite substrate) with the STM. This measurement gave an average particle diameter of ~16 ± 1.5 nm. Considering that tip–cluster interactions can change the apparent size of measured features,[4] this diameter is excellent agreement with the 14.5-nm colloid diameter measured by TEM in this and in previous work.[8]

Though $xy$ scans with the STM accurately reflected gold particle diameters, we found that the height mode was not quantitatively reliable. Generally, the STM gave particle heights in the $z$ direction varying between 1.0 and 2.0 nm, a dimension considerable smaller than the 15-nm gold particle diameter. We believe that the contracted dimension in the $z$ direction is a result of operating the microscope in the constant height mode rather than a flattening of the gold colloid particle on the graphite surface. Hence dimensions measured by tunneling are more reliable in the $xy$ than in the $z$ direction, and we conclude that the STM can be used as a reliable and semiquantitative tool for measuring the shape and dimensions of colloidal metallic particles deposited on conducting substrates.

After our initial characterization of single, isolated colloidal particles with the STM, we began to explore the properties of colloidal aggregates. The particles were aggregated by adding 1–3 drops of 1 M NaCl or 1 M $NaClO_4$ to 5 $cm^3$ of the colloidal suspension. After the addition of the salt solutions, the wine-red Au suspension turned blue, indicating that the small aggregates of gold were beginning to form.[7] At this stage several drops of the suspension were deposited onto a freshly cleaved HOPG substrate and evacuated to dryness. The water was removed at a reduced pressure of $10^{-3}$ Torr without allowing the sol to solidify and sublime. As described earlier, we modified the graphite surface with 1-propanol and deposited the aggregates both at ambient temperatures and at 110 °C. Elevated temperatures did not change the structure or distribution of aggregates but did speed up the removal of solvent and propanol.

Figure 2 shows typical STM and TEM images of colloidal gold aggregates flocculated under these conditions. Samples for TEM analysis were obtained by depositing the colloids on carbon-coated copper grids. The STM images of the flocculated colloid are very similar to the appearance of the aggregates by TEM: the individual particles appear to be physically touching but rarely fused together. As with the isolated particles the aggregates were stable for periods of several hours, and they could be imaged under a wide variety of bias conditions with little effect on their appearance.

One of the most important issues in colloid science concerns the nature of the electric double layer which provides the repulsive Coulombic barrier that keeps the particles in suspension. We hoped to use the STM to study the local character of the double layer by aggregating the colloids with different flocculating agents. For example, ionic salts are known to induce aggregation by causing the collapse of the diffuse double layer surrounding each colloidal particle, while molecular adsorbates are thought to cause aggregation by displacing more weakly bound charged species from the colloid surface. These different agents should produce colloidal surfaces with significantly different electrical and molecular characteristics.

Though flocculating with ionic salts produced aggregates with excellent tunneling characteristics, we were not as successful with the molecular flocculating agent, tetrathiafulvalene (TTF).[12] In fact we never obtained stable STM images from colloids flocculated with TTF, even though TEM micrographs show that these aggregates are identical with those aggregated with salt. We speculate that adsorbed TTF forms an insulating barrier around the colloid surface that prevents tunneling from occurring. Thus, to obtain the best STM images of flocculated colloids, it seems necessary to aggregate with ionic agents which screen the Cou-

(7) Hillier, J.; Turkevitch, J.; Stevenson, P. C. *Trans. Faraday Soc.* **1951**, 55

(8) Weitz, D. A.; Lin, M. Y.; Sandroff, C. J. *Surf. Sci.* **1985**, *158*, 147. The concentration of sodium citrate used in the synthesis of the gold colloids is incorrect in this reference. It should be $10^{-2}$ M not $10^{-3}$ M.

(9) Creighton, J. A.; Blatchford, C. G.; Albrecht, M. G. *J. Chem. Soc., Faraday Trans. 2* **1979**, *75*, 790

(10) Sandroff, C. J.; Herschbach, D. R. *Langmuir* **1985**, *1*, 73

(11) Nanoscope II, Digital Instruments, Inc., 6780 Cortona Drive, Santa Barbara, CA 93117

(12) Deckman, H. W.; Dunsmuir, J. H.; Ingersoll, S. M. *Tennol. B* **1983**,

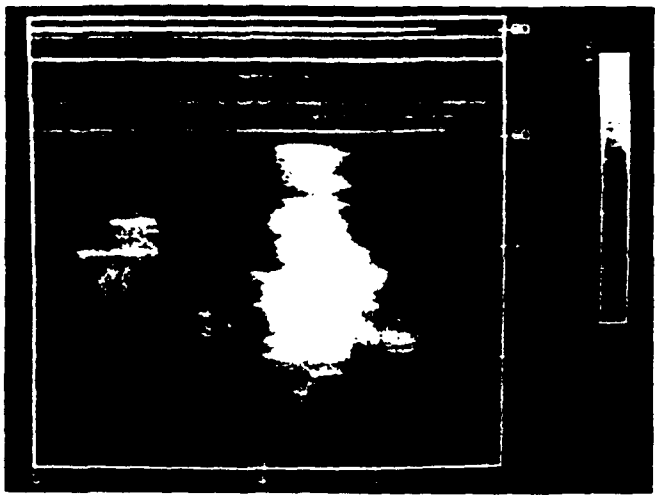


**Figure 2.** STM and TEM images of colloidal gold aggregates. (a, top) STM image on graphite; (b, bottom) TEM image on carbon-coated copper grid. The colloid sizes were found to be ~15 nm by both techniques.

ombic interaction between particles without hindering the tunneling process.

While exploring the properties of colloidal aggregates we often noticed that the STM images contained sharp spikes. Believing these were due to the presence of codeposited salts, we treated the aggregated suspensions with ion-exchange resin[3] to reduce the concentration of ions in solution. Figure 3 displays a remarkable STM image obtained after the aggregated colloids were treated with ion-exchange resin. This image consists of roughly 50 "atoms" which have assumed a highly ordered hexagonal array that measures 150 nm × 150 nm. Each of the "atoms" in the lattice has a diameter of ~14 nm, and a two-dimensional Fourier transform identified the lattice constant to be ~24 nm.

Since previous work had demonstrated that charged colloidal particles deposited from solution onto smooth surfaces can sometimes crystallize in hexagonal lattices,[4] we originally associated these STM images with our sols with each "atom" identified as a single gold particle. However several characteristics of the arrays argue against their being lattices of colloidal gold particles. First, the individual particles are extremely uniform

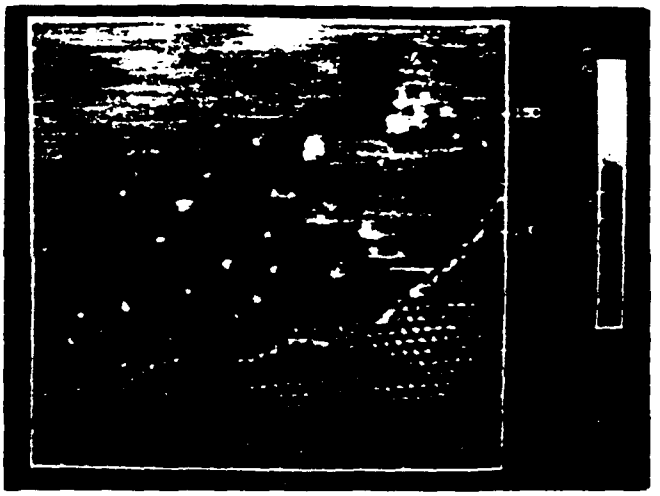

**Figure 3.** STM image of anomalous long-range order on graphite. The periodicity of the hexagonal array was 7.5 nm and it extended over an area of ~150 × 150 nm². The arrays were always observed near a terrace like the one seen in the lower part of the figure.

in size, much more uniform than isolated particles appear when seen by either TEM or STM. Also the particles in the lattice do not conduct as much current as isolated gold particles do under identical experimental conditions. Finally, images qualitatively similar to those in Figure 3 were obtained after the deposition of colloidal dispersions which were not treated with ion-exchange resin. Under these circumstances the ionic strength of the sol is high, and the long-ranged Coulombic forces necessary to induce two-dimensional crystallization should not be present.

We speculate that this highly regular lattice is associated with the graphite substrate itself. Indeed similar images have been obtained from graphite surfaces after the deposition of organic salts from solutions which contained no dispersed particles.[5] Moreover, very recent studies of graphite surfaces by STM have appeared, and almost identical images were obtained where no deliberate adsorption of material occurred.[6] Kuwabara et al.[6] argue that the anomalous long-range order seen on graphite can be attributed to Moiré interference between two slightly misoriented layers of graphite. However, it is possible that several mechanisms are operating simultaneously to give rise to the long-range order on graphite. Indeed, preliminary computer simulations show that anomalous long-range order can develop when a graphite flake picked up by the tip slides across the graphite substrate.

In conclusion, we have shown that the STM can be used with some confidence in the study of the properties of metal colloids. The physical dimensions of colloidal particles can be measured with reasonable accuracy in the plane of the substrate, and large aggregates can be readily images so long as electrically insulating molecules are not adsorbed on the colloid surface. Under some conditions it is possible to observe highly ordered hexagonal arrays on graphite surfaces. Although the origin of this array is not well understood, we believe it is a phenomenon associated with the graphite surface itself. Since the lattice parameter of the ordered array is comparable to the size of colloidal particles, it is important to exercise care when using the STM to study colloids or other macromolecular species adsorbed on graphite surfaces.

*Acknowledgment.* We thank R. S. Robinson for helpful criticism. This research was supported in part by the National Science Foundation under grant CHE-8912674 and by a grant by the Air Force Office of Scientific Research.

[3] We found that unaggregated sols were not ion-exchange resin [illegible]

[4] Sanders, J. V. [illegible] Discuss. Faraday Soc. 1951, 11, 264.

[5] Evans, J. W.; Hubacek, J. S.; Trammell, G. T.; Skala, S.; Brucker, G. P.; Shanes, J. G.; Keyes, M. P. J. Vac. Sci. Technol. 1988, A6, 45.

[6] Kuwabara, M.; Clarke, D. R.; Smith, D. A. Appl. Phys. Lett. 1990, [illegible]

Surface Science Letters 241 (1991) L11–L15
North-Holland



Surface Science Letters

# Scanning tunneling microscopy: a critical view of tip participation

J.F. Womelsdorf [a], M. Sawamura [a] and W.C. Ermler [a,b]

[a] Department of Chemistry and Chemical Engineering, [b] Department of Physics and Engineering Physics, Stevens Institute of Technology, Hoboken, NJ 07030, USA

Received 17 July 1990; accepted for publication 21 September 1990

A model for the scanning tunneling microscope (STM) experiment is presented which explicitly treats the STM tip as a polyatomic crystalline surface. The net tunneling current is the sum of all tunneling occurrences from each tip atom to every substrate atom. With the aid of computer simulations, the atomic resolution of an hexagonally close-packed substrate with a nearest neighbor distance of 0.245 nm is reproduced using an hexagonally close-packed tip with a nearest neighbor distance of 0.277 nm. The resulting periodicity of the image is independent of tip size. The recent observations of anomalous long range periodicity is explained by employing the model in a simulation of a 2.7 nm super lattice.

Since its introduction [1,2], scanning tunneling microscopy (STM) has found immediate acceptance as a powerful tool for surface analysis. Current and future applications of this technology is highly dependent on our understanding of the measurement technique. This Letter presents a new model for describing the STM experiment based on mutual scanning between the tip and surface. This model of the STM experiment is shown to reproduce atomic resolution of ordered surfaces, as well as provide a general explanation of anomalous long range periodicity that has been recently observed [3–5].

As a first approximation, it is generally believed [6] that the STM current image results from an electron of a lone tip atom tunneling to a single surface atom when an external bias potential of appropriate sign is applied. The exponential dependence of tunneling current on both interatomic distance and barrier height of the tunneling electron selects for a single dominant tunneling pathway. This results in the ability to map out the electron orbital charge density of the surface as a function of tunneling current when a tip is scanned parallel to the surface. This mechanism, although it correctly explains many phenomena associated with STM images, does not predict the long range periodic structures that are often observed [3–5].

We propose a new interpretation of the STM experiment for tunneling to an ordered surface such as highly oriented pyrolytic graphite (HOPG) from a metal tip having a close-packed structure. The proposed mechanism is predicated on the following STM experimental model. Firstly, that microscopically, a pure metal tip is crystalline with the (111) surface dominating in many cases. Secondly, that it is possible that tunneling can occur from every tip atom to every surface atom. The net tunneling current is initially assumed to be a simple summation of all individual tunneling occurrences which are assumed to be independent and behave according to the Tersoff and Hamann equations [7–9]. Finally, defects and step edges that posses lower barrier heights than their corresponding bulk surfaces will appear as adatoms and contribute uniquely to the resulting image.

The modeling of a sharp metal tip as an ordered crystal surface is a logical assumption based on the following developments. Iijima et al. [10] have observed large metal clusters containing over 1000 atoms which maintain single crystal structure with a tendency to maximize the (111) surface area

under TEM experimental conditions ($1.3 \times 105$ electrons per ångström per second). Clusters of as few as 500 atoms experienced frequent rearrangement to new single crystal structures. This work suggests that even under highly energetic conditions large close-packed metal clusters are crystalline. This work has been confirmed by Malm et al. [11]. Trevor et al. [12] observed that metal surfaces which have undergone electrochemical oxidation/reduction similar to some STM tip preparations tend to minimize defects, holes, and step edges preferring to maximize crystal plane areas. Perhaps the most compelling evidence for a planer tip comes from work done by Colton et al. [13]. This group showed that graphite pencil lead or graphite coated tungsten could be used as an STM tip to reproducibly image HOPG with atomic resolution. Finally, the STM experiment itself has failed to show that pure metal surfaces contain stable adatoms under STM experimental conditions. This conclusion is based on the lack of published data supporting the presence of adatoms on pure metal surfaces under STM conditions. It is therefore logical that the tip be treated on the same footing as any other close-packed metal. In fact, the distinction between tip and substrate is purely configurational having no special significance when considering the relative motion and interactions between the two surfaces.

The net tunneling current from the (111) surface of a metal tip to a coplaner (111) surface of a metal substrate is given by

$$I_{\text{total}} = \sum_i \sum_j I_{ij}(i, j), \tag{1}$$

$$I_{ij}(i, j) = A \exp\left\{-a\left[(x_{ij} - x_{lk})^2 + (y_{ij} - y_{lk})^2 + (z_{ij} - z_{lk})^2\right]^{1/2}\right\}. \tag{2}$$

where eq. (1) is a simple summation over all tip/surface tunneling currents and (2) is Tersoff and Hansma's familiar result [7,9]. As the tip is moved to a new position this current varies. Since both surfaces, which can initially be considered infinitely extended in parallel planes, inherently posses translational symmetry in both the $x$ and $y$ directions, the net current is periodic having a period related to the smaller atomic spacings.

This can be exemplified using the following gedanken experiment. Consider two coplaner infinite lattices that are superimposed on each other with one lattice translated with respect to the other in the lattice plane. An observer could then record, at some finite interval in the plane, a unique set of images for each of the configurations as one lattice is translated a distance corresponding to the period of the smaller lattice spacing. Due to the translational symmetry of the two lattices, each subsequent set of images would be identical to the initial set. In fact, since the direction of the translation is arbitrary, only the first half of the images of the initial set will be unique.

Consider next the STM experiment. It is known that as a crystal surface of a tip is scanned across a crystal surface of a substrate, the periodicity corresponding to the smaller atomic periodicity (substrate or tip) will be imaged. Furthermore, it is known that HOPG contains two inequivalent carbon sites [14] resulting in the STM image dominated by the tunneling contribution of one of these atoms. Fig. 1 reports the results of a series of two dimensional simulations where a multi-atom tip (with the nearest neighbor distance 0.277 nm corresponding to platinum) has scanned a 25 atom substrate (with nearest neighbor distance of 0.245 nm corresponding to the beta–beta carbon distances in HOPG). Within the constraints of the independent multiple tunneling assumption, described above, it is evident that multiple atom tips do not necessarily yield multiple images. It is clear from these two dimensional cross sections that the multi-atom tip, with a larger interatomic distance, correctly reproduces the simulated current image of HOPG. The simulation was simplified using a straight forward reduction of variables [16] and performed in a constant height mode in keeping with recent experimental observations [5]. Fig. 1 shows that neither the atomic periodicity nor the corrugation amplitude is effected by tip size.

If the surface, with the smallest atomic spacing, contains a defect which results in a lower barrier height than that of the bulk surface [15], a long range hexagonally close-packed image with a periodicity much larger than the substrate is observed. This results from the surface-to-defect tunneling path of the large atomically spaced surface to the

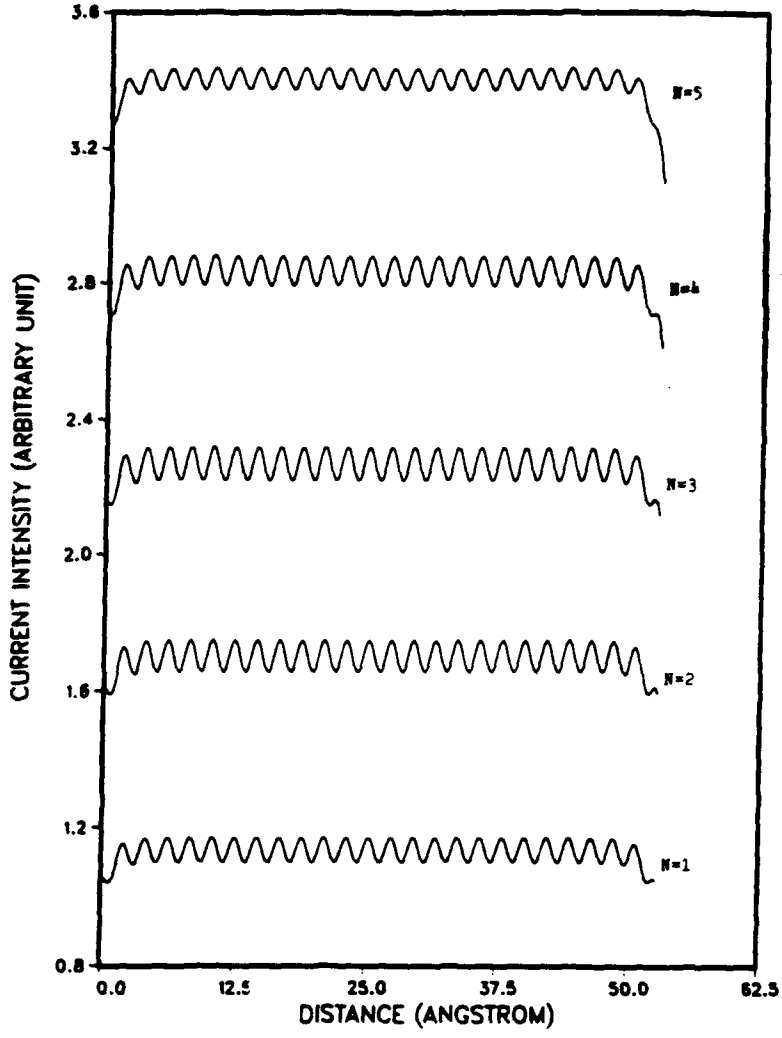


Fig. 1. A two-dimensional cross section of a simulated STM constant height image as a function of tip size. The number of tip atoms, which are separated by 0.277 nm, is indicated next to each curve. The substrate is represented by 25 atoms separated by 0.245 nm. Note that a multiple atom tip does not necessarily produce a multiple image under this independent tunneling assumption. The edge distortions are caused by over scanning the substrate surface.

surface defect of the smaller atomically spaced surface. In essence, the defect scans the larger lattice of the surface as the tip translates across the substrate. Therefore, the image of the tip is added to the net current image as produced by the defect. Since the defect must result in a lower barrier height in order to act as a pseudo-tip, it contributes significantly to the net current image. Thus, the resulting STM image is the *superposition* of both the tip and substrate images. Fig. 2 exhibits a simulation of the image due to a 35 × 15 atom hexagonally close-packed tip scanning a 35 × 15 hexagonally close-packed substrate which contains a single defect.

The superposition of the tip and substrate image can result in a variety of large, long range periodicities. This is because the $xy$-plane of the tip will be oriented at an angle $\eta$ ($0 < \eta < 30°$) relative to the $xy$-plane of the surface. The intensity of the resulting image varies as a function of the

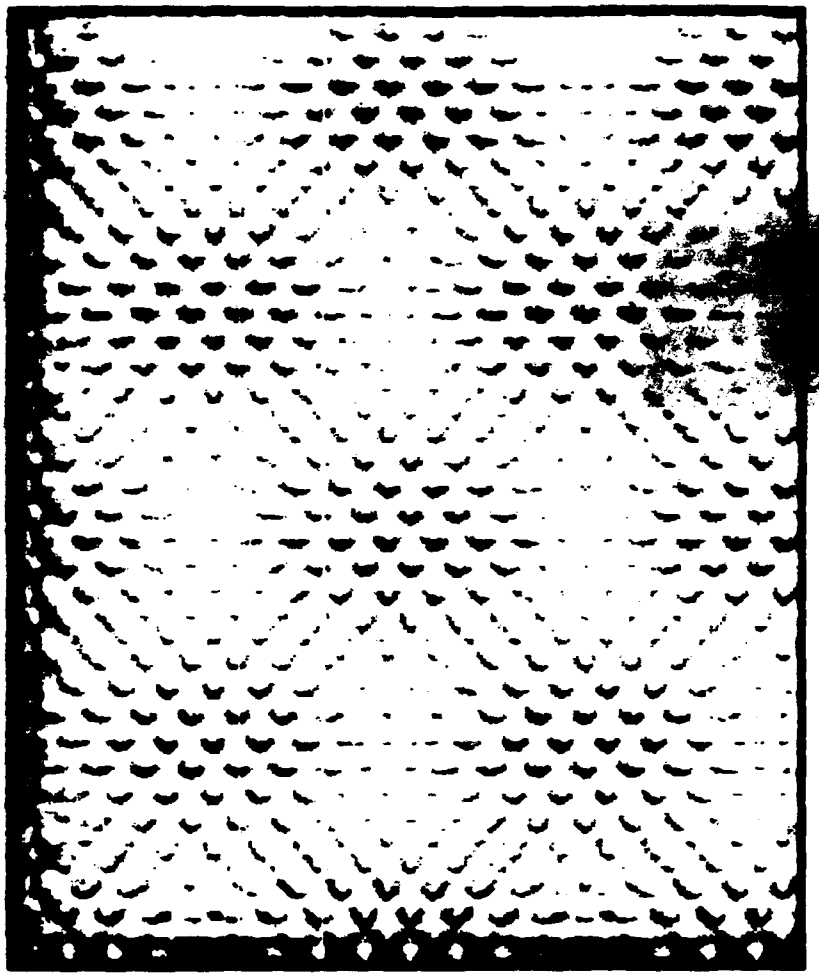

Fig. 2. Long range periodicity simulated by the superposition of a (111) fcc surface with a nearest neighbor distance of 0.277 nm which is coplanar and rotated by $\eta = 0°$ with respect to an hexagonal latuce with a nearest neighbor distance of 0.245 nm. The image is 3.82 by 8.58 nm. and clearly shows a long range periodicity of approximately 2.87 nm. (The apparent compression of the hexagonal structure in the image is due to the graphical output device and is not a feature of the data.)

phase of the two images. which is a function of their atomic surface periodicities as well as the angle $\eta$ between them.

Long range periodic structures on graphite have been previously reported [3,4]. In many cases. these structures have been observed to be associated with graphite defects [3–5]. In our experience they usually can be associated with basal plane step edges [5]. The carbon atoms lying at step edges are unique with respect to bulk graphite carbon atoms due to their unfilled (open-shell) atomic orbital. If those step edge atoms have significantly different ionization potentials in comparison to the defect free graphite. they should logically constitute low barrier height defects. Hence. what appears in some STM images to be long range periodicity can be produced by point defects located at basal plane step edges.

Although we have chosen to investigate the special case of a coplanar tip and substrate. we do not wish to imply that this is representative of the STM experiment in general. Clearly the effects of non-coplanarity need to be investigated in a more thorough study. However. the reader is reminded

that the anomalous long range corrugations such as those reported to be associated with HOPG [3,5] are also special case images which are not representative of the typical graphite surface. Furthermore, the restrictive condition that the STM tip contain a large planar surface can be lessened by recognizing that STM tips have been shown to adsorb large HOPG flakes [17] which are inherently planar.

We do not disagree that many STM experiments can be modeled by assuming a single atom tip. This is reasonable since a microscopically crystalline tip will have edges and corners and it is unlikely that the substrate will be coplaner with a crystal face of the tip. However, since most tips are made of bulk material (tungsten or platinum wire, for example) and upon initial current flow there exists sufficient energy, possibly due to resistive heating, for the tip to anneal to its lowest energy interatomic orientation. It is still unclear if a planar tip will be unable to reproduce sharp step images as some have suggested. It is also unclear to what extent the coplanar configuration can be relaxed such that long range periodicity can still be produced. However, we have shown that a multi-atom crystal domain STM tip can explain both atomic periodicity and the anomalous long range order often observed on graphite.

This research is supported in part through the Air Force Office of Scientific Research and by the National Science Foundation under grant No. CHE-8912674. We are also grateful to Professor D.M. Kalyon and Dr. J. Wang for access to the graphical facilities used in preparation of this manuscript.

## References

[1] G. Binnig, H. Rohrer, Ch. Gerber and E. Weibel, Phys. Rev. Lett. 49 (1982) 57.
[2] G. Binnig, H. Rohrer, Ch. Gerber and E. Weibel, Appl. Phys. Lett. 40 (1982) 178.
[3] M. Kuwabara, D.R. Clarke and D.A. Smith, Appl. Phys. Lett. 56 (1990) 2396.
[4] J.W. Lyding, J.S. Hubacek, G. Gammie, S. Skala, R. Brockenbrough, J.R. Shapley [illegible] J. Vac. Sci. Technol. A 6 (1988) 363.
[5] J.F. Womelsdorf, W.C. [illegible] unpublished.
[6] R.J. Hamers, Annu. Rev. Phys. Chem. 40 (1989) 531.
[7] J. Tersoff and D.R. Hamann, Phys. Rev. Lett 50 (1983) 1998.
[8] J. Tersoff and D.R. Hamann, Phys. Rev. B. 31 (1985) 805.
[9] N.D. Lang, Phys. Rev. B. 34 (1986) 5947.
[10] S. Iijima, in: Microclusters, Eds. S. Sugano, Y. Nishina and S. Ohnishi (Springer, Berlin, 1987) p. 186.
[11] J.-O. Malm and J.-O. Bovin, Surf. Sci. 200 (1988) 67.
[12] D.J. Trevor, C.E.D. Chidsey and D.N. Loiacono, Phys. Rev. Lett. 62 (1989) 929.
[13] R.J. Colton, S.M. Baker, R.J. Driscoll, M.G. Youngquist, J.D. Baldeschwieler and W.J. Kaiser, J. Vac. Sci. Technol. A 6 (1988) 349.
[14] G. Binnig, H. Fuchs, Ch. Gerber, H. Rohrer, E. Stoll and E. Tosatti, Europhys. Lett. 1 (1986) 31.
[15] B. Krahl-Urban, H. Wagner and R. Butz, Surf. Sci. 93 (1980) 423.
[16] The reduction of variables was accomplished as follows. The distance term in the exponent was expressed in Cartesian coordinates. Since the simulation was performed in constant height mode, the constants in the exponential (height, work function, etc ...) were grouped together and set arbitrarily equal to one as was the pre-exponential factor. This simplification was employed since the low bias tunneling relationships, previously derived by Tersoff and Hamann (ref. [8,10]) are assumed to be correct. It was found that assigning to the exponential constant values between 0 and 100 simply scales the z-component (i.e. amplitude) of the image. We found this simplification acceptable since corrugation amplitude is not the focus of this study.
[17] T. Tiedje, J. Varon and J. Stokes, J. Vac. Sci. Technol. A 6 (1988) 372.

# Ab Initio Study of the Electronic Spectrum of a $Cs_{11}O_3$ Cluster

Ping Wang

Department of Chemistry and Chemical Engineering

Stevens Institute of Technology

Hoboken, New Jersey 07030

and

Walter C. Ermler

Department of Chemistry

The Ohio State University

Columbus, Ohio 43210

(J. Chem. Phys., accepted 2/11/91)

**ABSTRACT**

Geometries and electronic states of the cesium suboxide cluster $Cs_{11}O_3$ are investigated using ab initio Hartree-Fock calculations. Relativistic effective core potentials are employed to represent core electrons in the atoms while Gaussian-type orbital basis sets are used to describe the valence electrons. Interatomic distances are optimized for the ground electronic state. The workfunction of $Cs_{11}O_3$ is calculated as 0.65 eV, in excellent agreement with an experimentally determined value of 0.7 Ev for bulk cesium suboxide. Mulliken populations of negatively charged and neutral $Cs_{11}O_3$ clusters have been calculated and indicate that upon ionization the emitted electron exits a molecular orbital encompassing the outermost cesium layer of the cluster.

*Permanent address of Walter C. Ermler

electron spectroscopy by de-excitation of metastable noble gas atoms (MDS) to follow the continuous oxidation of cesium films.[8] This group applied UPS for a finite information depth and MDS for the properties of the outermost atomic layer. The experimental results show that small [illegible] of $O_2$ cause the formation of a "monoplane" of $Cs_{11}O_3$ [illegible]ich $O^{2-}$ ions are incorporated below the surface, while the surface itself consists solely of Cs atoms. The workfunction of $Cs_{11}O_3$ is decreased in comparison to pure Cs metal. A theory of the workfunction of cesium suboxide and a model of its electronic structure was proposed by Burt and Heine[9] based on Simon's studies of the crystallography of cesium suboxide.[10] They determined that a substantial drop in workfunction is to be expected in going from Cs to $Cs_{11}O_3$ due to changes in boundary conditions on the conduction electrons.

The present work investigates a cesium suboxide cluster $Cs_{11}O_3$ using ab initio calculations. The geometry of the cluster in low-lying electronic states is studied. The workfunction of the cluster is calculated and Mulliken populations are analyzed.

## II. CALCULATIONS

The average relativistic effective potentials (AREP)[11] for oxygen were obtained from Pacios and Christiansen.[12] They used a refined version of the Dirac-Fock based

relativistic effective core potential procedure of Lee, Ermler and Pitzer[13] to compute AREP's of Li through Ar. They also reported small optimized Gaussian-type orbital (GTO) basis sets for the valence electrons of Li through Ar. The AREP and Gaussian-type basis set used for cesium were taken from Ross et al.[14]

2-electron core and 6-electron valence spaces for oxygen and 46-electron core and 9-electron valence spaces for cesium were chosen. In cesium, the five s-type and five p-type GTO's are contracted to three s- and two p-type functions, respectively.

In the RHF calculations, one- and two-electron matrix elements involving symmetry-adapted linear combinations of GTO's were calculated using "equal contribution" integral program of Pitzer and Hsu.[15] The wavefunctions and energies were calculated using a restricted-Hartree-Fock self-consistent-field program.[16]

Geometry optimizations were performed beginning with the crystal structure of $Cs_{11}O_3$[10] using a one-dimensional "breathing" model. The equilibrium geometry was then obtained from a plot of energy versus breathing radius. The geometric parameters associated with the minimum energy for this curve were then used in RHF calculations to obtain the corresponding energy.

Electronic state optimizations were performed for anionic, neutral and cationic clusters and the corresponding workfunctions were extracted.

## III. RESULTS

Table I shows the coordination numbers of the $Cs_{11}O_3$ cluster. The structure of the $Cs_{11}O_3$ cluster can be described as being formed by layers of Cs and O atoms (see Fig.1). The upper layer consists 3 CsB atoms possessing a $C_3$ rotation axis. The middle layer consists of 3 OA and 3 CsA atoms. The lower layer is structurally similar to the upper layer and spaced from the middle layer by the same distance as the upper layer. The two CsC atoms are nested somewhat closer to the middle layer than the upper and lower layers and lie along the $C_3$ axis.

The abovementioned AREP's and contracted GTO basis sets lead to Hartree-Fock energies of -19.84218 and -15.64121 hartrees for the cesium and oxygen atoms, respectively[15]

Table II shows the structural parameters of $Cs_{11}O_3$ obtained experimentally by Simon and Westerbeck.[10] The cluster geometry was optimized and the effectsd of geometric changes on total energies are shown in Table III. The geometric parameters associated with the minimum energy for this correspond to a 7% expansion of the crystal structure of Table 2.

Tables IV-VI show total valence energies of several low-lying electronic states for anionic, neutral and cationic clusters, respectively. All calculations correspond to the average energy of molecular orbital configurations.[17]

We chose to treat such averaged spin states because the size of the cluster (11 Cs, 3 O and 117 valence electrons) results in severe computational complexity. All electronic state optimizations were performed at the 7% swelled equilibrium geometry of Table III and the lowest states were found for the negative, neutral and positive clusters. It is noteworthy that the negatively charged cluster is found to be the most stable.

Mulliken populations on each of the atoms in the ground states of the negative, neutral and positive clusters are listed on Table VII. By comparing the electron populations on each type of atom in the negative and neutral clusters, it is clearly seen that the ionized electron comes from the outermost cesium layer.

The energies of the highest occupied molecular orbitals (HOMO) and lowest unoccupied MO's (LUMO) are listed in Table VIII. The energies of the HOMO's of all the clusters are negative. However, the energies of the LUMO's for the positive cluster are all negative, those for neutral cluster being partially negative and partially positive, and those for negative cluster all positive. These indicate that both positive and neutral clusters are electron deficient and the negative cluster is the most stable. This conclusion is reinforced by comparing their total energies. The workfunction of the cluster, obtained by subtracting the total energy of the negative cluster from that of neutral cluster, is 0.651 eV. This may be compared to the

corresponding value of 0.700 eV calculated using Koopmans' theorem.[18]

## IV. DISCUSSION

The $Cs_{11}O_3$ cluster model studied is shown in Fig. 1. It has the layer symmetry of the bulk crystal and has four unique atoms. The cluster has $D_{3h}$ point group symmetry and represents a fragment of the bulk crystalline solid. The use of the $D_{3h}$ point group symmetry and averaged relativistic effective core potential to replace the core electrons for $Cs_{11}O_3$ led to substantial reductions of the numbers of two-electron integrals that must be computed and processed for each SCF calculation.

The contractions of the basis sets for cesium and oxygen atoms leave the outermost (smallest exponent) primitive functions uncontracted, making single contracted functions of the innermost (largest exponent) primitives. This permits the linear SCF-MO coefficient of the outer function, having maximum amplitude in the interatomic region, to respond to the changes which occur upon cluster formation.

The interatomic distances were initially determined from the lattice constants of crystalline $Cs_{11}O_3$[13] (see Table II) and the geometry optimization was carried out using a breathing model. The results appearing in Table 3 indicate that the total energy of the cluster reaches

minimum at 7% expansion of the crystalline size and the naked cluster is stable in the gas phase. The total energy of the cluster is lower by 81.5 kcal/mole than that due to the summation of the energies of the separated atoms.

The electronic state optimizations were carried out for negative, neutral and positive clusters. The procedures are similar to those following by Ermler et al. in their studies of the properties of large Be clusters.[19] The results appearing in Table IV-VI show that the most stable electronic state has an open shell configuration and that the negative $Cs_{11}O_3^-$ cluster is the most stable. The behavior of the lowest electronic state is similar to that of $Be_{63}$[19], and is indicative the onset of the bulk characteristics, i.e., the presence of a partially filled band in which spin couplings are not important energetically and electrons are highly delocalized. This provides some justification for carrying out electronic state optimizations based on averaged energy of configuration states for open shell cases.

The conclusion that the most stable cluster is negatively charged is supported by HOMO and LUMO analyses. As shown in Table VIII, the six LUMO's for the lowest-energy configuration of the positive cluster $Cs_{11}O_3^+$ are all negative and the majority of the LUMO's for the neutral cluster $Cs_{11}O_3$ are negative, indicating that the positive and neutral system are electron deficient for the low-lying states. The singly charged anionic $Cs_{11}O_3^-$ was then studied

in an attempt to satisfy this electron deficiency. The results appearing in the Table VIII for $Cs_{11}O_3^-$ show that its six HOMO's are all negative and all of its LUMO's are positive, indicating that the electrophilicity of the system has been quenched and addition of one electron to the neutral cluster increases its overall stability. These findings are similar to those reported by Marino et al. on their studies of the layered semiconductor cluster $Bi_6I_{18}$.[20]

Charge per atom values appearing in Table VII indicate that the predominant interlayer interactions occur between the CsC and OA atos (Fig. 1) for the lowest-energy state of $Cs_{11}O_3^-$. This was also observed for the other five low-lying states of $Cs_{11}O_3^-$. However, those for $Cs_{11}O_3$ and $Cs_{11}O_3^+$ indicate that predominant interlayer interactions occur between two layer six CsB atoms and three OA atoms (see Fig.1). By comparing charge per atom values in the negative and neutral clusters, we also found that the values for oxygen are constant at -1.59 whereas those for the CsB and CsC atoms are changed by +0.34e and -0.41e, respectively. A detailed analysis of Mulliken populations reveals the following: (a) In ionization from the negative cluster $Cs_{11}O_3^-$ to the neutral cluster $Cs_{11}O_3$, the electron exits from the outermost cesium layer. and (b) the predominant interlayer interactions change from CsC-OA to CsB-OA.

The workfunction of the cesium suboxide is one of its most important properties. Our calculated results show that $Cs_{11}O_3^-$ has very low workfunction, consistent with that

experimentally for cesium suboxides.[7] Two theoretical values correspond to a calculation of the workfunction as the difference between total energy of $Cs_{11}O_3^-$ and $Cs_{11}O_3$ and to Koopmans' theorem. In the latter case, two inherent approximations can result in a more reasonable value of the workfunction for systems with large numbers of electrons: (a) The "frozen orbital" approximation. This assumes that the spin orbitals for the N-electron states are identical with those for the (N+1)-electron states. This approximation neglects relaxation of the spin orbitals in the (N+1)-electron state to produce a workfunction that is too positive. (b) "constant differential correlation effects" approximation. The single determinant wavefunction leads to well-know errors in description of instantaneous electron correlation effects and one must go beyond the Hartree-Fock approximation in order to recover such corrections to Koopmans' theorem. In particular, correlation energies are larger for the system havig more electrons. Therefore, correlation effects tends to cancel the relaxation error for the workfunction. Our model $Cs_{11}O_3^-$ cluster contains 118 valence electrons and the calculated workfunction value using Koopmans' theorem is 0.7 eV, which is comparable with that of 0.65 eV using the energy difference between two Hartree-Fock calculations. By comparing our calculated workfunction values with experimental value, it is seen that Koopmans' theorem gives a value in close agreement with experiment. This close agreement between SCF, Koopmans'

theorem and experimental values indicates that since $Cs_{11}O_3^-$ is a system with large number of electrons, Koopmans' theorem is applicable and may be expected lead to an accurate workfunction.

Gregory et al.[7] reported the workfunction of cesium suboxide to be 0.7 eV. To obtain this value, they studied the oxidation of cesium using ultraviolet photoemission spectroscopy. They carried out the experiment in a stainless-steel ultrahigh-vacuum system with a base pressure of about $3x10^{-10}$ Torr and measured the distribution curves (DEC) using a standard retarding potential system.[21] They found that upon exposure of a fresh cesium film to oxygen, a very narrow peak which grew with increasing exposure appeared in the DEC's about 2.6 eV below the Fermi level ($E_f$). This peak is associate with oxygen ions dissolved below the surface of the cesium metal. After $3x10^{-5}$ Torr/sec of exposure, additional structure began to appear and the structure associated with the oxides changed with increasing oxygen exposure. At 500 L oxygen exposure the workfunction reached a sharp minimum of 0.7 eV, which was obtained from the DEC's by subtracting the width of the EDC from the photon energy used to produce the DEC's. The structure of present model cluster is consistent with this experimental observation, viz. oxygen ions dissolved in the cesium metal below the surface.

Burt and Heine[9] studied cesium suboxide by calculating

the band structure using a layer method. Their model solid is an FCC lattice of hard spheres with a constant potential between, a lattice constant of 30 a.u corresponding to the suboxide $Cs_{11}O_3$ was used. The model of the electronic structure of the system proposed by Burt and Heine is composed of one region approximating cesium metal with other regions, occupied by oxygen ions; the latter highly repulsive to the conduction electrons. Their calculated reduction in workfunction compared with cesium metal for $Cs_{11}O_3$ is 0.9 eV. This result is in general agreement with the drop in workfunction upon oxidation of thick cesium films observed by Gregory and with the present calculations. In their studies, the lower workfunction of the cesium suboxide monolayer film compared with that of bulk cesium was explained as a quantum size effect. That is, confinement of an electron to a monolayer raises its kinetic energy and hence the Fermi energy, leading to an equivalent decrease in workfunction. This claim is further verified by our calculations.

Woratschek et al.[8] presented evidence for a quantum size effect for the conduction electrons during oxidation Cs. This group studied the continuous oxidation of a Cs film using ultraviolet photoelectron spectroscopy and electron spectroscopy by deexcitation of metastable noble gas atoms. They found that the transition from metallic Cs to $Cs_{11}O_3$ leads to a twofold increase of the intensity of electron emission from the valence band, even though the

concentration of conduction electrons is reduced by about 50%. This is attributed to a quantum size effect.[22] They also found that a thin layer of $Cs_{11}O_3$ was created by exposing a clean Cs surface to small amount of $O_2$. The resulting workfunctions were 2.0 eV for Cs-poly and 1.5 eV for $Cs_{11}O_3$-poly. Although the workfunction values are different from those observed by Gregory et al.,[7] Burt et al.,[9] and with the present work, the decrease in workfunction compared with Cs-poly for $Cs_{11}O_3$-poly is still in general agreement with the present calculations and other experiments.

A very recent study by Limberger and Martin[23] reported that with increasing oxidation of the cesium clusters the IP decreases and reaches a minimum at $Cs(Cs_2O)_n$. They investigated cesium and cesium oxide clusters by ionization in a one-photon experiment by means of a tunable CW dye laser and a mass spectrometric detection system. The interpretation of the ionization threshold was given in terms of a displaced harmonic oscillator model which leads to a relation between adiabatic and vertical ionization potential. Their findings support our results as in the following manner: (1) Stability of the negatively charged cluster. In the bulk, they found that the oxygen appears as an oxide $O^{2-}$, a peroxide $O_2^{2-}$, or a superoxide anion $O_2^-$. These observations indicate that the negative cluster $Cs_{11}O_3^-$ is the most stable, in agreement with our calculated results. (2) Influence of the number (n) of

cesium atoms per cluster. Their experimental results show that $Cs_nO_m$ cluster with n an odd number has a lower IP than those with n even because those with odd n contain an unpaired electron. This finding is also consistent with our model which includes 11 cesium atoms and an open-shell ground state. (3) Influence of the number (m) of oxygen atom per cluster. A doped oxide cluster $Cs(Cs_2O)_m$ containing one excess cesium has the lowest IP. Our model could be written as $Cs_5(Cs_2O)_3$ and is in general agreement with $Cs(Cs_2O)_m$ when the number of cesium atoms in the cluster remains odd. (4) The cluster has several isomeric forms, each with its own threshold. This may explain the workfunction difference between our calculated value for $Cs_{11}O_3$ and that observed by Woratschek et al., that is, $Cs_{11}O_3$ could have stable isomers possessing different workfunctions.

## V. CONCLUSIONS

Our findings regarding the workfunction of $Cs_{11}O_3^-$ provide a theoretical basis for experimental observations of very low workfunctions for cesium suboxides. The consistency between calculated and experimental values indicates that our model provieds a good representation of the cesium suboxide surface. Mulliken population analysis reveals that the ionized electron comes from the outermost cesium layer.

## ACKNOWLEDGMENTS

This research was supported in part by the Air Force Office of Scientific Research and by the National Science Foundation under Grant CHE-8912674. The Ohio Supercomputer Center and the Pittsburgh Supercomputing Center are acknowledged for grants of Cray Y-MP time. We are grateful to Professor Milos Seidl for advice and suggestions.

**REFERENCES**


1. B. Hellsing, Phys. Rev. B 40, 3855 (1989).
2. E. G. Michel, J. E. Ortega, E. M. Dellig, M. C. Asensio, J. Ferron and R. Mirand, Phys. Rev. B 38, 13 399 (1988).
3. J. E. Ortega, E. M. Dellig, J. Ferron and R. Mirand, Phys. Rev. B 36, 6213 (1987).
4. A. H. Sommer, J. Appl. Phys. 51, 1254 (1980).
5. C. T. Campbell, J. Catal. 106, 301 (1987).
6. M. Seidl, W. E. Carr, S. T. Melnychuk, A. E. Sousis, J. Isenberg and H. Huang, Surface Production of Negative Hydrogen Ions, Proc. SPIE Symposium on Innovative Science & Technology, edited by H. E. Brandt 1061, 547 (1989).
7. P. E. Gregory, P. Chye, H. Sunami, W. E. Spicer, J. Appl. Phys. 46, 3525 (1975).
8. B. Woratschek, W. Sesselmann, J. Kuppers, G. Errl, H. Haberland, J. Chem. Phys. 86, 2411 (1987).
9. M. G. Burt and V. Heine, Solid State Phys. 11, 961 (1978).
10. V. [illegible]Simon, Z. Anorg. Allg. Chem. 395, 301 (1973).
11. P. A. Christiansen, W. C. Ermler, K. S. Pitzer, Ann. Rev. Phys. Chem. 36, 407 (1985).
12. L. F. Pacios and P. A. Christiansen, J. Chem. Phys. 82, 2664 (1985).
13. Y. S. Lee, W. C. Ermler, and K. S. Pitzer, J. Chem.

Phys. 67, 5861 (1977)

14. R. B. Ross, J. M. Powers, T. Atashroo, W. C. Ermler, L. LaJohn and P. A. Christiansen, J. Chem. Phys. in press
15. R. M. Pitzer and H. L. Hsu, private communication.
16. R. M. Pitzer, private communication.
17. J. C. Slater, Quantum Theory of Atomic Structure, McGraw-Hill, NY, 1960.
18. A. Szabo and N. S. Ostland, Modern Quantum Chemistry: Introduction to Advanced Electronic Structure Theory, MacMillan, New York (1982).
19. W. C. Ermler, R. B. Ross, C. W. Kern, R. M. Pitzer and N. W. Winter, J. Phys. Chem. 99, 3042 (1988).
20. M. M. Marino, M. Sawamura, W. C. Ermler and C. J. Sandroff, Chem. Phys. Lett. 163, 202 (1989).
21. C. R. Eden, Rev. Sci. Instrum. 41, 252 (1970).
22. M. Sawamura and W. C. Ermler, J. Phys. Chem. 94, 7805 (1990).
23. H. G. Limberger and T. P. Martin, J. Chem. Phys. 90, 2979 (1989).

Table I. Coordination Numbers of the $Cs_{11}O_3$ Cluster.[a]

| Atom | Number |
|---|---|
| CsA[b] | 3 |
| CsB[c] | 6 |
| CsC[d] | 2 |
| OA[e] | 3 |

[a]See Fig. 1.

[b]CsA = Cs1; 2; 9.

[c]CsB = Cs5; 6; 7; 8; 10; 11.

[d]CsC = Cs3; 4.

[e]OA = O1; 2; 3.

Table II. Geometric Structure of the $Cs_{11}O_3$ Cluster

| Atom Pair | Interatomic Distance (A) |
|---|---|
| Cs3 - Cs4 | 3.653(2) |
| Cs3 - Cs1; 2; 9 | 3.786(3); 3.783(3); 3.766(2) |
| Cs4 - Cs1; 2; 9 | 3.754(3); 3.741(3); 3.769(3) |
| Cs3 - Cs5; 7; 10 | 4.165(3); 4.153(3); 4.123(3) |
| Cs4 - Cs6; 8; 11 | 4.153(3); 4.156(3); 4.185(3) |
| Cs1 - Cs5; 6; 10; 11 | 4.244(4); 4.304(3); 4.250(4); 4.344(3) |
| Cs2 - Cs7; 8; 10; 11 | 4.310(3); 4.327(3); 4.311(4); 4.285(4) |
| Cs9 - Cs5; 6; 7; 8 | 4.275(4); 4.370(3); 4.388(3); 4.310(3) |
| Cs5 - Cs6 | 4.022(3) |
| Cs7 - Cs8 | 4.103(4) |
| Cs10 - Cs11 | 4.063(4) |
| O1 - Cs1; 2; 3; 4; 10; 11 | 2.940(14); 2.914(15); 2.970(14); 2.957(13); 2.688(14); 2.760(15) |
| O2 - Cs2; 3; 4; 7; 8; 9 | 2.967(13); 2.981(14); 2.964(14); 2.731(14); 2.731(14); 2.918(13) |
| O3 - Cs1; 3; 4; 5; 6; 9 | 2.916(14); 2.982(14); 2.921(14); 2.684(15); 2.763(14); 2.948(13) |
| O1 - O2; 3 | 4.061(20); 4.021(18) |
| O2 - O3 | 4.037(20) |

Table III. Geometry Optimization of $Cs_{11}O_3^-$

| Expansion (percent of the lattice parameters)[a] | Total Energy E (a.u) |
|---|---|
| 50% | -265.0296602077 |
| 25% | -265.2343008441 |
| 15% | -265.2982444057 |
| 10% | -265.3162851913 |
| 7% | -265.3200065394 |
| 5% | -265.3181039860 |
| 4% | -265.3164955496 |

[a]See Table 2.

Table IV. Electronic State Optimization for $Cs_{11}O_3^-$.

| State[a] | MO Configuration[b] | | | | | | Total Energy |
|---|---|---|---|---|---|---|---|
| | $10a_1'$ | $4a_2'$ | $8a_2''$ | $12e'$ | $8e''$ | $2a_1''$ | E (a.u.) |
| 1 | 2 | 0 | 1 | 3 | 0 | 0 | -265.320006 |
| 2 | 2 | 0 | 2 | 2 | 0 | 0 | -265.313010 |
| 3 | 0 | 0 | 2 | 4 | 0 | 0 | -265.259282 |
| 4 | 1 | 0 | 2 | 3 | 0 | 0 | -265.293672 |
| 5 | 2 | 0 | 0 | 4 | 0 | 0 | -265.309983 |

[a]Average energy of configuration. Ref. 17.

[b]Occupations of the outermost MOs' are shown.

Table V. Electronic State Optimization for $Cs_{11}O_3$.

| State[a] | MO Configuration[b] | | | | | | Total Energy |
|---|---|---|---|---|---|---|---|
| | $10a_1'$ | $4a_2'$ | $8a_2''$ | $12e'$ | $8e''$ | $2a_1''$ | E (a.u.) |
| 1 | 2 | 0 | 1 | 2 | 0 | 0 | -265.296097 |
| 2 | 2 | 0 | 0 | 3 | 0 | 0 | -265.286243 |
| 3 | 2 | 0 | 2 | 1 | 0 | 0 | -265.287395 |
| 4 | 1 | 0 | 1 | 3 | 0 | 0 | -265.278357 |
| 5 | 1 | 0 | 0 | 4 | 0 | 0 | -265.264475 |

[a]Average energy of configuration. Ref. 17.

[b]Occupations of the outermost MOs' are shown.

Table VI. Electronic State Optimization of $Cs_{11}O_3^+$.

| State[a] | MO Configuration[b] | | | | | | | Total Energy |
|---|---|---|---|---|---|---|---|---|
| | $10a_1'$ | $4a_2'$ | $7a_2''$ | $8a_2''$ | $12e'$ | $8e''$ | $2a_1''$ | E (a.u.) |
| 1 | 2 | 0 | 2 | 0 | 2 | 0 | 0 | -265.200801 |
| 2 | 2 | 0 | 2 | 1 | 1 | 0 | 0 | -265.209878 |
| 3 | 2 | 0 | 2 | 2 | 0 | 0 | 0 | -265.199121 |
| 4 | 1 | 0 | 2 | 1 | 2 | 0 | 0 | -265.198115 |
| 5 | 2 | 0 | 1 | 0 | 3 | 0 | 0 | -265.130255 |

[a]Average energy of configuration. Ref. 17.

[b]Occupations of the outermost MOs' are shown.

Table VII. Population Analysis for Cluster Ground States.

| A[a] | B[b] | s-type | p-type | Total | C[c] | D[d] |
|---|---|---|---|---|---|---|
| $Cs11O_3^-$ | OA | 5.825 | 16.934 | 22.759 | 7.59 | -1.59 |
| | CsA | 6.916 | 18.764 | 25.679 | 8.56 | 0.44 |
| | CsB | 15.950 | 36.856 | 52.806 | 8.80 | 0.20 |
| | CsC | 3.635 | 13.120 | 16.755 | 8.38 | 0.62 |
| $Cs_{11}O_3$ | OA | 5.825 | 16.944 | 22.769 | 7.59 | -1.59 |
| | CsA | 7.205 | 18.671 | 25.875 | 8.62 | 0.37 |
| | CsB | 14.274 | 36.503 | 50.778 | 8.46 | 0.54 |
| | CsC | 3.681 | 12.896 | 17.577 | 8.79 | 0.21 |
| $Cs_{11}O_3^+$ | OA | 5.825 | 16.949 | 22.774 | 7.59 | -1.59 |
| | CsA | 7.214 | 18.563 | 25.777 | 8.59 | 0.41 |
| | CsB | 13.528 | 36.288 | 49.815 | 8.30 | 0.70 |
| | CsC | 4.849 | 12.784 | 17.633 | 8.82 | 0.18 |

[a]Cluster.

[b]Type of atom (See Table I and Fig. I.)

[c]Gross atomic population.

[d]Charge per atom.

Table VIII. HOMO and LOMO Energies of $Cs_{11}O_3$, $Cs_{11}O_3$ and $Cs_{11}O_3^+$ in Their Lowest-Energy States

| Cluster | Orbital | HOMO (a.u.) | LUMO (a.u) |
|---|---|---|---|
| $Cs_{11}O_3^-$ | $a_1'$ | -0.0436 | 0.0492 |
| | $a_2'$ | -0.1285 | 0.0977 |
| | $a_2''$ | -0.0377 | 0.0140 |
| | e' | -0.0257 | 0.0341 |
| | e' | -0.1339 | 0.0566 |
| | $a_1''$ | -0.6163 | 0.1236 |
| $Cs_{11}O_3$ | $a_1'$ | -0.1003 | -0.0103 |
| | $a_2'$ | -0.1964 | 0.0334 |
| | $a_2''$ | -0.0989 | -0.0454 |
| | e' | -0.0877 | -0.0470 |
| | e" | -0.2022 | -0.0009 |
| | $a_2''$ | -0.6870 | 0.0590 |
| $Cs_{11}O_3^+$ | $a_1'$ | -0.1587 | -0.0704 |
| | $a_2'$ | -0.2667 | -0.0321 |
| | $a_2''$ | -0.1615 | -0.1057 |
| | e' | -0.1517 | -0.1294 |
| | e" | -0.2732 | -0.0598 |
| | $a_1''$ | -0.7590 | -0.0070 |

## Figure Captions

Figure 1. The $Cs_{11}O_3$ cluster from several perspectives.

Figure 2. Total valence energy (a.u.) vs. geometry for a $Cs_{11}O_3^-$ cluster.

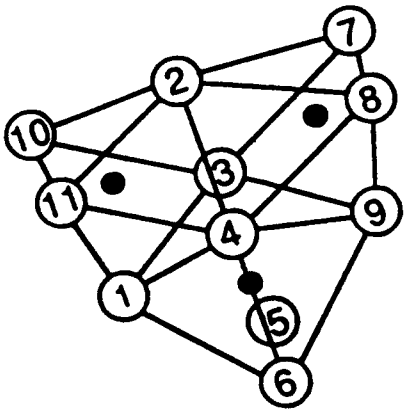


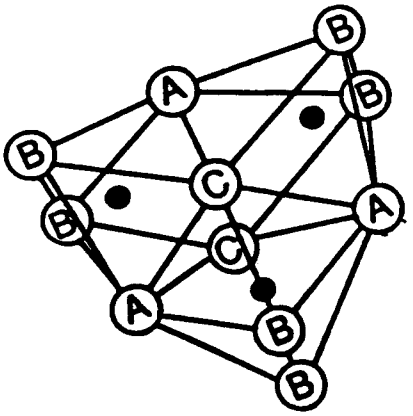


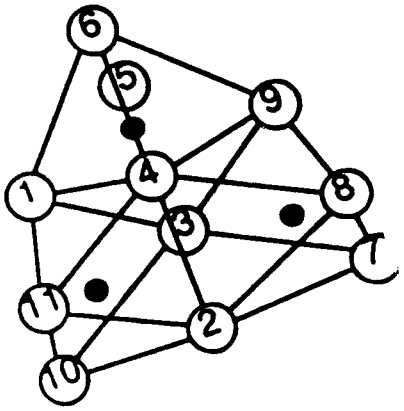


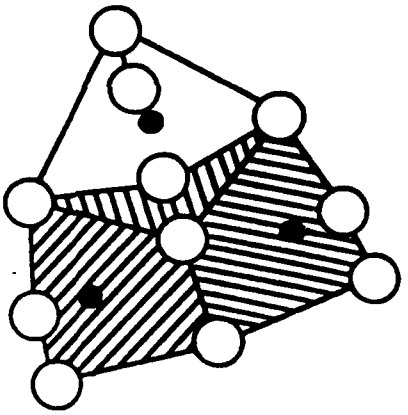

Cs

O

Fig. 2

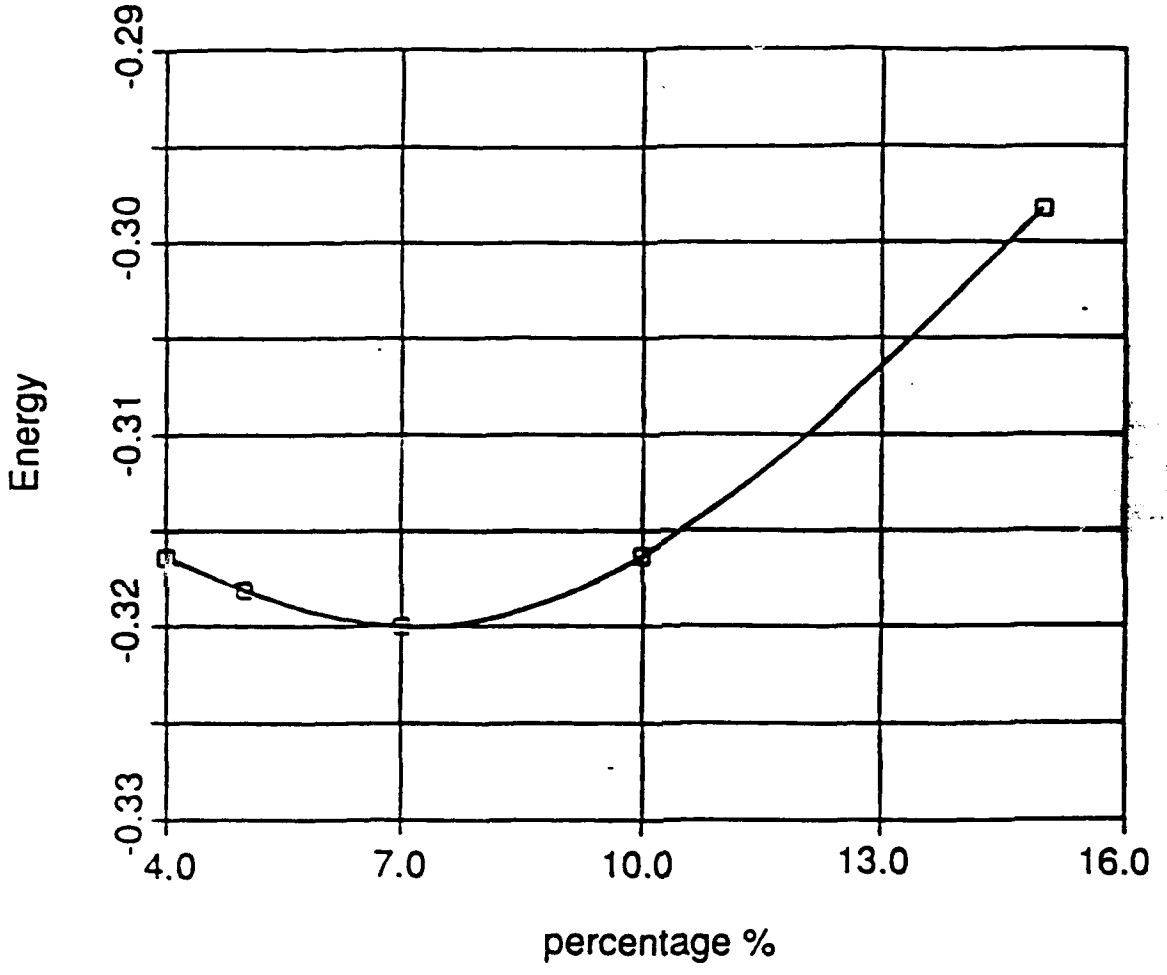

# Ab Initio Study of Hydrogen Adsorption on Be (0001)

M. M. Marino

Department of Chemistry and Chemical Engineering*

Stevens Institute of Technology

Hoboken, New Jersey 07030

and

W. C. Ermler

Department of Chemistry

The Ohio State University

Columbus, Ohio 43210

(J. Chem. Phys. accepted 2/11/91)

## ABSTRACT

Hydrogen adsorption on the (0001) beryllium surface is modelled using a $Be_{45}$ cluster containing seven layers. The ab initio Hartree-Fock calculations employ effective core potentials and full $D_{3h}$ point group symmetry. Six low-lying electron configurations are investigated and the effect of electron spin coupling on the adsorption process is discussed. The adsorption of H on Be is calculated to be stable by 20 kcal/mol and lowers the work function by 1.3 eV.

## I. INTRODUCTION

The use of metal clusters to represent bulk surfaces involved in adsorption phenomena is widespread.[1-4] A good model of the adsorption process, however, requires the use of clusters large enough to describe the metal surface and its interaction with the adsorbate, while remaining small enough for the application of accurate theoretical treatments. Beryllium has been widely used for such studies because it is the smallest atom with a closed-shell ground electronic state to exhibit metallic character.[5-10] The toxicity of beryllium, however, has limited its use experimentally. Nevertheless, two recent experimental studies have investigated the adsorption of Hydrogen on beryllium metal.[11,12] The former study[11] was concerned with $H_2$ adsorption on polycrystalline Be, while the latter[12] involved the effects of $H_2$, H and D on the (0001) surface of beryllium metal. The experimental data, in conjunction with theoretical calculations, can be used for the development of more reliable models for adsorption.

The model of the beryllium surface used in this study consists of a seven-layer cylindrical piece from a wafer having Be-Be internuclear distances equal to those in the bulk metal. Work function values, the effect of spin coupling on the cluster and net charge differences between neutral and [illegible] clusters are analyzed to determine how closely the model approximates bulk behavior. Where possible, comparisons between theory and experiment are made. Finally, adsorption energies are reported and the effects of H adsorption on the Be surface are discussed in the context of adsorbate plus substrate as a supermolecule.

## II. CALCULATIONS

The model system is taken as a cylindrical piece from a Be wafer whose surface corresponds to the (0001) hcp metal face. Table I defines all the cylinders of a given radius which may be formed from a wafer of a given thickness. The seven-layer wafer in this study has a radius $R_3$ which corresponds to a one unit cell step along the a-direction. Be-Be internuclear distances are taken as those in the bulk hcp metal (a=2.29Å, c=3.58Å).[13] The resulting cylinder has $D_{3h}$ point-group symmetry, and the adsorption of atomic hydrogen, one on the top surface and one on the bottom surface of the cluster is modeled such that the three-fold symmetry and horizontal mirror plane are preserved. The Be-H internuclear distances are varied in a series of self-consistent field (SCF) calculations. The hydrogenated $Be_{45}$ cylinder is shown in Fig. 1. Results obtained using this system are compared to those calculated by treating an identical bare $Be_{45}$ cylinder.

Calculations were accomplished on a Cray Y-MP supercomputer using programs based on the "equal contribution theorem" for two-electron integrals.[14] Ab initio restricted closed-shell and restricted open-shell Hartree-Fock calculations corresponding to an average energy of configuration as well as to the energies for pure spin couplings were carried out on numerous low-lying states of each cluster. (The average energy of configuration is defined as the weighted mean of the energies of all the multiplets for the configuration.[15]) Multiconfiguration self-consistent field (MCSCF) calculations involving two configurations were also carried out for selected electronic states. The calculations required about one hour of Cray Y-MP time for each geometric orientation. The following basis sets of contracted Gaussian-type functions were used for beryllium and hydrogen, respectively: (3s2p)/[2s1p][16] and

(4s1p)/[2s1p].[17] Ab initio effective potentials (EP)[18] were used to represent the 1s core electrons in Be.[16] (Valence SCF energies for atomic Be and H are -0.95083, -0.49928 hartrees, respectively, for the basis sets used in this study.)

## III. RESULTS

Total valence energies for six low-lying electronic states are given in Table II. These results are reported for both the equilibrium hydrogen-to-Be-plane distance and at the near dissociative limit of 10Å. All of the energies correspond to triplet spin couplings with the exception of state 2, which is the lowest-lying closed shell singlet state found. Table III shows the effects of electron correlation, proper dissociating wavefunctions and spin coupling for the lowest-lying electron configuration calculated at the minimum $H\text{-}Be_{surface}$ distances of 0.86Å and at the dissociative limit of 10Å. Table IV contains energy values at dissociation for state 6, a low-lying MO configuration having the largest number of open-shell electrons.

Total SCF energies for the ground state of H and of each cluster, as well as calculated adsorption energies are given in Table V. Theoretical work functions are shown in Table VI. The first values in each row were calculated as the difference between the total valence SCF energy of the neutral cluster and that of the ion resulting from the removal of one electron from the highest occupied orbital of the cluster. The values immediately following are due to Koopmans' theorem and correspond to the negative of the energy of the molecular orbital (MO) from which the electron was ionized. Experimental values are also shown.[11]

Atomic net electron charge values are given in Table VII, as

calculated using a Mulliken population analysis.[19] Values of R in this table correspond to the optimum H atom-to-surface distance for the lowest-lying electronic state. This distance was calculated as the minimum of a curve fit to SCF energies for three or more surface-adsorbate separations.

## IV. DISCUSSION

Only two of the six low-lying electron configurations found, states 1 and 6 of Table II, dissociate properly at the restricted Hartree-Fock level of approximation. The remainder of the states lie significantly higher in energy at dissociation. An analysis of their Mulliken populations indicates that the net charges on the H atoms at 10Å separation ($R_\infty$) are as high as 0.5 electron/atom, clearly indicative of an improper dissociation limit.

All of the open-shell states appearing in Table II are coupled as triplets. Tables III and IV show the effects of spin coupling on the energy of the $Be_{45}H_2$ system. Both the two configuration MCSCF and the pure spin triplet calculations (Table III) yield the same energy at dissociation (-45.57065 hartrees). However, the improperly dissociating singlet spin state is significantly higher in energy (144 kcal/mol higher). The average energy of configuration calculation also yields a much higher energy (by 94 kcal/mol), but this calculation, as mentioned previously, reflects a weighted average of the energies for all the multiplets of a particular configuration.[15] Therefore, the higher energy is a consequence of the contribution from the singlet component of the multiplet. These results indicate that the unpaired electrons in the overall cluster must be coupled as triplets with respect to each other to insure proper dissociation in a

single configuration treatment. According to Mulliken population analyses, these electrons correspond solely to hydrogen 1s electrons at $R_\infty$. Although the energies are not identical, the MCSCF result also agrees well with that of the pure spin triplet case at equilibrium, the discrepency between the two being approximately 6 kcal/mol, which is attributed to electron correlation effects. However, even at this short distance, coupling the unpaired electrons singlet as opposed to triplet results in a 20 kcal/mol increase in energy.

The effects of spin coupling on the $Be_{45}H_2$ system at dissociation were further studied using state 6 of Table II. This is the highest spin electron configuration (quintet) found to dissociate properly. The energies for various spin states of this configuration were calculated. These results appear in Table IV. Three states, the quintet, triplet and first singlet, have energies which are nearly identical. The second singlet, however, is 160 kcal/mol higher in energy. Again, the average energy of configuration calculation reflects the contribution of the second singlet state. As with the previous results, the three low-lying states in Table IV have the two unpaired electrons corresponding to the hydrogen 1s electrons coupled triplet with respect to each other, while the less stable singlet state has these electrons coupled singlet. The coupling of the unpaired electrons associated primarily with Be orbitals does not affect the energy significantly. For example, the triplet spin state and the more stable singlet spin state have the unpaired Be electrons coupled singlet and triplet, respectively, yet the energy difference between the two is only 2.4 Kcal/mol. We are encouraged by this behavior since it is expected if the $Be_{45}$ cluster provides an accurate model of the bulk surface, which is obviously not affected by spin considerations.

The total adsorption energy of $Be_{45}H_2$ is 19.72 kcal/mol·atom (Table

V). This energy was determined two ways. First, the adsorption energy was calculated as the total energy difference between the lowest-lying electronic state found at equilibrium and at dissociation. Second, the adsorption energy was defined as the difference between the energy of the lowest-lying electronic state found at equilibrium and the sum of the energies for the lowest-lying electronic state found for bare $Be_{45}$ plus two ground state H atoms. Both methods yielded values of 19.72 kcal/mol·atom. Fig. 2 shows a plot of energy vs H to Be surface distance. A barrier of 24.68 kcal/mol (12.34 kcal/mol·H atom) occurs before H adsorbs to the $Be_{45}$ surface.

A very recent experimental study by Ray et al. investigated the effects of H and $H_2$ adsorption on the (0001) surface of Be metal using high resolution electron energy loss spectroscopy (HREELS), thermal desorption spectroscopy (TDS) and workfunction measurements.[12] This group found no evidence for the dissociative or molecular chemisorption of $H_2$ at the temperatures investigated, in agreement with previous experimental work.[11] They also found, however, that H does adsorb on Be and reported the energy barrier to recombinative desorption, obtained using TDS, as ranging from 0.7 to 1.2 eV (16.1 to 27.7 kcal), depending on the degree of H coverage. This barrier energy is equal to the sum of the adsorption site binding energy and the barrier to dissociative adsorption. This value is in excellent agreement with our calculated adsorption energy of 0.85 eV or 20 kcal/mol·atom (Table V).

The convergence of both methods to the same value for the adsorption energy indicates that the lowest-lying electronic state correlating to the dissociative limit has been determined accurately. Such a determination is pivotal because properties such as work functions, adsorption energies and charge distributions, which indicate the chemical nature of the system, are

sensitive to the electronic state chosen. In our previous work,[11] we concluded that H does not chemisorb to $Be_{45}$ since no shift in the workfunction of the $Be_{45}$ surface occurred upon H adsorption. Furthermore, the net charge distribution difference between $Be_{45}^{+}$ vs. $Be_{45}$ and $Be_{45}H_2^{+}$ vs. $Be_{45}H_2$ were nearly identical, indicating that the ionization process was not affected by the presence of hydrogen. In the present calculations, however, a lower-lying electronic state has been found for both $Be_{45}$ and $Be_{45}H_2$. Although the adsorption energy corresponding to this state is only 1.56 kcal/mol·atom lower than was determined previously, the workfunction of $Be_{45}$ is now 4.4 eV (Table VI), in close agreement with the experimental value of 3.92 eV.[20] Adsorption of H onto $Be_{45}$ lowers the work function to 3.14 eV, a shift of 1.29 eV. No work function shift is observed experimentally for the $H_2$/Be system.[11] However, a direct comparison between the experimental and theoretical work function shifts in this case cannot be made since the experiment involved sputtered $H_2$ and polycrystalline Be. In such a process, H adsorption is necessarily preceded by $H_2$ dissociation, which requires approximately 104 kcal/mol at room temperature.[21] This is considerably more than the calculated 20 kcal/mol bond formed between hydrogen and the $Be_{45}$ surface. Consequently, it is more energetically favorable for hydrogen to remain as $H_2$, unless, of course, the surface plays a heretofore unclear catalytic role in lowering the energy needed to break the H-H bond. In either case, the focus of the present calculations is to study the interaction of H with the Be surface and not the dissociation of $H_2$. For the H/Be (0001) system, however, the work function of Be reaches a minimum (-0.56 eV) for a coverage of approximately 0.4 and then reaches a limiting value of -0.44 eV as the H coverage is increased. This is also in good agreement with our calculated work function lowering of 1.3 eV (0.65 eV/atom). It is pointed out,

however, that Ray et al.[12] believe their values correspond to adsorption of H on a bridge site, whereas the present study investigates H adsorption on one type of trigonal site (eclipsed site).

Net charge differences appearing in Table VII indicate that for both $Be_{45}$ and $Be_{45}H_2$, the largest fraction of the donated electron comes from MO's involving the surface atoms. This behavior is requisite if the $Be_{45}$ cluster is to provide an adequate representation of the bulk metal since the work function is a surface property. Adsorption of H increases the ability of the surface to release an electron to some degree (0.48 vs 0.60 for the bare cluster vs the hydrogenated cluster, repectively). However, there is no net charge transfer between the adsorbed hydrogen and the surface, indicating an essentially covalent interaction between the two.

In this study, H approaches the Be surface directly above the center of a triangle of Be atoms located on the surface, the center of which is located above a Be atom situated in a layer next to the surface (Fig. 1). This is called the eclipsed site. There are three other possible sites for adsorption. These are the Be-Be midpoint, directly overhead and open sites. The first has the adsorbate approaching the Be surface directly between two Be atoms located on the surface. The second involves adsorption directly above a Be atom located on the surface. The open site has the adsorbate approaching the surface directly above a triangle of Be atoms located on the surface, directly below which there is no Be atom.

The adsorption of H onto Be clusters modelling the bulk surface has also been studied at the SCF level of theory by other groups. In the following discussion the notation $Be_n(a,b,c,...)$ will be used. Here n refers to the number of atoms comprising the Be cluster and a, b, c, etc., are the number of atoms in the surface layer, the layer directly beneath the surface, the second layer beneath the surface, and so on, respectively.

In all cases, unless otherwise stated, the cluster interatomic separations were frozen at the bulk metal values.

Cox and Bauschlicher[8] studied the adsorption of H in the directly overhead position on a $Be_7(7,0)$ and $Be_{10}(7,3)$ cluster. Adsorption of H on a bond midpoint site was modelled using a $Be_{15}(10,5)$ cluster. They obtained adsorption energies of 65.5, 21.22 and 53.7 kcal/mol for the three above-mentioned sites, respectively. They further conclude that in two previous studies of H adsorption on Be, one using clusters or up to 22 atoms[22] and one using a $Be_{36}$ cluster[7], the chemisorption energy changed by approximately 10% in going from a 22-atom cluster to a 36-atom cluster and by about 30% in going from a $Be_{10}$ or $Be_{13}$ cluster to a $Be_{36}$ cluster.

In another study, Bauschlicher and Bagus[5] reported adsorption energies of 64.0, 47.8, and 35.8 kcal/mol for H adsorption on the directly overhead site of $Be_7(7,0)$, the eclipsed site of $Be_7(6,1)$ and the bond midpoint site of $Be_{10}(10,0)$, respectively. Calculations by Bagus et al.[7] on the $Be_{14}(14,0)H$ system found the directly overhead site, with a desorption energy of 59.0 kcal/mol, to be a more stable site for H adsorption than the bond midpoint, open or eclipsed sites (53.1, 56.1 and 56.1 kcal/mol, respectively). H adsorption on $Be_{22}(14,8)$, on the other hand, is predicted to be more stable for the open site (55.1 kcal/mol) than for the bond midpoint, eclipsed or directly overhead sites (53.4, 51.9, and 31.4 kcal/mol, respectively). Finally, the most stable site for H adsorption on a $Be_{36}(14,8,14)$ cluster was predicted to be the open site, also (57.7 kcal/mol), with the bond midpoint, eclipsed and directly overhead sites (43.7, 42.3 and 31.6 kcal/mol, respectively) giving rise to lower adsorption energies. Clearly, $Be_{36}$ and $Be_{22}$ give rise to the same ordering in the stability of the adsorption energy with respect to bonding site. However, with the exceptions of the directly overhead and open sites, the

predicted adsorption energies for a given site on these two clusters differ by as much as 9.7 kcal/mol.

The results reported here, along with those cited from previous studies, indicate the importance of cluster choice in modelling the Be metal surface involved in H adsorption. It must be ascertained that the cluster model adequately represents the bulk surface, or the calculated results will correspond to H adsorption on a specific electronic state of a cluster rather than on the (0001) Be surface. This explains the discrepancies in adsorption energies among the various studies cited. We believe that the energies arising from calculations on small clusters correspond to H adsorption on clusters rather than on the Be surface.

There are two critical steps in establishing a valid model of H adsorption on a surface. First, the cluster representing the surface must be large enough to model the bulk solid accurately. Second, the ground electronic state of the system must be determined. A recent study[11] of H adsorption on the Be (0001) surface investigated three possible cluster models of the bulk surface: $Be_{19}(6,7,6)$, $Be_{33}(7,6,7,6,7)$ and Be45(6,7,6,7,6,7,6). The first and third modelled adsorption on an eclipsed site, while the second involved adsorption on the directly overhead site. Since the adsorption site in $Be_{19}$ is identical to that in $Be_{45}$, results for both systems should agree. However, the calculated shift in the ionization potential of $Be_{19}$ due to H adsorption was 0.0 eV, while that corresponding to H adsorption on $Be_{45}$ was 1.4 eV. The work functions of $Be_{19}$ and $Be_{45}$ were calculated as 5.0 and 4.4 eV, with the experimental value being 3.9 eV. These discrepancies were explained using total net charge differences between neutral and ionized clusters. In the case of $Be_{19}$, ionization of the cluster indicated participation in charge redistribution by both the surface and middle layers. Since electron

emission occurs from the surface of the bulk metal and should not involve the middle layers, it was concluded that $Be_{19}$ is too small to model the Be (0001) surface. As previously stated, net charge differences for $Be_{45}$ (and $Be_{45}H_2$) indicate that the largest fraction of the donated electron comes from MO's involving the surface atoms (see Table VII). Since the work function is a surface property, this must be the case if the $Be_{45}$ cluster adequately models the bulk. Furthermore, the calculated work function of $Be_{45}$ is only 0.5 eV greater than the experimental value of 3.92 eV.[11]

A study by Pacchioni et al.[23] found the directly overhead site on a $Be_7(7,0)$ cluster to be more stable (48.3 kcal/mol) than the bond midpoint or open sites (35.7 and 11.7 kcal/mol, repsectively). They further point out that this finding holds only for single-layer models of the bulk metal. As more layers are are added, the bond-midpoint and open sites become more favored than the directly overhead site.[6,7] This is in agreement with our $Be_{33}$ ( directly overhead site) and $Be_{45}$(eclipsed site) models of adsorption. While H is not predicted to adsorb on $Be_{33}$,[11] it does adsorb on $Be_{45}$ by 19.7 kcal/mol (see Table V). Both clusters are multilayered cutoffs of the bulk, with $Be_{33}$ containing 5 layers and $Be_{45}$ containing 7 layers.

As pointed out earlier, the $Be_{45}$ cluster in this work contains Be-Be interatomic distances equivalent to the bulk metal values, and the cluster is, in effect, a cylindrical "plug" from the bulk metal (Table I). This approximation is valid since experimental evidence indicates that the Be surface does not reconstruct.[24] Furthermore, Cox and Bauschlicher[8] studied the effects of relaxation on $Be_7(7,0)$, $Be_{10}(7,3)$ and $Be_{15}(10,5)$ clusters due to H adsorption. Adsorption energies due to relaxation effects were calculated as 66.9, 21.4 and 55.6 kcal/mol, respectively, while the energies arising from adsorption on an unrelaxed substrate were reported as

65.5, 21.2 and 53.7 kcal/mol, respectively (refer to earlier discussion). They predict that neglect of relaxation effects results in only a 2 kcal/mol error in the calculated binding energies.

The final important point to consider when modelling H adsorption on a metal surface is the method of determining the ground electronic state of the system. This is imperative since the chemical nature of the system is, in effect, mainly determined by the ground electronic state. We have already discussed the errors resulting from improperly predicting the ground electronic state of $Be_{45}$ and $Be_{45}H_2$ in our previous work. Another example of the ambiguities or problems which may arise from the choice of ground electronic state can be seen in the studies of Paccioni et al.[23] and Cox and Bauschlicher.[8] The latter reported relaxation effects in the geometry of Be clusters due to H adsorption (refer to prior discussion). However, this group chose the ground state of the $Be_7$ system to be closed shell in order to avoid the effects of dangling orbitals on the energy of the system. Pacchioni et al.[23] attribute this shrinking to the choice of electronic state. This group found that the relaxation effects occurred in different directions for different electronic states and that they also depended on the choice of theoretical method (all electron vs pseudopotential at both the SCF and CI levels of theory). The effects of relaxation on the adsorption energy, they suggested, should be investigated further with other cluster models.

Panas et al.[25] studied the cluster convergence of chemisorption energies. This group generated molecular orbitals using SCF calculations and included correlation corrections via a one reference state contracted CI procedure. They studied H adsorption in the fourfold hollow position of Ni(100) using seven Ni clusters ranging in size from $Ni_5(4,1)$ to $Ni_{50}(16,9,16,9)$ to represent the Ni surface. They found a marked

difference in the calculated chemisorption energies of the clusters depending on the method used to determine the lowest-lying electronic state at short and long distances (the chemisorption energy being defined as the defference between the energies of these two states). This group concludes that the determination of the chemisorption energy is greatly improved by requiring that the cluster systems first be excited into a proper bonding state and then defining the chemisorption energy as the difference in the energy corresponding to this state at short and long distances plus the energy needed for excitation. In the present study, no restrictions were imposed on the symmetry and spin of the wavefunction at short and long distances. However, applying the rules outlined by Panas et al. led to the same value for the adsorption energy. Thus the energy value reported here is expected to be accurate.

One last point must be mentioned. All of the results reported in the current study were calculated at the SCF level of approximation. It is therefore necessary to estimate the extent to which electron correlation corrections will affect the current results. Rubio et al.[26] studied the effect of electron correlation on the process whereby H adsorbs to small (three to seven atoms) Be clusters. They determined, using data obtained at both the SCF snd CI levels, that SCF theory is qualitatively accurate to describe the interaction of H with the clusters. The changes in the H-to-Be-surface distances and in the calculated adsorption energies were quite small. A study by Siegbahn et al.[27] of $H_2$ dissociation on the Ni(100) surface using Ni clusters with as many as 34 atoms to represent the surface also determined that the SCF treatment was adequate for a qualitative description of the chemisorption process. Given these findings and the fact that the $Be_{45}H_2$ system is quite large (92 valence electrons) the incremental effects of electron correlation on the results reported

here are expected to be small.

## V. SUMMARY AND CONCLUSIONS

An accurate model of the adsorption process requires that the surface be modelled by a cluster which provides an adequate representation of the bulk structure. Once this is done, it is equally important to determine accurately the lowest-lying electronic configuration of the cluster-adsorbate system. We conclude that $Be_{45}$ provides an accurate model of the Be (0001) surface for several reasons. First, this cluster is not affected by spin considerations, as is expected for solid surfaces. Spin coupling affects the total energy only when electrons corresponding to hydrogen orbitals are involved. Second, the ionization potential of $Be_{45}$ at 4.4 eV is close to the value of 3.9 eV for bulk Be metal. Third, Mulliken population analyses indicate that the electron emitted during ionization is donated from the surface layers, which is also the case for bulk metal surfaces. Fourth, previous studies have indicated the need for clusters several layers thick to accurately model H adsorption.[7,11,27] $Be_{45}$ is a seven-layer cluster based on hcp bulk lattice constants. The lowest-lying electronic state of the $Be_{45}H_2$ system has been determined. An indication of the reliability of this determination is the fact that the workfunctions of the cluster and the bulk metal, at 4.4 and 3.9 eV, respectively, differ by only 0.5 eV. In our previous study[11], the improperly chosen ground electronic state caused the predicted cluster workfunction to be 1.25 eV lower than the current value and 0.77eV lower than that of bulk Be. A second indication that the ground state is correct is the convergence of the calculated adsorption energies to the same value using two different methods. This is expected if the true ground

electronic state has been found for both systems. In the present case, the systems were $Be_{45}$ + 2H and $Be_{45}H_2$ at infinite Be-H separation. Finally, the agreement between the MCSCF calculations and the calculations on the triplet spin states indicates that the bulk of the differential correlation energy is accounted for by requiring the electrons corresponding to H to be coupled as triplets. The resulting electronic states can thus be described adequately using single configuration SCF-MO calculations.

Finally, the results for H adsorption on $Be_{45}$ indicate that H adsorbs at an eclipsed site of Be (0001) by 20 kcal/mol and that the adsorption process lowers the workfunction of the cluster from 4.4 to 3.1 eV, or 1.3 eV. Since no charge transfer is observed between hydrogen and the Be surface, the adsorption process involves a primarily covalent interaction between the two.

## ACKNOWLEDGMENTS

This research was supported in part by the National Science Foundation under grant No. CHE-8912674 and by a grant from the Air Force Office of Scientific Research, which included Cray Y-MP time at the Ohio Supercomputing Center. The Pittsburg Supercomputing Center is acknowledged for a grant of Cray Y-MP time.

REFERENCES


*Permanent address of WCE.

1. R.P. Messmer, D.R. Salahub, K.H. Johnson and C.Y. Yang, Chem. Phys. Lett. 51, 84 (1977).
2. M.E. Geusic, M.D. Morse and R.E. Smalley, J. Chem. Phys. 82, 590 (1985).
3. I. Panas, P. Siegbahn and U. Wahlgren in ACS Symposium Series 394, The Challenge of d and f Electrons, Theory and Computations, D.R. Salahub and M.C. Zerner, ed. (American Chemical Society, 1989).
4. W. Ravenek and F.M.M. Geurts, J. Chem. Phys. 84, 1613 (1986).
5. C.W. Bauschlicher and P. Bagus, Chem. Phys. Lett., 90, 355 (1982).
6. G. Angonoa, J. Koutecky, A.N. Ermoshkin and C. Pisani, Surf. Sci. 138, 51 (1984).
7. P.S. Bagus, H.F. Schaefer and C.W. Bauschlicher, J. Chem. Phys. 78, 1390 (1983).
8. B.N. Cox and C.W. Bauschlicher, Surf. Sci. 102, 295 (1981).
9. C.W. Bauschlicher, D.H. Liskow, C.F. Bender and H.F. Schaefer III, J. Chem. Phys. 62, 4815 (1975).
10. C.W. Bauschlicher, Chem. Phys. Lett., 117, 33 (1985).
11. M.M. Marino, W.C. Ermler, G.S. Tompa and M. Seidl, Surf. Sci. 208, 189 (1989).
12. K.B. Ray, J.B. Hannon and E.W. Plummer, Chem. Phys. Lett. 171, 469 (1990).
13. R. G. Wyckoff, Crystal Structures, 2nd ed. (Interscience, New York, 1974).
14. R. M. Pitzer, J. Chem. Phys. 58, 3111 (1973) and private communication.

15. J.C. Slater, Quantum Theory of Atomic Structure, vol. 1 (McGraw-Hill, New York, 1960).

16. W. C. Ermler, C. W. Kern, R. M. Pitzer and N. W. Winter, J.Chem. Phys. 84, 3937 (1986).

17. T. H. Dunning, Jr. J. Chem. Phys. 53, 2823 (1970); ibid. 55, 3958 (1971).

18. P. A. Christiansen, W. C. Ermler and K. S. Pitzer, Annu. Rev. Phys. Chem. 36, 407 (1985).

19. R. S. Mulliken, J. Chem. Phys. 23, 1833 (1955).

20. G.S. Tompa, M. Seidl, W.C. Ermler and W.E. Carr, Surf. Sci. 185, L453 (1987).

21. See, for example, J.D. Roberts and M.C. Caserio, Basic Principles of Organic Chemistry (W.A. Benjamin, Inc., New York, 1964) and references therein.

22. C.W. Bauschlicher, P.S. Bagus and H.F. Schaefer, IBM J. Res. Develop. 22, 213 (1978).

23. G. Pacchioni, W. Pewestorf and J. Koutecky, Chem. Phys. 83, 201 (1984).

24. R.S. Zimmer and W.D. Robertson, Surf. Sci. 43, 61 (1974).

25. I. Panas, J. Schüle, P. Siegbahn and U. Wahlgren, Chem. Phys. Lett. 149, 265 (1988).

26. J. Rubio, F. Illas and J.M. Ricart, J. Chem. Phys. 84, 3311 (1986).

27. P.E.M. Siegbahn, M.R.A. Blomberg and C.W. Bauschlicher, J. Chem. Phys. 81, 2103 (1984).

Table I. Be Clusters by Coordination Cylinder and hcp Layer.

| Cylinder Height (z-coord.) | $R_0$ | | | | $R_1$ | | | | $R_2$=a | | | | $R_3$ | | | |
|---|---|---|---|---|---|---|---|---|---|---|---|---|---|---|---|---|
| ∞c/2 | | | | | | | | | | | | | | | | |
| . | | | | | | | | | | | | | | | | |
| . | | | | | | | | | | | | | | | | |
| 3c/2 | | | | 0 | | | | 3 | | | | 3 | | | | 6 |
| c | | | 1 | 1 | | | 1 | 1 | | | 7 | 7 | | | 7 | 7 |
| c/2 | | 0 | 0 | 0 | | 3 | 3 | 3 | | 3 | 3 | 3 | | 6 | 6 | 6 |
| 0 | 1 | 1 | 1 | 1 | 1 | 1 | 1 | 1 | 7 | 7 | 7 | 7 | 7 | 7 | 7 | 7 |
| - c/2 | | 0 | 0 | 0 | | 3 | 3 | 3 | | 3 | 3 | 3 | | 6 | 6 | 6 |
| - c | | | 1 | 1 | | | 1 | 1 | | | 7 | 7 | | | 7 | 7 |
| -3c/2 | | | | 0 | | | | 3 | | | | 3 | | | | 6 |
| . | | | | | | | | | | | | | | | | |
| . | | | | | | | | | | | | | | | | |
| -∞c/2 | | | | | | | | | | | | | | | | |
| No. Atoms | 1 | 1 | 3 | 3 | 1 | 7 | 9 | 15 | 7 | 13 | 27 | 31 | 7 | 19 | 33 | 45 |

Table II. Restricted Hartree-Fock Adsorption Energies of States of $Be_{45}H_2$.

| State No. | MO Configuration[a] | | | | | | Energy[b] | |
|---|---|---|---|---|---|---|---|---|
| | $a_1'$ | $a_2'$ | $a_2''$ | $e'$ | $e''$ | $a_1''$ | $R_{eq}$ | $R_\infty$ |
| 1 | 1 | 2 | 1 | 4 | 4 | 2 | -45.601315 | -45.570651 |
| 2 | 2 | 2 | 2 | 4 | 4 | 2 | -45.604328 | -45.294292 |
| 3 | 1 | 2 | 2 | 1 | 4 | 2 | -45.625789 | -45.264307 |
| 4 | 2 | 2 | 2 | 2 | 4 | 2 | -45.633513 | -45.124689 |
| 5 | 2 | 2 | 2 | 1 | 1 | 2 | -45.613706 | -45.101965 |
| 6 | 1 | 1 | 1 | 1 | 4 | 2 | -45.591720 | -45.502133 |

[a]All open-shell states are triplet coupled. Occupations correspond to the number of electrons occupying the highest energy molecular orbital of a given symmetry.

[b]$R_{eq}$ and $R_\infty$ correspond to H-$Be_{surface}$ separations of 0.86Å and 10Å, respectively. Energies are in hartrees.

Table III. Adsorption Energies of $Be_{45}H_2$.[a]

| Type of Calculation | Energy at $R_{eq}$ | Energy at $R_\infty$ | $\Delta E_{adsorb}$ |
|---|---|---|---|
| MCSCF[b] | -45.61135 | -45.57065 | 12.77 |
| Average Energy[c] | -45.58827 | -45.42429 | 51.45 |
| Pure Spin Singlet | -45.56818 | -45.34371 | 70.43 |
| Pure Spin Triplet | -45.60132 | -45.57065 | 9.63 |

[a]Energies (hartrees) correspond to State 1 of Table II. $R_{eq}$ and $R_\infty$ correspond to H-$Be_{surface}$ separations of 0.86Å and 10Å, respectively. $\Delta E_{adsorb}$ is the difference between energies at these two distances (kcal/mol·H atom).

[b]Two-configuration MCSCF (see text).

[c]Average energy of configuration (see text).

Table IV. Restricted Hartree-Fock Energies of $Be_{45}H_2$ at Dissociation.[a]

| | |
|---|---|
| Average Energy[a] | -45.35865 |
| Pure Spin Singlet[b] | -45.50602 |
| Pure Spin Singlet[c] | -45.25044 |
| Pure Spin Triplet[d] | -45.50213 |
| Pure Spin Quintet | -45.50603 |

[a]Energies (hartrees) correspond to State 6 of Table II. H to $Be_{surface}$ separation is 10Å.

[b]Electrons in symmetry orbitals $a_1'$ and $a_2''$ are coupled triplet with respect to each other and singlet with respect to those in symmetry orbitals $a_2'$ and e' (See Table II).

[c]Electrons in symmetry orbitals $a_1'$ and e' are coupled triplet with respect to each other and singlet with respect to those in symmetry orbitals $a_2'$ and $a_2''$. (See Table II).

[d]The electron in symmetry orbital e' is coupled singlet to all the other open shell electrons, which are coupled triplet to each other (See Table II).

Table V. Energies of the $Be_{45}H_2$ System.

| Species[a] | Energy[b] |
|---|---|
| H | - 0.49928 |
| $Be_{45}$ | -44.57210 |
| $Be_{45}H_2$ ($R_{eq}$) | -45.63351 |
| $Be_{45}H_2$ ($R_\infty$) | -45.57065 |
| $Be_{45}H_2$ ($R_{eq}$) - $Be_{45}H_2$ ($R_\infty$) | 19.72 |
| $Be_{45}H_2$ ($R_{eq}$) - [$Be_{45}$ + 2H] | 19.72 |

[a] $R_{eq}$=0.86Å, $R_A$=10Å, where R is the Distance from H to the Be surface.

[b] First four values are in hartrees, while the last two are in kcal/mol·atom. All values correspond to the lowest-lying state found at that distance. All States are triplet coupled.

Table VI. Work Functions of $Be_{45}$ and $B_{45}H_2$ Clusters.

| Cluster | $\Phi$(ev)[a] |
|---|---|
| $Be_{45}$ | 4.62,4.43 |
| $Be_{45}H_2$ | 3.39,3.14 |
| Be (expt.)[b] | 3.92 |
| BeH (expt.)[c] | 3.92 |
| $\Delta\Phi[Be_{45}-Be_{45}H_2]$[d] | 1.23,1.29 |
| $\Delta\Phi[Be-BeH]_{expt.}$ | 0 |

[a] Where two values appear, these are Koopmans' theorem and $\Delta E_{SCF}$ values, respectively.

[b] Ref. 19.

[c] Ref. 11.

[d] Values correspond to a work function lowering.

Table VII. Atomic Populations of $Be_{45}$ and $Be_{45}H_2$.

| Cluster | Z-coord[a] | Atom Label[b] | No. Atoms[c] | Cluster Net Charge per Atom | $[Cluster]^+$ Net Charge per Atom | Total Net Charge Difference ($[Cluster]^+$ - Cluster) |
|---|---|---|---|---|---|---|
| $Be_{45}$ | 0 | BeO | 1 | 1.01 | 1.00 | -0.01 |
| | c/2 | BeA | 6 | 0.42 | 0.40 | -0.12 |
| | c/2 | BeC | 6 | -0.20 | -0.15 | 0.30 |
| | 0 | BeB | 6 | -0.33 | -0.31 | 0.12 |
| | c | BeH | 12 | -0.19 | -0.17 | 0.24 |
| | c | BeD | 2 | 1.36 | 1.34 | -0.04 |
| | 3c/2 | BeF | 6 | -0.14 | -0.14 | 0.00 |
| | 3c/2 | BeG | 6 | 0.02 | 0.09 | 0.48 |
| $Be_{45}H_2$ | 0 | BeO | 1 | 0.99 | 0.99 | 0.00 |
| | c/2 | BeA | 6 | 0.43 | 0.41 | -0.12 |
| | c/2 | BeC | 6 | -0.16 | -0.13 | 0.18 |
| | 0 | BeB | 6 | -0.36 | -0.32 | 0.24 |
| | c | BeH | 12 | -0.15 | -0.14 | -0.12 |
| | c | BeD | 2 | 1.31 | 1.29 | -0.04 |
| | 3c/2 | BeF | 6 | -0.18 | -0.17 | 0.06 |
| | 3c/2 | BeG | 6 | -0.04 | 0.06 | 0.60 |
| | R[d] | H | 2 | -0.01 | -0.01 | 0.00 |

[a] c=3.58Å

[b] See Fig. 2.

[c] No. of symmetry equivalent atoms

[d] R=0.86Å for Be plane to H distance. Be to H distance is 1.58Å.

FIGURE CAPTIONS

Fig. 1. $Be_{45}H_2$

Fig. 2. The potential energy curve for the approach of H to a rigid $Be_{45}$ surface having internuclear separations corresponding to bulk metal lattice constants. Total energies may be obtained by adding -45.00 h to the given values.

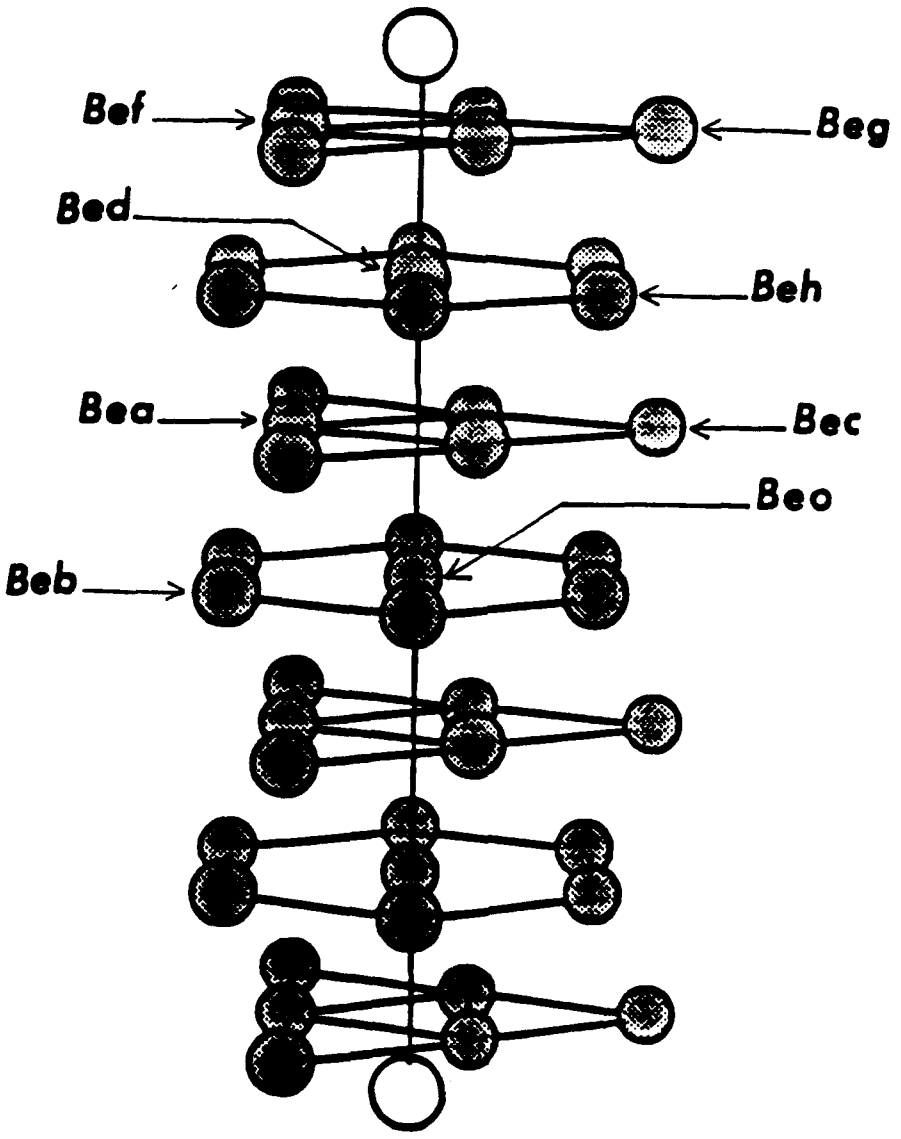
Bef
Beg
Bed
Beh
Bea
Bec
Beo
Beb

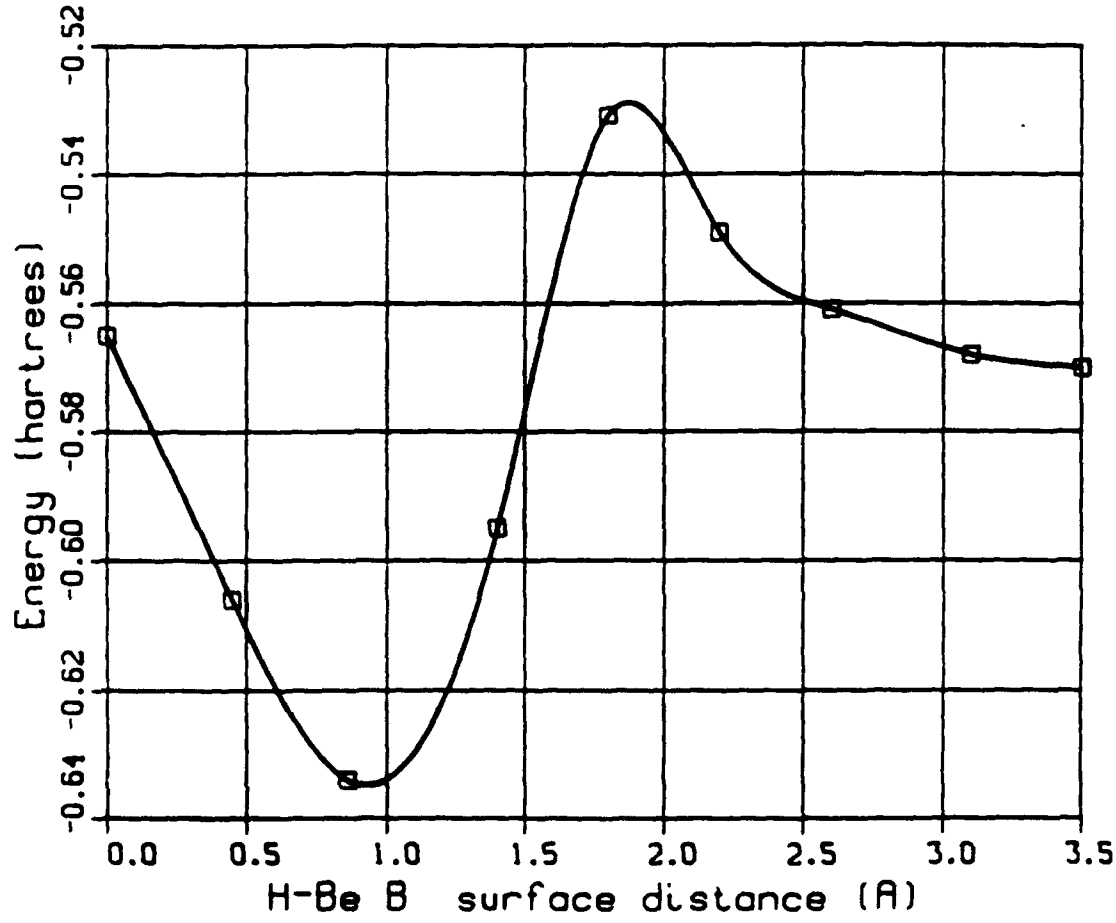
Energy (hartrees)
-0.52
-0.54
-0.56
-0.58
-0.60
-0.62
-0.64
0.0
0.5
1.0
1.5
2.0
2.5
3.0
3.5
H-Be B surface distance (A)

## 4. Publications


1. "Effects of Hydrogen and of Cesium Adsorption on a Beryllium Surface: A Theoretical and Experimental Study", Surface Science **208**, 189-204 (1989).
2. "Ab Initio Study of the Layered Semiconductor Cluster $Bi_6I_{18}$", M. M. Marino, M. Sawamura, W. C. Ermler and C. J. Sandroff, Chemical Physics Letters **163**, 202-6 (1989).
3. "Structure and Properties of Cesium-Coated Surfaces and the Effects of Hydrogen and Oxygen Implantation", W. C. Ermler and M. M. Marino, Proceedings of the SPIE OE/LASE '89 Conference on Microwave and Particle Beam Sources and Directed Energy Concepts, January 16-20, Los Angeles, CA, 1989, 13 pp.
4. "Ab Initio Study of the Geometry and Electronic Structure of Lead Iodide Semiconductor Clusters", M. M. Marino, M. Sawamura, W. C. Ermler and C. J. Sandroff, Physical Review B **41**, 1270-3 (1990).
5. "Ab Initio Study of Quantum Confinement Effects in $(PbI_2)_7$ Semiconductor Clusters", M. Sawamura and W. C. Ermler, The Journal of Physical Chemistry **94**, 7805-8 (1990).
6. "Ab Initio Studies on the $Li_2O$ Molecule and a $Cs_{11}O_3$ Cluster", P. Wang, M.S. thesis, Stevens Institute of Technology, 1990.
7. "Ab Initio Studies of Heterogeneous Atomic Clusters", M. M. Marino, Ph.D. thesis, Stevens Institute of Technology, 1990.
8. "Evolution of Quantum Confinement Effects in $PbI_2$ Semiconductor Clusters", M. Sawamura, Ph.D. thesis, Stevens Institute of Technology, 1990.
9. "Ab Initio Study of the Effects of Cesium, Hydrogen and Oxygen Adsorption on the Work Function of Beryllium", M. M. Marino and W. C. Ermler, Chemical Physics Letters, **176**, 36-40 (1991).
10. "Imaging of Colloidal Gold on Graphite by Scanning Tunneling Microscopy: Isolated Particles, Aggregates, and Ordered Arrays", J. F. Womelsdorf, W. C. Ermler and C. J. Sandroff, The Journal of Physical Chemistry, **95**, 503-5 (1991).
11. "Scanning Tunneling Microscopy: A Critical View of Tip Participation", J. F. Womelsdorf, M. Sawamura and W. C. Ermler, Surface Science **241**, L11-15 (1991).
12. "Ab Initio Study of the Electronic Spectrum of a $Cs_{11}O_3$ Cluster", P. Wang and W. C. Ermler, The Journal of Chemical Physics, in press.
13. "Ab Initio Study of Hydrogen Adsorption on Be (0001)", M. M. Marino and W. C. Ermler, The Journal of Chemical Physics, in press.

## 5. Professional Personnel

Dr. Walter C. Ermler, (Principal Investigator) Professor of Chemistry
Dr. Maria M. Marino, Graduate Research Assistant
Dr. Makoto Sawamura, Graduate Research Assistant
Ms. Ping Wang, Graduate Research Assistant
Mr. John F. Womelsdorf, Graduate Research Assistant

## 6. Interactions

### (1) Spoken Papers

1. "Ab Initio Studies of Cesiated Beryllium Clusters", American Conference on Theoretical Chemistry, Gull Lake, MN, July, 1987.
2. "Ab Initio Relativistic Calculations on Heavy Elements and Their Molecules", ACS National Meeting, New Orleans, LA, August, 1987.
3. "2-D Bulk Extension of Cylindrical Supermolecules: Ab Initio Studies of Cesiated Beryllium", ACS-NERM, Rochester, NY, October, 1987.
4. "2-D Bulk Extension of Cylindrical Supermolecules: Ab Initio Studies of Cesiated Beryllium", 17th Northeast Regional Meeting, American Chemical Society, Rochester, NY, November 8, 1987.
5. "Hydrogen and Cesium Adsorption on a Beryllium Surface", Clarkson University, Institute of Colloid and Surface Science Invited Seminar, March 17, 1988.
6. "An Ab Initio Study of Cs and H Adsorption on Be Metal", Molecular Spectroscopy Conference, The Ohio State University, Columbus, Ohio, June, 1988.
7. "An Ab Initio Study of Cs and H Adsorption on Be Metal", SPIE Conference, Los Angeles, CA, January, 1989.
8. "Structure and Properties of Cesium-Coated Surfaces", Physics Department Seminar Series on Atom-Surface Interactions, Stevens Institute of Technology, March, 1989.
9. "Ab Intio Studies of Lead Iodide Semiconductor Clusters", New Jersey Academy of Sciences, Wm. Patterson College, April, 1989.
10. "Ab Initio Study of Tungsten-Tip Graphite Surface Interactions of Scanning Tunneling Microscopy", March, 1990 Meeting of the American Physical Society, Los Angeles, CA.

11. "Ab Intio Potential Energy Surface for the Production of $H^-$ Ions from a Beryllium Surface", National Meeting of the American Chemical Society, Boston, MA, April, 1990.
12. "Ab Initio Calculation of Electronic Spectra of Semiconductor Clusters", Molecular Spectroscopy Conference, The Ohio State University, Columbus, Ohio, June, 1990.

**(2) Consultative and Advisory Functions**

None

7. **New Discoveries, Inventions or Patent Disclosures**

None

8. **Additional Statement**

None